Implementation of a lipid-coated membrane in a combined dissolution and permeation system and comparison to Caco-2 cell monolayers

Dissertation

zur Erlangung des Grades

des Doktors der Naturwissenschaften

der Naturwissenschaftlich-Technischen Fakultät III

Chemie, Pharmazie, Bio- und Werkstoffwissenschaften

der Universität des Saarlandes

von

Sandra P. Gantzsch

Saarbrücken

2013

Tag des Kolloquiums:	08.10.2013
Dekan:	Prof. Dr. Volkhard Helms
Berichterstatter:	Prof. Dr. Claus-Michael Lehr
	Juniorprof. Dr. Thorsten Lehr
Vorsitz:	Prof. Dr. Gerhard Wenz
Akad. Mitarbeiter:	Dr. Stefan Boettcher

Die vorliegende Arbeit entstand auf Anregung und unter Anleitung von

Herrn Prof. Dr. Claus-Michael Lehr

in Zusammenarbeit mit der

Sanofi-Aventis Deutschland GmbH

am Lehrstuhl für Biopharmazie und Pharmazeutische Technologie

an der

Universität des Saarlandes

Abstract

For the development of solid oral dosage forms the determination of drug release and permeability is of particular importance. To be close to real human conditions, the use of systems which combine testing of both parameters is meaningful. Therefore, an apparatus was developed especially for this approach which uses well-established Caco-2 cells as permeation barrier. Circumventing some drawbacks of Caco-2 cells, several non-cellular barriers were developed for classical transport experiments, which are known as so-called parallel artificial membrane permeability assays.

In the present work a non-cellular permeation barrier was developed especially for the use in the combined dissolution and permeation apparatus and successfully characterized regarding its coatig assembly, stability and permeation properties in comparison to Caco-2 cell monolayers for both drug solutions and solid oral dosage forms. This artificial membrane presents a valuable alternative to Caco-2 cells.

Furthermore, the suitability of the combined apparatus to analyze effects of excipients, in particular P-glycoprotein inhibitors, was tested. Due to the construction of the apparatus the absorptive transport could only be determined which resulted in much smaller inhibition effects. The results obtained with drug solutions and tablets indicated a limited use of the combined system in this context necessitating further investigations.

Zusammenfassung

Während der Entwicklung von festen oralen Arzneiformen ist die Bestimmung der Wirkstofffreisetzung sowie der Permeabilität von besonderer Bedeutung. Um nah an menschlichen Bedingungen zu sein ist die Verwendung von Systemen, die beide Parameter kombinieren, sinnvoll. Daher wurde ein Gerät speziell für diesen Ansatz entwickelt, welches etablierte Caco-2 Zellen als Permeationsbarriere nutzt. Um einige Nachteile von Caco-2 Zellen zu umgehen, wurden verschiedene nicht-zelluläre Barrieren für den Einsatz in klassischen Transportversuchen entwickelt, die als parallele artifizielle Membran-Permeabilitäts-Assays bekannt sind.

In dieser Arbeit wurde eine nicht-zelluläre Barriere speziell für den Einsatz in einem kombinierten Freisetzungs- und Permeationsgerät entwickelt und erfolgreich bezüglich Coatingaufbau, Stabilität und Permeationseigenschaften im Vergleich zu Caco-2 Zellen sowohl mit Wirkstofflösungen als auch mit Tabletten charakterisiert. Diese künstliche Membran stellt eine wertvolle Alternative zu Caco-2 Zellen dar.

Des Weiteren wurde der Einsatz des Gerätes zur Analyse von Hilfsstoffeffekten, insbesondere P-Glykoprotein Hemmer, getestet. Aufgrund des Geräteaufbaus konnte nur der absorptive Transport bestimmt werden, was in viel geringeren Transportereffekten resultierte. Die Ergebnisse, welche mit Lösungen sowie Tabletten erzielt wurden, weisen auf eine eingeschränkte Verwendung des kombinierten Gerätes in diesem Zusammenhang hin und erfordern weitere Untersuchungen.

Table of contents

1 Introduction

For the bioavailability of orally applied drugs liberation and absorption are essential parameters, and as such are parameters considered by the LADME model. This model summarizes the five main processes involved in pharmacokinetics as being liberation, absorption, distribution, metabolism and excretion. Since liberation and absorption are of vital importance for clinical efficacy and may easily be optimized during drug formulation development, many efforts have been made to achieve standardized determination of drug release and permeability close to human conditions, especially in case of solid dosage forms. Currently, both parameters are analyzed as individual attributes using different standard methods.

1.1 *In vitro* dissolution testing of orally applied drugs

Dissolution testing is the most commonly used technique for the determination of drug release. Validated dissolution models are described in the European Pharmacopoeia (Ph. Eur.) as well as in the United States Pharmacopoeia (USP) and consequently have become standard methods in formulation development and pharmaceutical quality control. Among them, USP apparatus 1 and 2 (basket and paddle apparatus respectively) are widely used. In order to be close to *in vivo* conditions the test conditions such as temperature, pH or composition of the dissolution media have been refined. In this context, the development of simulated intestinal fluids by the group of Dressman et al. [1] should be particularly mentioned. Various groups have established different versions of FaSSIF (fasted state simulated intestinal fluid) and FeSSIF (fed state simulated intestinal fluid) and described the use of such media for dissolution as well as for permeation approaches [1-7]. Even the USP describes a version of simulated intestinal fluid [8]. The main modification between the different versions is the concentration of bile salts like lecithin or sodium taurocholate.

Another apparatus used for dissolution testing is the flow through dissolution cell (USP apparatus 4). The technique of flow through dissolution measurement is advantageous especially for poorly soluble compounds, due to the better maintenance of sink conditions [9]. Furthermore, the continuous flow of medium

and the thereby constant removal of dissolved drug allows the determination of dissolution closer to the *in vivo* situation. Moreover, this device enables faster and easier change of dissolution media throughout the experiment and therefore the *in vivo* situation can easily be mirrored.

While determination of drug release with apparatus 1 and 2 directly leads to cumulative released amounts, apparatus 4 enables the time dependent determination of concentration changes in a differential form. The use of apparatus 4 therefore requires an additional conversion step of the measured released drug concentration in order to evaluate the total released amount.

1.2 Determination of permeability

A categorization of active pharmaceutical ingredients (APIs) with respect to biorelevant parameters has been described in the Biopharmaceutics Classification System (BCS) introduced by Amidon et al. [10]. As a guide to predict drug absorption after oral administration, the US Food and Drug Administration (FDA) accepted this system, which classifies APIs according to their intestinal permeability and their aqueous solubility (Table 1.1). According to the FDA an API is considered as highly soluble when the highest dose strength is soluble in 250 ml or less of aqueous media over the pH range of 1-7.5 [11]. If 90 % or more of the applied dose is absorbed in humans the API is considered as highly permeable [11].

Table 1.1. Biopharmaceutics Classification System (BCS) according to Amidon et al. [10]

Class	Solubility	Permeability
I	High	High
II	Low	High
III	High	Low
IV	Low	Low

The measurement of intestinal permeability is more challenging compared to dissolution testing due to the fact that it is a more complex process. Due to its large surface area, resulting from villous structures and epithelial folding, the small

intestine is the predominant organ for drug absorption of orally administered dosage forms. A drug can permeate the intestinal barrier via different pathways, which are illustrated in Figure 1.1. In the presence of a concentration gradient permeation via both the transcellular and the paracellular pathway is a passive process (Figure 1.1 A and B), which depends on the physicochemical parameters of the drug substance. Paracellular transport occurs as a diffusion process in between the cells crossing the interconnecting tight junctions through pores. This pathway is preferred by hydrophilic drug substances as transcellular transport is hindered by the lipophilic character of the cell membrane. Lipinski´s rule of 5 describes the limitations of transcellular transport [12]. For high transcellular permeability of a drug molecule to be likely to occur, at least three of the following criteria should be fulfilled:

1. Maximum 5 H-bond donors
2. Maximum 10 H-bond acceptors
3. A molecular mass less than 500 Da
4. A logP lower than 5

Apart from passive transport mechanisms, intestinal absorption can also take place by active transport via transporter proteins. This enables the permeation of substances which are excluded from passive pathways due to their physicochemical properties. Active transport can be concentration gradient driven (Figure 1.1 C) but may also occur against a concentration gradient (Figure 1.1 D and E). In the second case, energy (e.g. ATP) is required, and may facilitate transport from both the luminal side to the blood (influx) as well as from inside of the cell to the luminal side (efflux). Further processes which may occur in conjunction with drug permeation include vesicular transport following transcytosis or endocytosis (Figure 1.1 F), and enzymatic metabolism during transcellular transport (Figure 1.1 G).

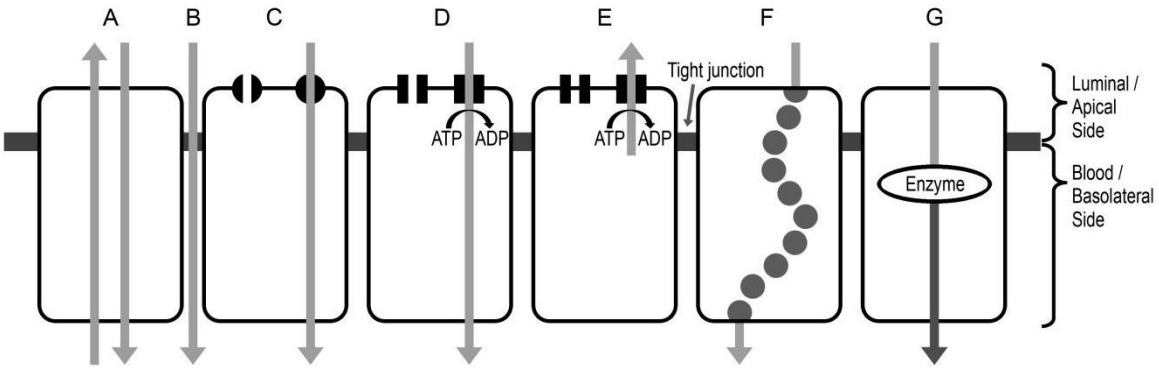

Figure 1.1. Scheme of possible permeation pathways at the intestinal barrier. Passive transcellular transport (A), passive paracellular transport (B), carrier-mediated transport (C), active transport (D), active efflux under ATP consumption (E), vesicular transport after apical endocytosis (transcytosis) (F), passive transcellular transport modified by enzymatic metabolism (G).

Apart from *in vivo* studies in humans, further biological models can be used for the evaluation of intestinal permeation of pharmaceutical compounds. This includes *in vivo* or *in situ* animal models, *in vitro* studies using excised animal or human intestinal tissues, such as the everted gut sac model, as well as *in vitro* studies using monolayers of cultured epithelial cells [11]. However, non-cellular permeation models based on lipid-infused artificial membranes also have an increasing importance for the determination of permeability due to the possibility of automation in high throughput systems. An overview of the relevant artificial models can be found in Chapter 1.4.

In vitro permeation experiments are mostly performed in 6-, 12-, 24- or 96-well plates in an incubator to ensure controlled conditions together with stirring or shaking. These conditions will be mentioned as classical static setup in the following chapters.

The most commonly used way to assess and compare results obtained from permeability experiments is by the calculation of the apparent permeability coefficient (P_{app}) [13]. This value represents the combined effects of all pathways across the barrier including the cell membrane, the tight junctions as well as the unstirred water layer at the membrane. The P_{app} value is equal to the flux per surface area and initial drug concentration. Thereby, the flux is calculated from the cumulative amount of drug substance in the receiver compartment versus time according to Fick´s first law, under assumption of steady state. It can be

determined for the absorptive as well as for the secretory direction of drug transport.

1.2.1 Caco-2 cell culture model

One of the widely used and well-established cellular *in vitro* models for the small intestine is the Caco-2 cell monolayer [14, 15]. Caco-2 cells were first isolated from the colonic adenocarcinoma of a Caucasian male in 1977. They are characterized by their physiological similarity to the human intestinal epithelium, which can explain their high acceptance as a model for the human intestinal epithelial barrier. Under standard culture conditions Caco-2 cells are able to differentiate spontaneously after reaching confluence. They do not only form a brush border membrane but also functional tight junctions. Furthermore, they express efflux pumps e.g. MDR1 and BCRP as well as active transporters like MCT1 and PepT1. All this properties are advantageous with respect to the use of Caco-2 cells for transport studies, as they enable analysis of specific uptake mechanisms. A good correlation between human intestinal absorption and Caco-2 cell permeability has been demonstrated in various studies [16, 17]. In contrast to the above mentioned advantages of this cell line, the evaluation of metabolism during transport in a Caco-2 cell model is limited due to the low expression of CYP3A4, the major enzyme for metabolism of marketed drugs. This drawback can be minimized by transfection of cells with the CYP3A4 gene or induction of the gene using vitamin D3 [18, 19].

1.2.2 Active efflux by P-glycoprotein

P-glycoprotein (P-gp) is often described as the most important efflux protein in humans. It belongs to the ATP binding cassette (ABC) family of transporters. At several barriers in the human body, P-gp plays a significant role [20]. Due to its anatomical location, this efflux transporter functions to protect the body against toxic xenobiotics [21]. For instance, it transports compounds from intestinal mucosal cells into the lumen, at the blood-brain-barrier towards the blood or in the kidneys into the urinary system [22, 23]. Most of the substances which are P-gp substrates are hydrophobic in nature [21]. In the gastrointestinal tract, the

transporter is located on the apical surface of epithelial cells of the small and large intestine [20]. Consequently, the oral bioavailability of certain substances may be reduced by the activity of P-gp [24]. Nevertheless, the clinical effect of P-gp inhibition is discussed controversial. The *in vivo* relevance of P-gp is affected both by the affinity of the API to efflux systems and by the luminal concentration of API. For example, an increased oral bioavailability of paclitaxel was demonstrated when co-administered with cyclosporine A (CysA), which is known to be a potent P-gp inhibitor [25]. Furthermore, in healthy volunteers the same effects were described when CysA was given in combination with TPGS [26]. Nevertheless, there are also statements that the influence of P-gp is less important than the influence of CYP especially with regard to the occurrence of drug-protein interactions [21].

1.3 Rationale and state of the art of combined dissolution and permeation measurement

As described above drug release and permeability are usually analyzed separately.

However, permeability can be influenced by excipients and different drug release profiles. Analysis of the impact of drug formulations on gastrointestinal permeability as well as a direct correlation of dissolution and permeation is therefore impeded by the design of commonly employed *in vitro* dissolution and permeation tests. Thus, a combined method for simultaneous dissolution and permeation experiments would be highly desirable to detect potential interactions between drug and excipients, and to assess the impact of any such interactions. For this reason, different systems have been developed combining dissolution and permeation in one apparatus.

The first approach was described by Ginski et al. [27]. In their continuous dissolution/Caco-2 system dissolution is performed in a paddle apparatus according to the USP (apparatus 2). Permeation takes place in a side-by-side diffusion cell, where a Caco-2 cell monolayer is mounted. Both parts are connected with a peristaltic pump for media transfer. As no drug is allowed to leave the system, the setup can be seen as a closed system. Therefore, the

generated concentration time trends have a lower *in vivo* relevance, and efflux or uptake transporters may become saturated.

The second approach and the first open system was published by Kobayashi et al. [28], which also takes the change of pH during the intestinal passage of drugs into account. As a kind of flow through dissolution device serves a stirred glass vessel at pH 1. A second glass vessel connected to the first with a pump is used for pH adjustment to pH 6. This vessel is followed by a side-by-side diffusion chamber, where permeation over a Caco-2 cell monolayer takes place.

A third approach especially designed for the investigation of poorly water soluble drugs was described by Kataoka et al. [29]. In this closed system dissolution and permeation take place in the same vessel. The device is divided by a Caco-2 cell monolayer into an apical and a basolateral compartment. The system was constructed in a downsized setup in relation to *in vivo* conditions; the drug was also applied in suspension or powder in clinical doses which were adapted accordingly to the setup size. Later on Kataoka et al. [6, 30, 31] published different applications for their system such as the investigation of food effects, formulation effects or efflux by P-gp. However, dissolution and permeation were not performed at the same time in this approach. Therefore, the author of this thesis remarks that the system can be understood as a combined and simultaneous setup only in limited form.

Based on these three approaches a system combining dissolution and permeation in one apparatus (d/p-system) was developed by Motz et al [32, 33] for the evaluation of complete solid oral dosage forms. Having an open system and using dynamic flow conditions provides a closer simulation of the conditions in the human body. The apparatus consists of three main parts. The current construction of the d/p-system is schematically shown in Figure 1.2. The first part is a flow through dissolution cell (USP apparatus 4). It is connected inline with the second part, where permeation takes place. The permeation module enables the mounting of a Transwell® with a Caco-2 cell monolayer in a custom-made flow through permeation cell (FTPC). The third part includes automated sampling and detection devices using a sequential injection analysis (SIA). As dissolution and permeation requires different flow rates the dissolution and permeation modules are connected with each other by a stream splitter. The system was tested for its ability to allow for measurement of both dissolution and permeation using

propranolol tablets with different release kinetics and dosage strengths. The system was refined by Muendoerfer et al. [34]. Firstly, the system was improved to allow the measurement of lowly permeable compounds (BCS class III and IV). In particular, a second valve, pump and autosampler for basolateral sampling were installed, the volume of the basolateral compartment was downsized and a magnetic stirrer was implemented. Secondly, the system was extended by a tool for online measurement of the transepithelial electrical resistance (TEER) value. Therefore, electrodes were integrated into both sides of the FPTC, which can be connected to a voltohmmeter (EVOM). This new tool enables the monitoring of the barrier integrity throughout the dissolution and permeation process. This is of particular importance in such a combined system, as for example, it is well known that excipients can open tight junctions and thereby can enhance the passive permeation of drug substances.

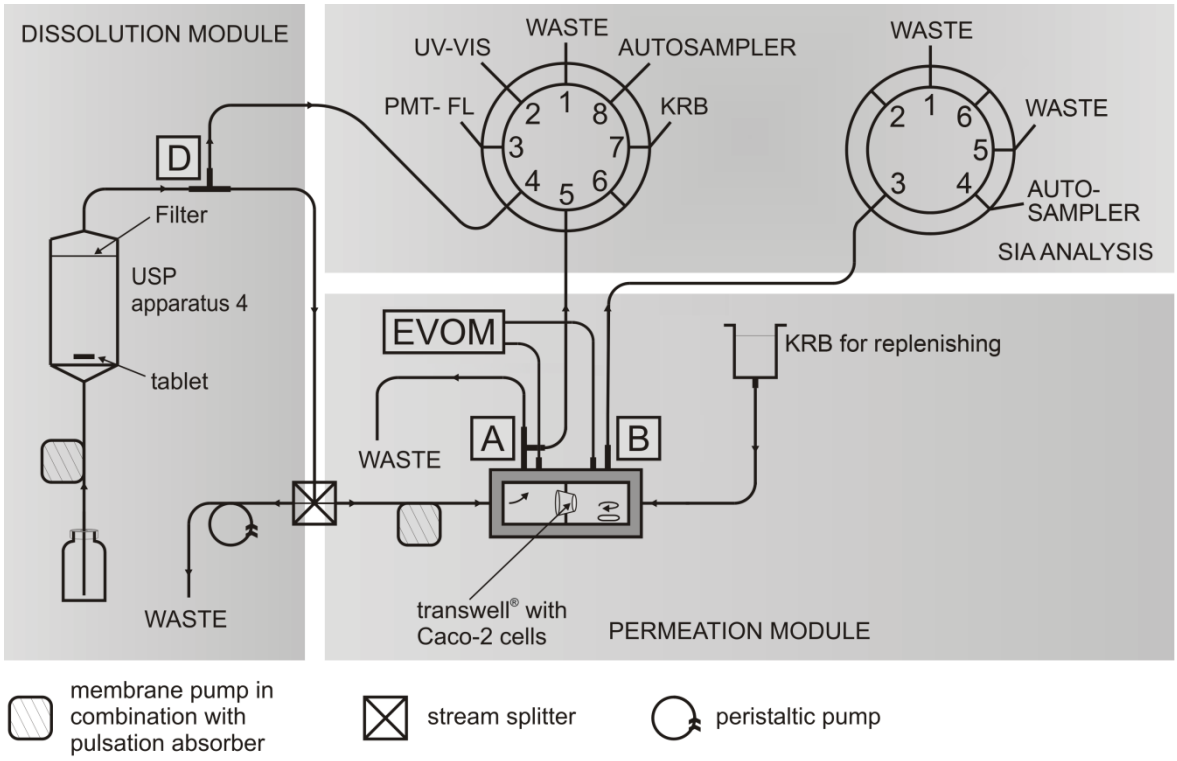

Figure 1.2. Scheme of the combined dissolution and permeation system according to Motz et al. and Muendoerfer et al. [32-34].

In contrast to the classical static setup, permeation experiments performed in the d/p-system and particularly in the FTPC are mentioned as being conducted under dynamic flow conditions in the following chapters.

1.4 State of the art: artificial membrane / non-cellular permeation barrier

Although Caco-2 cell monolayer has become one of the standard *in vitro* models for the determination of intestinal permeability [35], the use of cellular assays is associated with certain drawbacks. Long cultivation times, problems with contamination or incompatibility with some dissolution media should be mentioned as examples of such drawbacks. Due to these disadvantages, there was a strong need for the development of permeation models which do not utilize cells. Over the last years a high throughput model known as parallel artificial membrane permeability assay (PAMPA) has been developed [36], which has rapidly grown in importance. The PAMPA model can be a helpful, fast and low cost add-on to cellular models [37]. Artificial membranes behave in a very similar manner to Caco-2 cells in passive diffusion studies [38]. In the following, some selected examples of PAMPA-like models are presented.

Kansy et al. [36] were the first to describe a non-cellular model based on lipids solved in an organic solvent serving as the PAMPA permeation barrier. This original method consisted of a highly porous microfilter which was infused with a solution of egg lecithin (10 % w/v) dissolved in n-dodecane [36, 37]. The investigator chose to use phosphatidylcholine as a lipid due to its prevalence in mammalian membranes.

Since 1998 the PAMPA technique has been refined and has undergone substantial development to a more and more versatile method for permeability testing. Based on the first description of PAMPA many of the following systems were made of phosphatidylcholine dissolved in n-dodecane. As the source of lipid is mostly egg lecithin, these models are often classified as egg-PAMPA [37]. In order to mimic the high prevalence of sterols in mammalian membranes, some of these assays supplement phosphatidylcholine with cholesterol [37].

Due to egg lecithin sourcing and extraction processes, the quality and composition of the lipid for egg-PAMPA can change from batch to batch. This could be disadvantageous with respect to the reproducibility of assay results and may also

lead to higher inter-laboratory variations. Therefore, a synthetic lipid could be advantageous with respect to these points.

A solution of 2 % w/v of the synthetic phospholipid dioleoylphosphatidylcholine (DOPC) in n-dodecane was the basis for the first commercially available PAMPA lipid formulation [39-41]. However, it was soon replaced by the double-sink-assay (DS-PAMPA). This improved formulation is again based on a lecithin lipid combination (20 % w/v mixture of phospholipids) dissolved in n-dodecane [42, 43]. Furthermore, the experimental conditions were changed to a two gradient system, hence the name double-sink. The first sink condition is realized by a pH gradient between the aqueous compartments, mimicking the gastrointestinal and blood environment. Depending on the drug substance the pH of the donor compartment can be adjusted from 3 to 10, while the pH of the acceptor compartment is fixed at 7.4. As the second sink condition surfactants in micellar form are added to the acceptor compartment, where they act as chemical scavengers [37, 42].

Another approach to more closely mimic the lipid composition in biological membranes was described by Sugano et al. [44, 45]. In this study a mixture of cholesterol, phosphatidylcholine, phosphatidylethanolamine, phosphatidylserine and phosphatidylinositol dissolved in 1,7-octadiene was used. This biomimetic phospholipid mixture is described as being similar to the composition of the brush border membrane [46].

Additionally to PAMPA methods using diverse lipids dissolved in an organic solvent, Wohnsland and Faller [47] described a phospholipid-free assay using only an inert solvent, namely n-hexadecane (HDM-PAMPA). In comparison to other models this HDM-PAMPA leads to longer assay times [37].

Most of the published PAMPA methods utilize a hydrophobic filter membrane as support for the impregnated lipid solution. Although each system appears to work well and has shown promising correlation to human absorption, the long transport time and slow permeation rate in these systems in general is a disadvantage. Therefore, Zhu et al. [48] described a system using a hydrophilic PVDF membrane as support, which decreased the transport period and increased the permeation rate.

In principle all these PAMPA variants are characterized by an aqueous drug solution and an aqueous acceptor buffer separated by a phospholipid-infused or organic solvent-infused filter membrane [37]. As a high throughput method

PAMPA experiments are mostly performed in 96-well plates in a classical static setup. Several problems are associated with this setup such as the maintenance of sink conditions or the presence of an unstirred water layer. Therefore, a PAMPA-like system for use under flow conditions appears meaningful.

A model suitable for the use not only under static conditions but also under flow conditions was described by Corti et al. [49]. Here again, a lipid mixture (egg phosphatidylcholine and cholesterol) dissolved in an organic solvent (n-octanol) was used to impregnate a membrane [49, 50]. The impregnated membrane was inserted into a diffusion cell, connected to a donor and acceptor compartment by a peristaltic pump. The system can be seen as a closed model, since no drug is allowed to leave the setup. Corti et al. [50] showed that for passively absorbed drugs, such an artificial membrane was a good predictor of oral absorption in humans.

As organic solvents employed for solvation of PAMPA lipid components are prone to interact with the supportive membrane, several efforts were undertaken to eliminate this risk. A model free of organic solvents was described for the first time by Flaten et al. [51]. This model was based on depositing lipids in the form of liposomes in order to form a permeation barrier, and was designed for use under classical static permeation conditions. In several studies [52-57] the authors showed the suitability of their artificial membrane. The barrier was stable towards pH changes and agitation. The use of simulated intestinal fluid as medium as well as the addition of tensides or co-solvents to the medium was shown to be possible. Furthermore, this permeation barrier could be used for melt extrudates in a static setup with previous dispersion of the formulation in buffer [58]. Nevertheless, this setup does not enable the use of undissolved formulations and the simultaneous investigation of drug release and permeation.

Another PAMPA model avoiding the use of organic solvent in excess was described by Chen et al. [59] as a lipid/oil/lipid tri-layer system. According to the hypothesis of the authors, the excess of organic solvent in the current assays is an additional permeation barrier leading to under-prediction of highly permeable substances. This could be avoided by the new model leading to a better predictability. In comparison to conventional PAMPA methods the coating of the membrane of the tri-layer system does not need to be performed immediately

before the assay. Therefore, the authors concluded that the day-to-day variability of the coating can be minimized and the reproducibility can be improved [59].

Originally the artificial membrane setups called PAMPA were developed for the investigation of gastrointestinal permeation, which was also the focus of this chapter. For the sake of completeness it should be mentioned that in the last years this approach has also been used for other permeation barriers like the blood-brain-barrier or the skin [60, 61].

1.5 Aim of the work

As known from *in vivo* data the addition of different excipients like P-gp inhibitors or solubilizers can influence the bioavailability of drug substances. This can be an effect of changes during the dissolution or the permeation as well as a combination of both. Therefore, it appears meaningful to test the d/p-system for its suitability to analyze such effects. The first aim of the work was to examine the influence of the release of excipients under dynamic flow conditions. For this, a suitable model substance had to be selected showing an increased absorptive transport under inhibition of efflux transporters. Furthermore, the effect of excipients on drug permeation was tested using Caco-2 cell monolayers and solid dosage forms containing a P-gp inhibitor.

The combined dissolution and permeation system was developed for the use of Caco-2 cell monolayers as the permeation barrier. Due to certain drawbacks including cultivation time or potential for contamination, the development of an alternative to cellular barriers was set as a second aim. Therefore, an artificial membrane coated with lipid was developed, characterized and implemented in the FTPC and compared with Caco-2 cells. In a further step, it was evaluated whether the artificial membrane was also suitable for the analysis of dosage forms such as tablets.

2 Selection of a drug substance to test efflux systems

Statement of authorship contribution:

The following author contributed to this chapter:
Sandra P. Gantzsch, Ulrich F. Schaefer, Claus-Michael Lehr, Co-operation partners from Sanofi-Aventis
The author of the thesis made the following contribution to this chapter.

1. Design of the project including formulation of problems to be tested and design of individual experiments:
   Contributed significantly

2. Planning of experiments and design of methods to answer the problems posed under # 1 including choice and development of the methods:
   Contributed significantly

3. Performance of experiments and data analysis:
   Essentially performed this study independently

4. Presentation, interpretation and discussion of the results obtained in article form:
   Essentially performed this study independently

2.1 Introduction

Besides the consideration of the BCS for the selection of a suitable substance for the evaluation of the effect of excipients with a particular focus on efflux transporters, the refined Biopharmaceutics Drug Disposition Classification System (BDDCS) should also be taken into account. This classification system was introduced by Wu and Benet in 2005 [62]. The BDDCS includes transporter effects and elimination routes in the classification of drug substances. According to this system, the four classes as defined in BCS are supplemented by the effect of transporters and the elimination (Table 2.1). Recently, a compilation of over 900 drugs to which the BDDCS was applied has been published [63].

Table 2.1. Biopharmaceutics Drug Disposition Classification System (BDDCS) according to Wu et al. [62]

Class	Transporter effects	Route of drug elimination
I	Minimal	Metabolism
II	Efflux transport predominate	Metabolism
III	Absorptive transport predominate	Renal/Biliary elimination
IV	Absorptive and efflux transport could be important	Renal/Biliary elimination

As it is often described as the most important efflux protein in humans, P-gp moved into the focus of this investigation. As already described in hapter 1.2.2, several studies reported the effect of P-gp inhibitors on the bioavailability of drug substances [64, 65]. Therefore, it appeared meaningful to test the d/p-system for its suitability to determine effects of P-gp inhibition and any accompanying permeation enhancement.

Prior to testing complete dosage forms, the aim of the study was to identify a substance which shows an increased permeation across Caco-2 cells under inhibition of P-gp in the established transport setups (classical static setup and d/p-system). According to the BDDCS, substances classified in class II or IV are of particular interest. For this purpose, four different substances were tested.

Firstly, furosemide was chosen as a potential substrate for initial tests due to the fact that the d/p-system has already been established for the testing of that drug substance. Furthermore, different studies describe the impact of P-gp on the absorption of furosemide [66, 67].
The second chosen compound was rhodamine 123. It is described as a substrate of P-gp and has shown increased permeation and decreased efflux in the presence of TPGS [68].
Domperidone was the third substance selected for testing. It is described as a good substrate for P-gp, although these studies concentrate on the blood-brain barrier [69, 70].
The last potential substance selected was talinolol. According to Wu et al. [62] it is classified as a BDDCS class II substance and is indicated as a P-gp substrate. Furthermore, *in vivo* studies have shown an increased bioavailability of talinolol in combination with TPGS [71].

Besides the selection of suitable drug substances, which are described as substrates of efflux transporters, an inhibitor for the transporter also needed to be selected. As a model for this, TPGS was chosen as a potential inhibitor of P-gp. Several studies have demonstrated an inhibitory effect of TPGS on P-gp. For example, the enhancing effect of TPGS on intestinal absorption of talinolol, paclitaxel and HIV protease inhibitors has been described [71-73]. Furthermore, there are dosage forms on the market containing TPGS. For example, a soft gelatin capsule formulation of amprenavir with TPGS is marketed under the name Agenerase.

2.2 Materials and methods

2.2.1 Materials

Furosemide (Synopharm GmbH & Co KG, Barsbuettel, Germany), rhodamine 123 (Sigma-Aldrich, Steinheim, Germany), domperidone and domperidone maleate (Transo-Pharm, Siek, Germany) and talinolol (extracted from Cordanum tablets, AWD.pharma, Radebeul, Germany) were used as model substances. TPGS 1000 was obtained from Sigma-Aldrich (Steinheim Germany). All buffer reagents were

purchased from Sigma-Aldrich (Steinheim, Germany) and were of cell culture tested grade. All reagents for high performance liquid chromatography (HPLC) quantification were obtained from Sigma-Aldrich (Steinheim, Germany) and were of HPLC gradient grade. High purity water was prepared by a Millipore Milli-Q Synthesis system (Merck Millipore, Darmstadt, Germany).

2.2.2 Cell culture

Caco-2 cells (clone C2Bbe1) were purchased from American Tissue Culture Collection (ATCC, Manassas, USA). Cells were grown in 75 cm² T-flasks in an incubator (37 °C, 5 % CO_2, 85 % relative humidity) to approximately 90 % confluence. Cell culture medium consisted of Dulbecco´s Modified Eagle´s Medium (DMEM, PAA Laboratories GmbH, Pasching, Austria) supplemented with 1 % non-essential amino acids (NeAA, PAA Laboratories GmbH, Pasching, Austria) and 10 % fetal calf serum (FBS, LONZA, Verviers, Belgium) and was changed every second day. Caco-2 cells were trypsinated after reaching targeted confluence and were seeded on permeable supports (Transwell® type 3460, Corning Inc., Acton, USA) at a density of 60,000 cells/cm². Passages 61-70 within 21-25 days after seeding were used for experiments.

2.2.3 Transepithelial electrical resistance (TEER) measurement

Before each experiment, the transepithelial electrical resistance (TEER) of the cell monolayer was measured with a handheld chopstick electrode (STX-2) and an epithelial voltohmmeter (EVOM, World Precision Instruments, Berlin, Germany). Only Transwells® showing TEER values above 300 Ω*cm² were used for transport experiments. The TEER value was measured in the same way also after a classical static transport experiment.

During a dynamic transport experiment in the d/p-system, the TEER value was monitored online using an EVOM connected to electrodes in the FTPC as described by Muendoerfer et al. [34]. Here, the TEER value was recorded every minute in a computer-controlled manner using LabVIEW software (Version 2009, National Instruments Germany GmbH, Munich, Germany).

2.2.4 Buffer solution

As a donor and acceptor medium Krebs Ringer Buffer (KRB) adjusted to pH 7.4 was used. Composition of the buffer was the following: 142.03 mM NaCl, 10.0 mM HEPES, 4.00 mM D-Glucose, 3.00 mM KCl, 1.41 mM $CaCl_2$, 2.56 mM $MgCl_2$ and 0.44 mM K_2HPO_4.

2.2.5 Classical static transport experiments

Prior to transport experiments, Caco-2 cell monolayers were washed with KRB and pre-incubated (30 min) with KRB. Subsequently, 1.5 ml KRB was added to the receiver (basolateral) compartment and 0.5 ml solution of the drug to the donor (apical) compartment (Table 2.2). Throughout the experiment, the inserts were shaken using an orbital shaker (IKA®-Werke GmbH and Co KG, Staufen, Germany) at 150 rpm in an incubator (37 °C). Samples (100 µl) were taken at defined time points from the receiver compartment over 180 min. The sample volume was replaced with fresh KRB. All experiments were performed at least three times. Mass balance was checked and confirmed after the experiments.

Table 2.2. Concentrations of the drugs used in classical static transport experiments and dynamic transport experiments.

Substance	Concentration
Domperidone	23.5 µM = 10 µg/ml
Domperidone maleate	23.5 µM = 12.7 µg/ml
Furosemide	1209.5 µM = 400 µg/ml
Rhodamine 123	13 µM = 4.94 µg/ml
Talinolol	27.5 µM = 10 µg/ml
TPGS	0.0025 %, 0.005 %, 0.01 %, 0.02 % (added to drug solution, 0.01 % = 66 µM)

2.2.6 Dynamic transport experiments

Dynamic transport experiments were carried out in the FTPC of the d/p-system at 37 °C. The flow rate of drug solution was adjusted to 1.0 ml/min, which has been

described as the optimal flow rate to maintain barrier integrity in particular [32]. As a basis for all donor solutions (apical compartment) and as acceptor medium (basolateral compartment) KRB was used. Drug concentrations in the experiments were the same as used for classical static transport experiments, and as such are also summarized in Table 2.2. Prior to mounting in the FTPC Caco-2 cell monolayers were washed twice and were pre-incubated with KRB for 30 min. Samples were collected automatically at certain time points from the basolateral side of the permeation cell by means of Sequential Injection Analysis (SIA equipped with FIAlab software (FIAlab instruments, Bellevue, USA)). Therefore, the basolateral side of the permeation module was directly connected to a syringe pump and an autosampler (Cetac ASX 260, Omaha, USA). The sample volume was automatically replaced with fresh KRB. All experiments were performed at least three times.

The program codes for the respective substance and sampling ports are given in Chapter 10.2 in the annexes.

It was ensured by a constant delivery from a reservoir that during the whole experiment the donor concentration at the apical side of the FTPC remained constant.

2.2.7 Quantification of drug substances

The concentration of substance in the basolateral compartment at each sampling time point was determined via HPLC or fluorescence measurement in a plate reader. For further details of the quantification method see Chapter 10.1 in the annexes.

2.2.8 Data treatment

The apparent permeability (P_{app}) for each substance across the Caco-2 cell monolayer was calculated according to the following equation (eq. 1) derived from Fick's law for steady state and sink conditions.

$$P_{app} = \frac{dQ}{dt} \times \frac{1}{A \times c_0} \qquad \text{(eq. 1)}$$

From the linear part of produced diagrams (increasing mass in the basolateral part versus time), the ratio dQ/dt [µg/s] was calculated. Furthermore, A [cm²] is the surface area of the cell culture insert and c_0 [µg/ml] is the donor concentration at t = 0 h.

P_{app} values were calculated for each transport experiment separately. For comparison of different experimental conditions the single values were averaged.

For the rating of the effect of the inhibitor on the permeation an inhibition ratio was calculated according to the following equation (eq. 2).

$$inhibition\ ratio\ = \frac{P_{app\ (with\ inhibitor)}}{P_{app\ (without\ inhibitor)}} \qquad \text{(eq. 2)}$$

The mean P_{app} values were taken from transport experiments in the absorptive direction (A→B).

For statistical analysis t-tests ($p \leq 0.01$) were performed using SigmaStat integrated in SigmaPlot version 11.0 (Systat Software GmbH, Erkrath, Germany).

2.3 Results and discussion

2.3.1 Monitoring of TEER value

For both, transport experiments under classical static conditions as well as in the FTPC, the TEER values were above 300 Ω*cm² at the end of each experiment. Thus, TPGS did not show any effect on the membrane integrity and the membrane was intact throughout the entire experiment.

2.3.2 Furosemide

Figure 2.1 shows the permeated mass of furosemide in a classical static transport experiment. The respective P_{app} values are summarized in Table 2.3. The P_{app} values of furosemide in combination with 0.005 %, 0.01 % and 0.02 % TPGS (t-test, $p \leq 0.01$) show a significant difference from experiments without TPGS. Also, a significantly different amount of permeated furosemide after 180 min was found in the presence of 0.01 % TPGS (t-test, $p \leq 0.01$).

For furosemide, in the classical static setup it was possible to detect an effect of the P-gp inhibition on the permeation of the drug substance and a significant difference was found in the presence of 0.01 % TPGS. Therefore, it was decided that subsequent experiments in the FTPC would focus on using a 0.01 % concentration of inhibitor.

Table 2.3. Overview of P_{app} values for furosemide. Data are presented as mean ± SD (n ≥ 3). Data marked with * are significantly different from P_{app} values without TPGS (t-test, p ≤ 0.01).

Addition of TPGS	P_{app} classical setup [$*10^{-6}$ cm/s]	P_{app} FTPC [$*10^{-6}$ cm/s]
Without	0.26 ± 0.07	0.18 ± 0.02
0.0025 %	0.27 ± 0.06	Not tested
0.005 %	0.38 ± 0.01*	0.23 ± 0.06
0.01 %	0.42 ± 0.05*	0.17 ± 0.02
0.02 %	0.43 ± 0.02*	Not tested

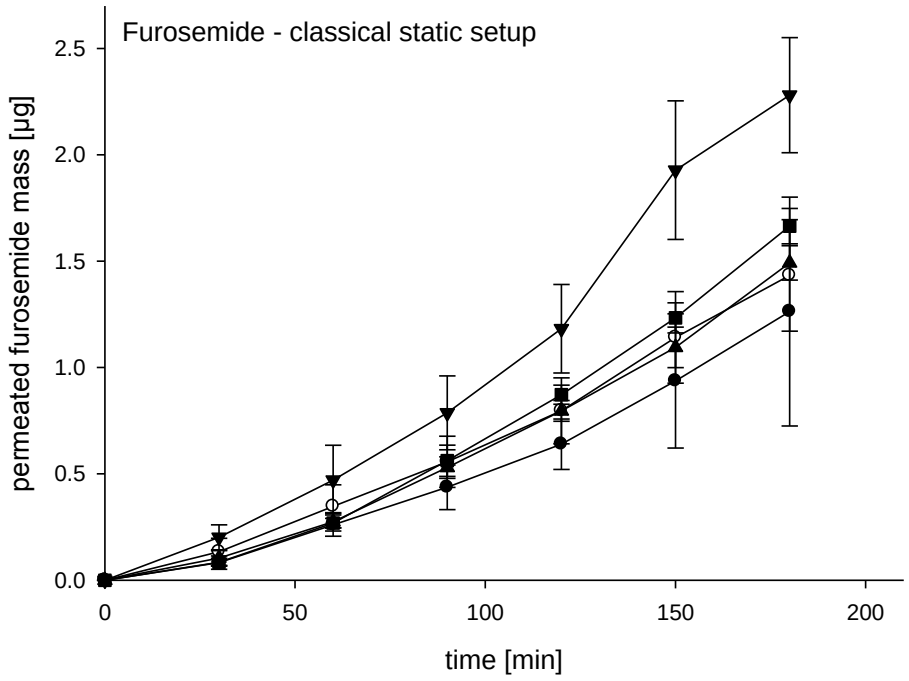

Figure 2.1. Permeated mass of furosemide in classical transport experiment. Experiments were performed without TPGS (○), with 0.0025 % (●), 0.005 % (▲), 0.01 % (▼) and 0.02 % (■) TPGS. Data are presented as mean ± SD (n ≥ 3).

Using the FTPC similar results were found for furosemide (Figure 2.2). The permeated mass of furosemide after 180 min was the same without and with 0.01 % TPGS. However, as no significant difference was found, a second concentration of TPGS was tested. The addition of 0.005 % TPGS already showed significant differences at least for the P_{app} values in the classical static transport experiments. In the FTPC, the permeated mass was found to be slightly higher with 0.005 % TPGS compared to furosemide alone. In the initial stages of transport experiments all three curves had the same slope. After 120 minutes the curve for furosemide transport in the presence of 0.005 % TPGS was observed to become steeper but nevertheless the difference was not significant. Also the P_{app} values (Table 2.3) obtained with TPGS were not significantly different from values without inhibitor (t-test, $p \leq 0.01$). Therefore, in the case of furosemide, the FTPC was not able to distinguish between non-inhibition and inhibition of P-gp by TPGS at the employed TPGS concentrations.

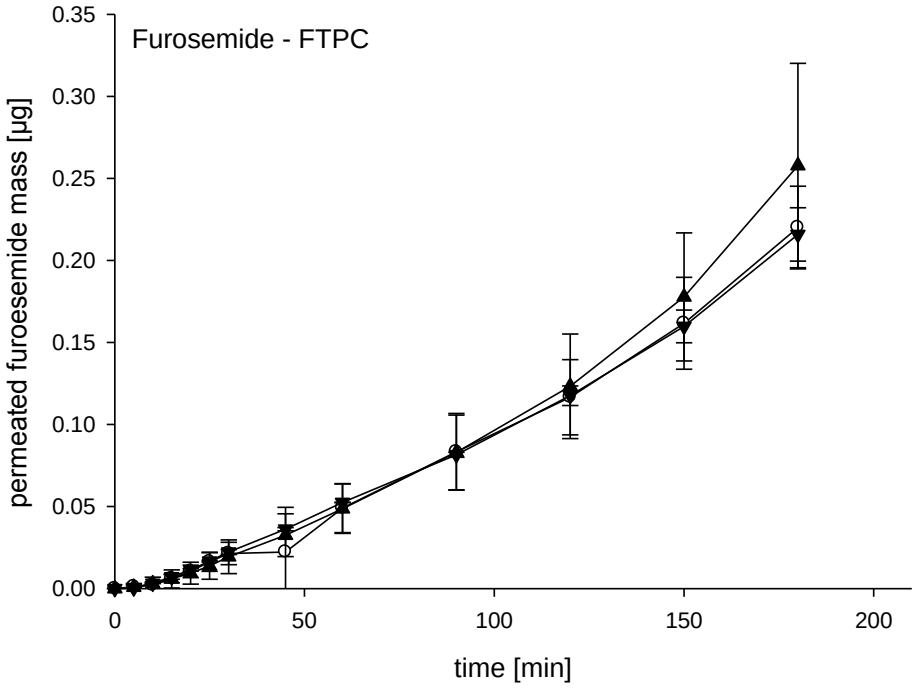

Figure 2.2. Permeated mass of furosemide in the FTPC. Experiments were performed without TPGS (○), with 0.005 % (▲) and 0.01 % (▼) TPGS. Data are presented as mean ± SD (n ≥ 3).

2.3.3 Rhodamine 123

The permeation profiles for rhodamine 123 under classical static transport conditions show only minor changes between the different concentrations of added TPGS (Figure 2.3). Looking at the P_{app} values (Table 2.4), a significant difference was only found between the experiments without TPGS and with 0.01 % TPGS (t-test, $p \leq 0.01$).

Table 2.4. Overview of P_{app} values for rhodamine 123. Data are presented as mean ± SD ($n \geq 3$). Data marked with * are significantly different from P_{app} values without TPGS (t-test, $p \leq 0.01$).

Addition of TPGS	P_{app} classical setup [$*10^{-6}$ cm/s]
Without	1.84 ± 0.67
0.0025 %	2.71 ± 0.52
0.005 %	2.10 ± 0.78
0.01 %	3.16 ± 0.54*
0.02 %	3.14 ± 2.46

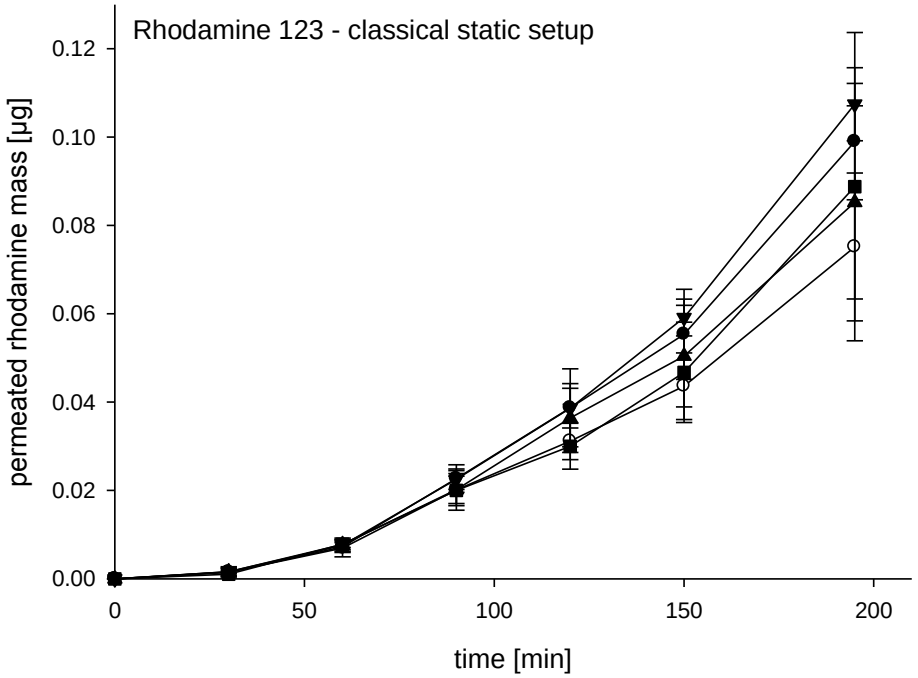

Figure 2.3. Permeated mass of rhodamine 123 in classical transport experiment. Experiments were performed without TPGS (○), with 0.0025 % (●), 0.005 % (▲), 0.01 % (▼) and 0.02 % (■) TPGS. Data are presented as mean ± SD ($n \geq 3$).

TPGS showed less influence on the permeation behavior of rhodamine 123 compared to furosemide. Since the FTPC was not able to show the influence of TPGS on furosemide permeation clearly, no further investigation of rhodamine 123 permeation in the FTPC was carried out.

2.3.4 Domperidone and domperidone maleate

The results for furosemide and rhodamine 123 in the classical static setup showed the greatest and most significant difference when adding 0.01 % TPGS to the drug solution. Therefore, the transport experiments with domperidone and domperidone maleate were only performed without and with 0.01 % TPGS.

Comparable results were obtained for domperidone and domperidone maleate in the classical setup and in the FTPC (Figure 2.4 and Figure 2.5).

The P_{app} values for the respective conditions are summarized in Table 2.5. Both domperidone and domperidone maleate show significantly different P_{app} values in combination with TPGS under classical static conditions as well as in the FTPC. Therefore, in contrast to the situation with furosemide, the FTPC was able to detect an effect of P-gp inhibition for these substances. This qualifies domperidone and domperidone maleate for further investigations with oral dosage forms.

Table 2.5. Overview of P_{app} values for domperidone and domperidone maleate. Data are presented as mean ± SD (n ≥ 3). Data marked with * are significantly different from P_{app} values without TPGS (t-test, p ≤ 0.01).

Addition of TPGS	P_{app} classical setup [$*10^{-6}$ cm/s]	P_{app} FTPC [$*10^{-6}$ cm/s]
Domperidone		
Without	4.21 ± 0.46	6.08 ± 0.52
0.01 %	6.96 ± 0.72*	8.69 ± 1.38*
Domperidone maleate		
Without	2.29 ± 0.62	8.11 ± 2.19
0.01 %	7.12 ± 0.52*	12.52 ± 1.40*

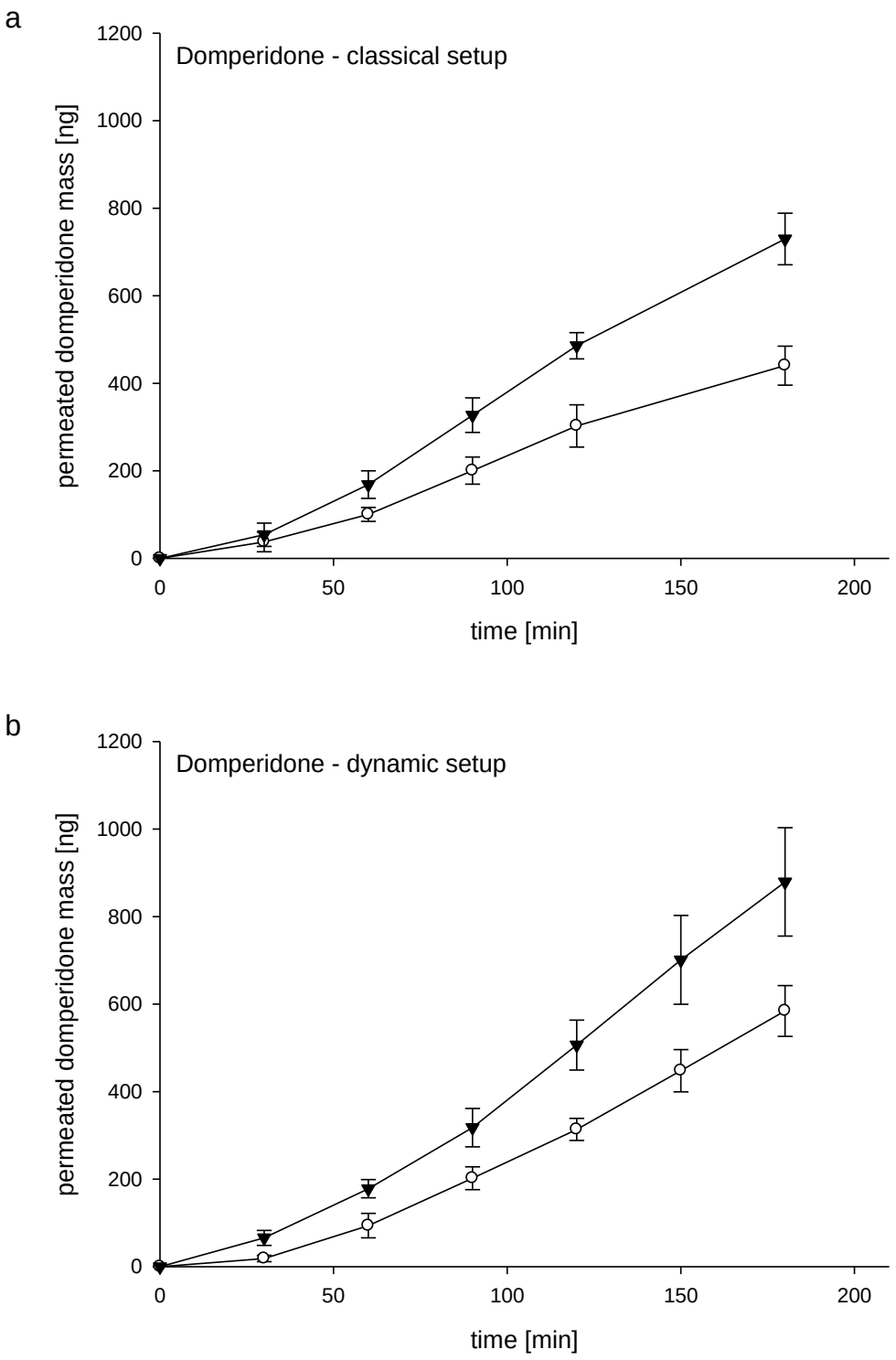

Figure 2.4. Permeated mass of domperidone in a classical transport experiment (a) and in the FTPC (b). Experiments were performed without TPGS (○) and with 0.01 % (▼) TPGS. Data are presented as mean ± SD (n ≥ 3).

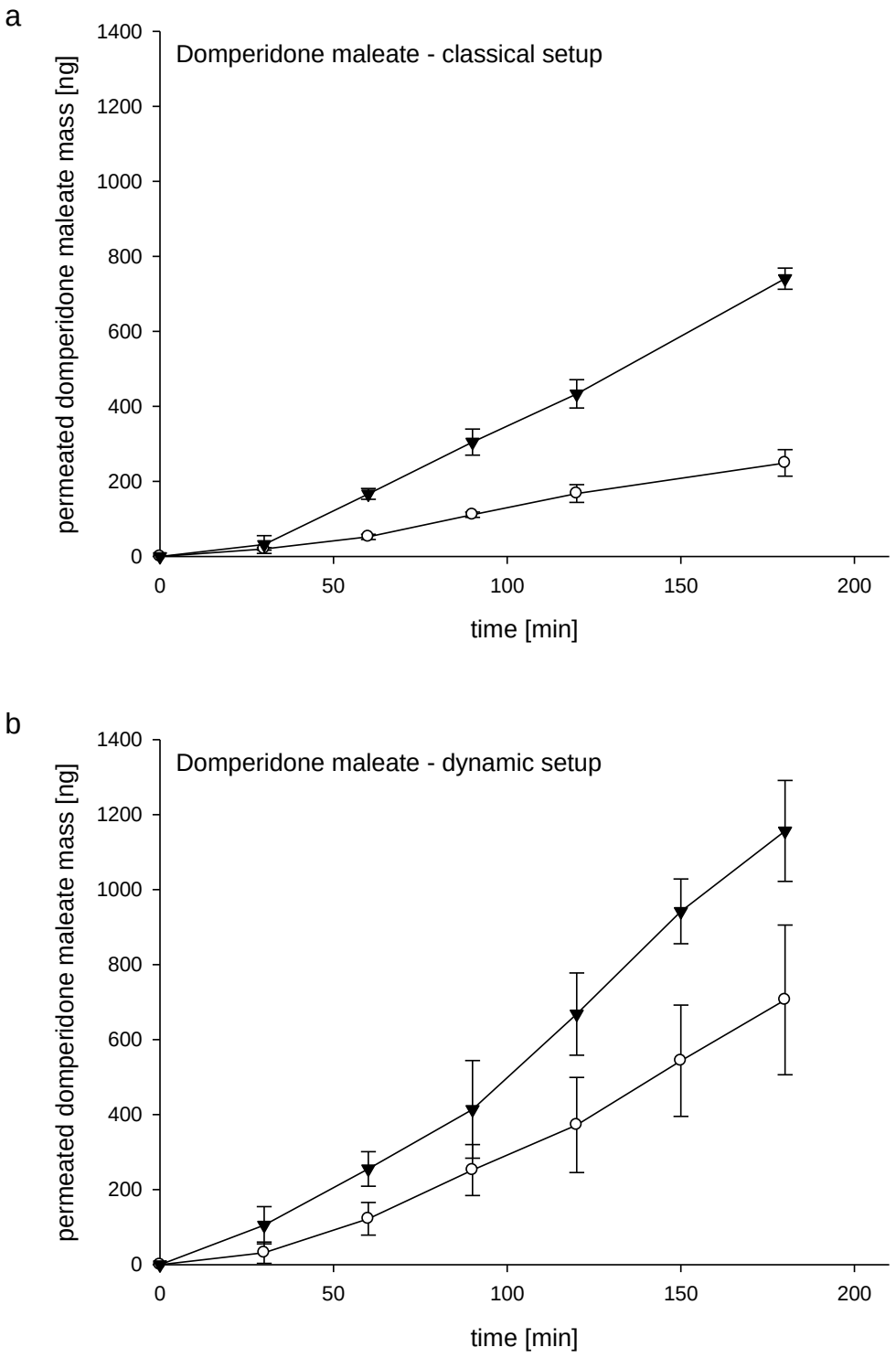

Figure 2.5. Permeated mass of domperidone maleate in a classical transport experiment (a) and in the FTPC (b). Experiments were performed without TPGS (○) and with 0.01 % (▼) TPGS. Data are presented as mean ± SD (n ≥ 3).

2.3.5 Talinolol

As well as for domperidone, experiments with talinolol were only performed without and with 0.01 % TPGS. Figure 2.6 shows the permeated mass of talinolol under classical static and dynamic flow conditions. While for the classical setup a significant difference between the permeated masses after 180 min was found, this could not be found in the FTPC. The P_{app} values summarized in Table 2.6 also confirm this result. Therefore, for talinolol the FTPC was not able to distinguish between non-inhibition and inhibition of P-gp, which was possible in a classical static setup. In comparison to the classical static setup, the results from the FTPC show higher standard deviations, thus preventing the occurrence of a statistically significant difference. Consequently, talinolol does not qualify for further investigation with tablets in the d/p-system.

Table 2.6 Overview of P_{app} values for talinolol. Data are presented as mean ± SD (n ≥ 3). Data marked with * are significantly different from P_{app} values without TPGS (t-test, p ≤ 0.01).

Addition of TPGS	P_{app} classical setup [*10^{-6} cm/s]	P_{app} FTPC [*10^{-6} cm/s]
Without	0.45 ± 0.13	1.50 ± 0.42
0.01 %	0.92 ± 0.19*	2.08 ± 0.63

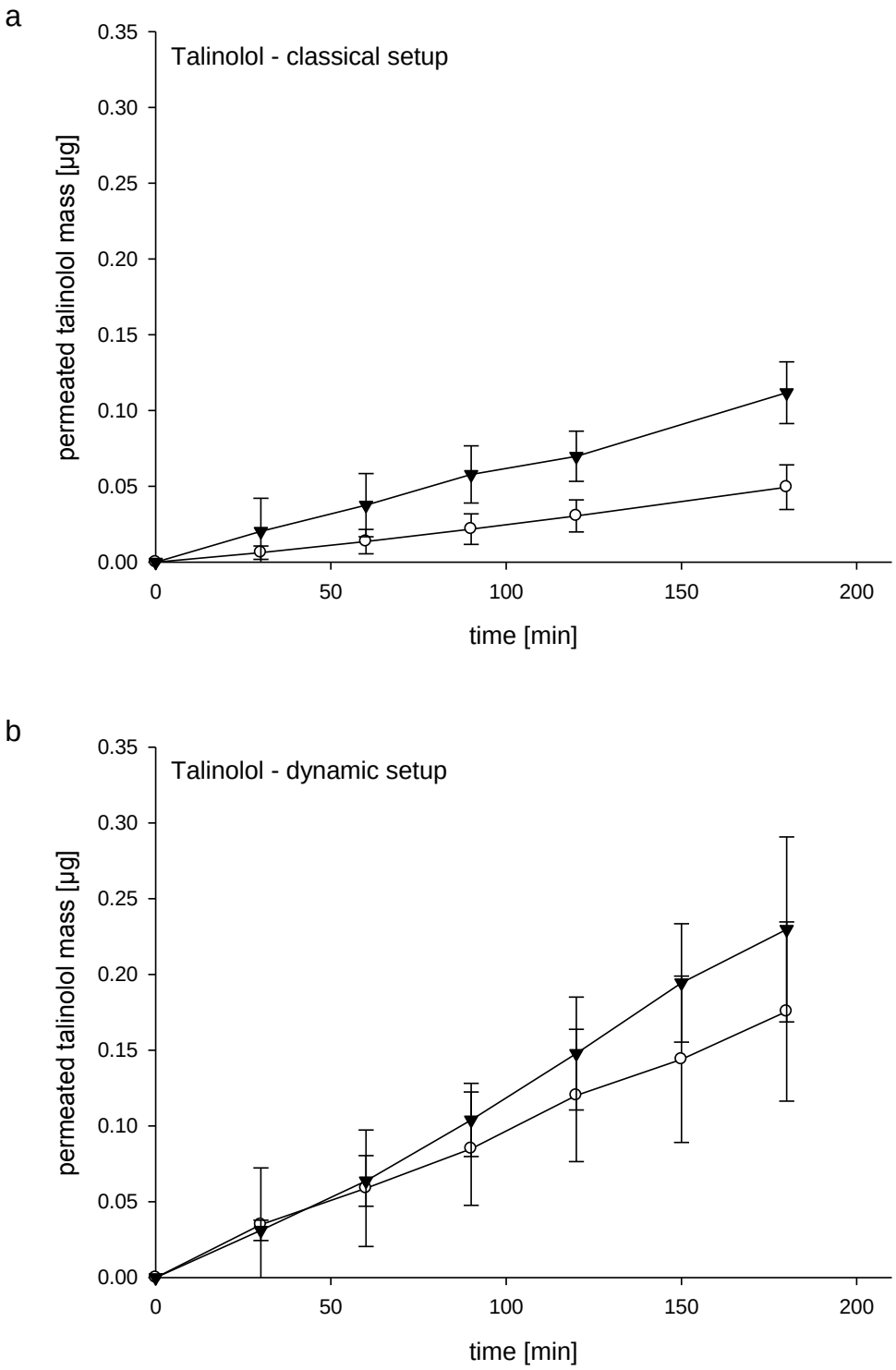

Figure 2.6. Permeated mass of talinolol in a classical transport experiment (a) and in the FTPC (b). Experiments were performed without TPGS (○) and with 0.01 % (▼) TPGS. Data are presented as mean ± SD (n ≥ 3).

2.3.6 Comparison of inhibition ratios

Generally the influence of efflux inhibitors is calculated according to equation 3 [21].

$$efflux\ ratio\ = \frac{P_{app\ (B\rightarrow A)}}{P_{app\ (A\rightarrow B)}} \qquad \text{(eq. 3)}$$

For the substances selected for investigation in the current work, high efflux ratios are described in the literature. For example, an efflux ratio of 15 to 36 has been described for domperidone [74].

In light of the intended purpose of the apparatus, only data for the absorptive transport (A→B) and not for the secretory transport (B→A) are available. This hinders the calculation of an efflux ratio. Therefore, for a better comparison of the obtained results, the inhibition ratio of 0.01 % TPGS was calculated according to equation 2 (Chapter 2.2.8) (Table 2.7). When considering all substances, the inhibition ratios are in the range between 1.6 and 3.1 for the classical static setup. For experiments in the FTPC the ratios show less variation, but are in accordance with the ratios obtained in the classical setup. Furthermore, for furosemide a ratio of approximately 1 was found in the FTPC indicating that there is no difference in the P_{app} values. Therefore, the FTPC is less sensitive in the detection of permeation differences caused by inhibition of P-gp. As mentioned previously, this might be due to the higher standard deviations of the results. The greatest inhibition ratios in the FTPC were found for domperidone maleate and domperidone, being the only substances with a significant difference in the P_{app} values in the classical static setup as well as in the FTPC.

Table 2.7. Comparison of inhibition ratio with 0.01 % TPGS.

Substance	Classical static setup	FTPC
Furosemide	1.62	0.94
Rhodamine 123	1.71	Not tested
Domperidone	1.65	1.43
Domperidone maleate	3.11	1.54
Talinolol	2.04	1.34

For better comparison of the obtained data with the literature, the inhibition ratios for results with rhodamine 123 and digoxin described in the literature [75] were calculated (Table 2.8). The literature ratios are within the range of the ratios found in this study. Especially the ratio for rhodamine 123 is comparable to the result from the literature confirming the found results.

Table 2.8. Inhibition ratios calculated from literature data [75]. Data were obtained in a classical static setup (absorptive direction) with TPGS or CysA as inhibitor.

Substance	Inhibition Ratio
Rhodamine 123, 13 µM	1.86 (with 33 µM TPGS ≙ 0.005 %)
	2.22 (with 15 µM CysA)
Digoxin, 1 µM	1.88 (with 33 µM TPGS ≙ 0.005 %)
	2.20 (with 15 µM CysA)

2.4 Conclusion

The selection test of different P-gp substrates showed that the effect of P-gp inhibition could not be detected *in vitro* easily especially when focusing on the absorptive transport direction. Furthermore, the FTPC was not always able to detect a difference in P_{app} values for all tested substances even if they showed a difference under classical static conditions. As domperidone maleate efflux inhibition was obvious in the classical transport setup as well as in the d/p-system, it is selected for further investigation of the onset-dynamics of TPGS as a P-gp inhibitor, which includes the evaluation of the effects of the inhibitor and the formulation on drug dissolution as well as permeation. Such an investigation requires the manufacturing of tablets. The results of this further examination are described in Chapter 3.

3 Feasibility of determining the effect of excipients in the d/p-system using tablets

Statement of authorship contribution:

The following author contributed to this chapter:
Sandra P. Gantzsch, Ulrich F. Schaefer, Claus-Michael Lehr, Co-operation partners from Sanofi-Aventis
The author of the thesis made the following contribution to this chapter.

1. Design of the project including formulation of problems to be tested and design of individual experiments:
   Contributed significantly

2. Planning of experiments and design of methods to answer the problems posed under # 1 including choice and development of the methods:
   Contributed significantly

3. Performance of experiments and data analysis:
   Essentially performed this study independently

4. Presentation, interpretation and discussion of the results obtained in article form:
   Essentially performed this study independently

3.1 Introduction

As described in Chapter 2, the pretest of the effect of P-gp inhibitors on the permeation of drugs using stock solutions of API and inhibitor show small increases in permeation in the apical to basolateral direction. Domperidone maleate in combination with TPGS was chosen for further investigations as an oral dosage form in the d/p-system, as this drug demonstrated the greatest effect of TPGS-induced P-gp inhibition on permeation in both classical and dynamic setups. Therefore, immediate release tablets (IR tablets) with domperidone maleate were manufactured using direct compression.

3.2 Materials and methods

3.2.1 Materials

Domperidone maleate was purchased from Transo-Pharm (Siek, Germany) and Kolliphor® TPGS was from BASF (Ludwigshafen, Germany). CapsuLac® 60 (lactose) was a kind gift from Meggle (Wasserburg, Germany), Microcell MC-102 (microcrystalline cellulose, MCC) was a kind gift from Lehmann & Voss & Co. (Hamburg, Germany), Kollidon CL was from BASF (Ludwigshafen, Germany), Aerosil 200 was from Degussa (Frankfurt, Germany) and Mg-stearate was from Fagron (Barsbuettel, Germany). All tablet excipients were of Ph. Eur. grade. All buffer reagents were purchased from Sigma-Aldrich (Steinheim, Germany) and were of cell culture tested grade. KRB was prepared as described in Chapter 2.2.4.

3.2.2 Cell culture

Cell culture was performed as described in Chapter 2.2.2.

3.2.3 TEER measurement

TEER was determined as described in Chapter 2.2.3.

3.2.4 Preparation of tablets

IR tablets with domperidone maleate were manufactured using direct compression. Ingredients were sieved (mesh size 1400 µm), blended in a turbula mixer (type T2C, Willy A. Bachofen AG Maschinenfabrik, Basel, Switzerland) for 5 min (25 rpm) and subsequently compressed using a Korsch EK 0 eccentric tablet press (Berlin, Germany) resulting in the production of tablets of mass 150 mg. Table 3.1 shows the composition of the tablets. Furthermore, tablets containing the API and the P-gp inhibitor TPGS were prepared as follows. TPGS was dissolved in ethanol and then granulated with lactose via wet granulation using a sieve (mesh size 1400 µm). Subsequent to sieving, the wet granulate was dried at room temperature for one day. Shortly before compressing, the remaining ingredients were added freshly sieved and were blended for 5 min in a turbula mixer, as described previously.

Table 3.1. Composition of domperidone maleate tablets

	Without inhibitor	With inhibitor
Domperidone maleate	10 %	10 %
TPGS	-	10 %
Lactose (CapsuLac® 60)	60 %	50 %
MCC (Microcell MC-102)	27 %	27 %
Kollidon CL	1 %	1 %
Aerosil 200	1 %	1 %
Mg-stearate	1 %	1 %

3.2.5 Characterization of tablets

Crushing strength was determined with the Erweka hardness tester type TBH 30 (Heusenstamm, Germany) and disintegration time was measured using the Sotax disintegration tester type DT 2 (Basel, Switzerland). Ten or six tablets were tested in each of these setups, respectively.

Content of tablets was tested by dissolving a tablet in 5.0 ml DMF by means of ultrasonication and filling up to 1000.0 ml with KRB followed by further ultrasonic treatment. Then, the solution was filtered through a cellulose acetate filter (pore

size 0.2 µm). The concentration was determined via HPLC. Three tablets were tested.

3.2.6 Combined dissolution and permeation experiment in the d/p-system

All experiments were performed with the d/p-system as it is described in Chapter 1.3 and depicted in Figure 1.2 using two tablets.

The dissolution module consisted of a flow through dissolution cell (USP apparatus 4, Sotax CE1, Sotax, Lörrach, Germany), whereas the permeation module consisted of a custom-made flow through permeation cell (FTPC). In the dissolution module the flow rate was set to 6.5 ml/min and in the permeation module to 1.0 ml/min. All streams were driven by membrane dosage pumps of type Stepdose 03® (KNF Neuberger, Freiburg, Germany) in combination with a pulsation absorber. The dissolution and permeation cells were submersed in a water bath at 37.0 °C.

The SIA system for automatically sampling consisted of the FIALab 3500 (FIALab instruments, Bellevue, USA) composed of a 2.5 ml piston pump and an eight port valve. Furthermore, the d/p-system consisted of an autosampler (Cetac ASX 260, Omaha, USA), the fluorescence detector PMT-FL (FIALab instruments, Bellevue, USA), a D 2000 light source and an USB 2000 UV-VIS spectrometer (Ocean optics, Dunedin, USA) and a 0.5 ml piston pump combined with a six valve port (FIALab instruments, Bellevue, USA).

Samples were collected automatically at sampling port D as indicated in Figure 1.2 (representing the dissolution process), A (representing the amount appearing in the apical compartment of the FTPC) and B (representing the amount permeated into the basolateral compartment of the FTPC) using the SIA module.

The system operated with FIAlab software for Windows® version 5.9.192 (FIALab instruments, Bellevue, USA).

The program codes for the respective substance and sampling ports are given in Chapter 10.2 in the annexes.

Prior to each experiment and mounting in the FTPC, Caco-2 cell monolayers were washed twice with KRB and equilibrated in KRB for 30 min in an incubator.

KRB was used both as a dissolution and permeation medium.

3.2.7 Quantification of drug substances

The concentration of substance at sampling ports D and A was determined by online detection using the SIA system. UV-absorbance at 285 nm was used for the online detection of domperidone maleate.
The concentration of substance in the basolateral compartment at each sampling time point was determined via HPLC. For further details of the quantification method see Chapter 10.1 in the annexes.

3.3 Results and Discussion

3.3.1 Characterization of domperidone maleate tablets

The determined properties of the tablets are summarized in Table 3.2.

Table 3.2. Properties of domperidone maleate tablets. Data are presented as mean ± SD (n ≥ 3).

	Without inhibitor	With inhibitor
Mass	149 ± 1 mg	150 ± 3 mg
Crushing strength	42 ± 5 N	26 ± 4 N
Disintegration time	14.3 ± 2.3 s	11.4 ± 3.5 min
Content domperidone maleate	16.99 ± 0.4 mg	16.52 ± 0.4 mg
Content TPGS	-	16.97 ± 0.2 mg

Although TPGS was granulated before compression for an easier handling, a sticking of the compounds could not be completely avoided. This resulted in a longer tablet disintegration time, as seen in Table 3.2. Therefore, the release of domperidone maleate from tablets with TPGS may be hindered and extended compared to tablets without TPGS.

3.3.2 Effect of TPGS on dissolution and permeation of domperidone maleate

The dissolution profiles of domperidone maleate tablets both without and with additional TPGS are shown in Figure 3.1. As already stated in the previous

chapter (3.3.1), the disintegration time of tablets with TPGS is longer than that of tablets not containing TPGS, which may lead to a comparatively extended release of TPGS-containing tablets. Indeed, tablets with TPGS show a lower maximum concentration and a longer release time. This does not completely confirm the assumption of an extended release but it is in accordance with the slower disintegration time.

By using two tablets at the same time, the concentration of domperidone maleate at sampling port A fitted to the dissolution data. Due to the longer release time the concentration at the apical side of the FTPC stays also longer at a higher level for TPGS containing tablets. Furthermore, there is a time shift of C_{max} as well as lower measured concentrations at sampling port A compared to port D, which can be explained by the construction of the d/p-system. These effects are a result of the spatial separation of dissolution and permeation modules, which are connected by tubes and a stream splitter as described by Motz et al. [32].

The dissolution profile of tablets with TPGS shows a wavelike pattern with small maximum peaks. This might be due to the hindered release of domperidone caused by the TPGS sticking. Furthermore, an encapsulation of API in TPGS micelles followed by a gradual release could possibly occur.

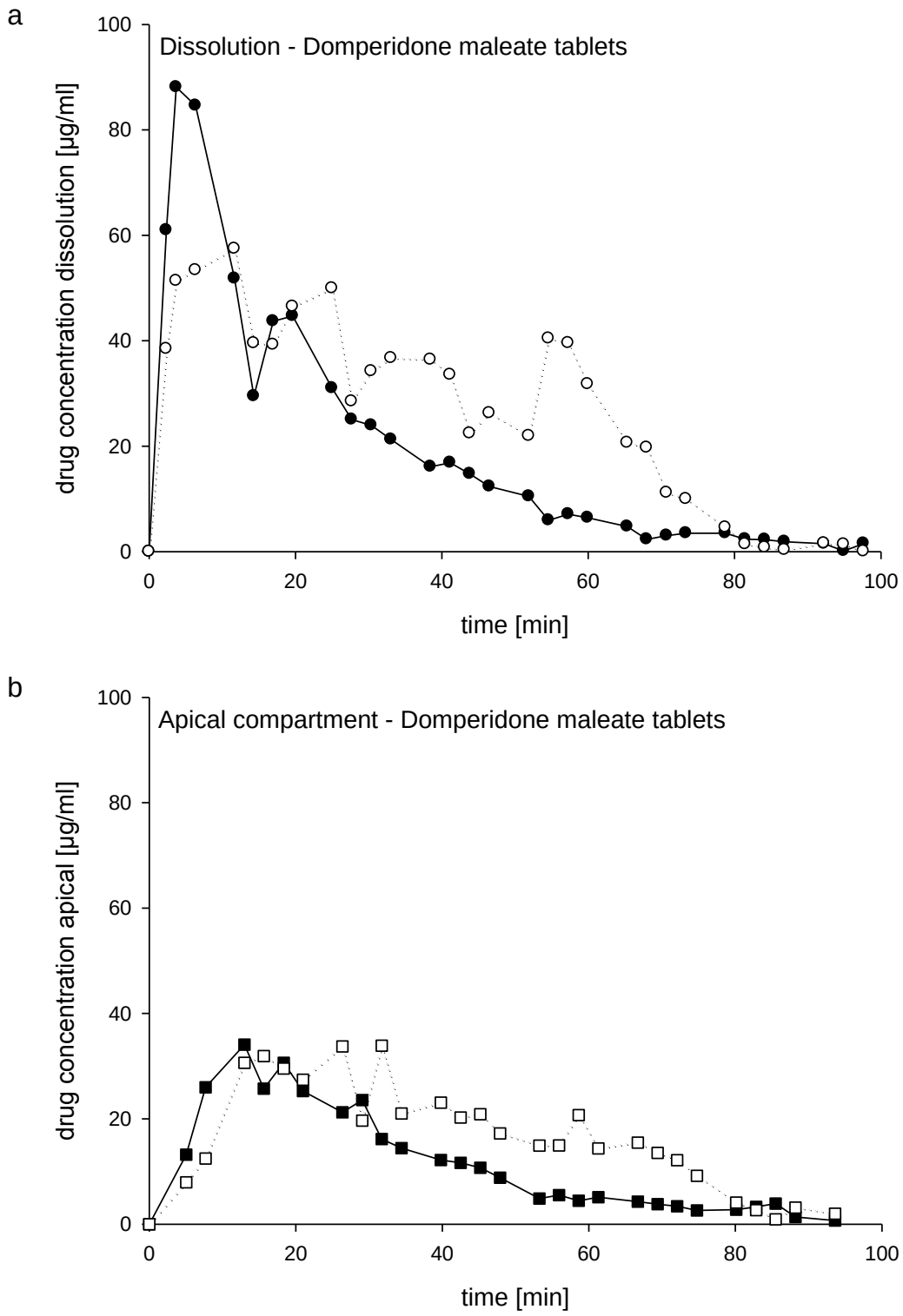

Figure 3.1. Concentration time trends for domperidone maleate tablets at sampling port D (a) and A (b) using 2 tablets. Closed symbols (●, ■) represent tablets without TPGS and open symbols (○, □) represent tablets with TPGS. For the sake of clarity, data are presented as mean values (n ≥ 3) without SD.

The permeation profiles of tablets in the absence and presence of TPGS are almost identical fitting with the concentrations measured at the apical side, which are also similar for both dosage forms (Figure 3.2). Even though the permeated mass after 240 min is slightly higher for the TPGS containing tablets, the difference is not significant (t-test, $p \leq 0.01$). Therefore, the expected inhibitory effect as predicted from the previous experiment with donor solutions cannot be found. Comparing the concentrations of drug present during the experiments, a concentration of about 40 µg/ml was achieved utilizing tablets as compared to stock solutions of 10 µg/ml. It is therefore possible that the efflux transporter is saturated using tablets and even without inhibitor a greater amount of drug remains at the basolateral side. Furthermore at higher donor concentrations, the same secreted amount has a lower weighting. Moreover, the inhibition of P-gp requires a certain pre-incubation time in order for the inhibitor to develop its full potential [76]. The occurrence of such a pre-incubation may have been hindered in the current studies due to the release kinetics of TPGS from the tablets. Therefore, the excipient may have no influence on the permeation in this study. A further possible reason for the found results might be the contact time of TPGS with the cell monolayer. TPGS is a hydrophilic substance and therefore does not have such a high affinity to cells. Due to the flow in the FTPC the contact time is limited and might be too short for TPGS to develop the full effect especially when it is not present in a constant concentration as it was the case for the previous study with drug solutions. A reduction of the flow rate in the FTPC should be tested to verify this.

Unfortunately, the release and the concentration of TPGS present cannot be measured within the d/p-system. Due to the SIA detection mechanism and a missing separation column, online detection is not possible. Different attempts were undertaken to determine the TPGS concentration offline by means of HPLC. A bottling of samples at sampling port D and A was successfully achieved. Nevertheless, a determination of TPGS at these sampling points was not possible. This might be caused by the occurrence of TPGS concentrations below the detection limit of the HPLC method.

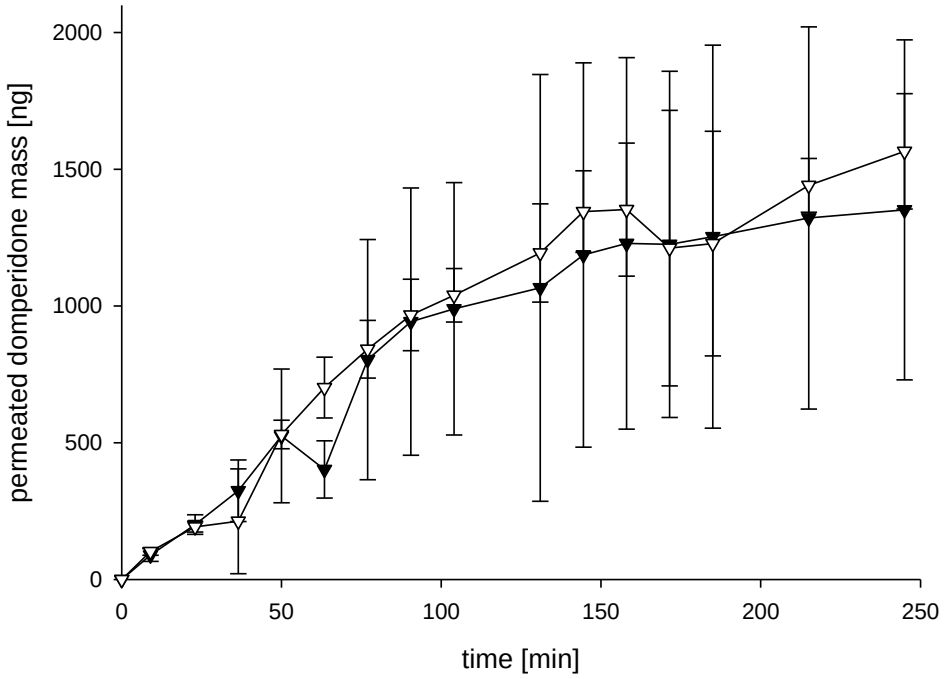

Figure 3.2. Permeated mass of domperidone maleate in the FTPC using 2 tablets. Closed triangles (▼) represent tablets without TPGS and open triangles (▽) tablets with TPGS. Data are presented as mean ± SD (n ≥ 3).

With respect to the tablets used in the current study, the presence of TPGS has an obvious effect on the dissolution of domperidone maleate but the effect on the permeation cannot be stated clearly. For that, further investigation using differing approaches would be valuable. Firstly, a preparation of tablets with very similar dissolution profiles would be necessary. Due to the physical behavior of TPGS and the occurrence of sticking during tablet compression, a similar dissolution profile to that exhibited by the TPGS-containing tablets could be achieved by the formulation of an extended release tablet without TPGS. The components of such a tablet would need to be granulated with a substance such as Eudragit® in order to achieve an extended release. Secondly, a formulation with an initial burst release of TPGS followed by a constant release of domperidone and TPGS could be considered as a means to provide a satisfactory pre-incubation period in which TPGS can interact with cells before exposure to the drug occurs. Another option which would not require a change in the formulation would be to add TPGS to the dissolution medium when using tablets without inhibitor. This approach could potentially resolve the release difficulties as well as the matter of contact time.

However, in spite of the promise of each of these described approaches, the identification and evaluation of an effect of TPGS on the permeation of P-gp substrates in the FTPC using solid oral dosage forms will be difficult due to the low concentration differences in the basolateral compartment of the FTPC.

3.4 Conclusion

The addition of TPGS to solid dosage forms leads to a different release profile of domperidone maleate. The permeation results obtained in initial work with stock solutions differ from those found here with the produced and tested tablets. The permeation of domperidone is not enhanced under inhibition of P-gp. Therefore, it cannot be stated clearly if the d/p-system is able to detect excipient effects on efflux systems such as P-gp when using solid oral dosage forms. Further investigations with improved formulations should be performed.

4 Development and characterization of a lipid-coated membrane for the d/p-system

Parts of this chapter are prepared for submission as journal article:

"Characterization and evaluation of lipid-coated membranes in comparison to Caco-2 cell monolayers for combined dissolution and permeation testing"

Statement of authorship contribution:

The following author contributed to this chapter:
A: Development of coating: Sandra P. Gantzsch, Ulrich F. Schaefer, Claus-Michael Lehr, Co-operation partners from Sanofi-Aventis
B: Raman microscopy: Sandra P. Gantzsch, Birthe Kann, Maike Windbergs, Ulrich F. Schaefer, Claus-Michael Lehr
The author of the thesis made the following contribution to this chapter.

1. Design of the project including formulation of problems to be tested and design of individual experiments:
    A: Contributed significantly
    B: Contributed significantly

2. Planning of experiments and design of methods to answer the problems posed under # 1 including choice and development of the methods:
    A: Contributed significantly
    B: Contributed significantly

3. Performance of experiments and data analysis:
    A: Essentially performed this study independently
    B: Contributed in collaboration

4. Presentation, interpretation and discussion of the results obtained in article form:
    A: Essentially performed this study independently
    B: Contributed significantly

4.1 Introduction

As already described in Chapter 1.2, the determination of permeability is mostly performed using cell based *in vitro* assays like the Caco-2 cell monolayer. Due to different drawbacks of cellular models like long cultivation times or incompatibility with some dissolution media, non-cellular *in vitro* assays known as PAMPA were developed. These lipid-based permeation models have the potential to overcome some of the cell-associated disadvantages. A transfer of this approach to the d/p-system appeared favorable to widen the field of application, especially to extend the time period to investigate dissolution and permeation of e. g. oral retard formulations. Furthermore, a transfer might contribute to a wider range of used dissolution and permeation media like simulated intestinal fluids (FaSSIF and FeSSIF). For a better comparability with Caco-2 cell monolayers, a change of the FTPC should be avoided. Consequently, the best opportunity seemed to be the coating of the same permeable support which is used for cell culture.

As a first clear step in development of a lipid-based permeation model, the aim of this study was to find a suitable lipid and coating procedure for a lipid-coated membrane, which could be used not only in a classical static permeation setup but also under dynamic flow conditions in the FTPC. Looking at the published PAMPA and PAMPA-like approaches a variety of lipids can be found, including lipids of natural origin like lecithin, as well as synthetic lipids such as DOPC. Initially, this study focused on the use of DOPC. As this lipid is produced synthetically, it always offers the same composition independent of the batch. Therefore, it holds promise for facilitating the generation of highly reproducible results. As an alternative, Lipoid E 80 (purified yolk lecithin) was taken. A combination of this lipid with cholesterol dissolved in n-octanol was described by Corti et al. [49] for the use in a closed system under flow conditions. Furthermore, Lipoid E 80 was used by Flaten et al. [51] for the coating of a membrane without use of organic solvent.

In a second step after defining a final coating procedure, an adequate physical characterization and evaluation of the lipid-coated membrane as well as the fabrication process was vital before starting further transport experiments.

The all-encompassing analysis of this model consisted of three aspects:

1) An analysis of the blank membrane, being the supportive layer for the coating, was required. Thereby, a special focus was placed on the pore morphology as drug substances primarily pass the membrane through the pores during transport experiments.
2) An extensive investigation of the physical lipid behavior on the membrane, including coating assembly, and within the pores was deemed necessary.
3) An overall evaluation of coating integrity after permeation experiments or exposure to dissolution medium was of vital importance. For API permeation studies a sufficient robustness of the coating against media is mandatory and therefore, needed to be evaluated.

For analyzing the above mentioned aspects the following techniques were used.

1) As a first attempt to specially characterize the stability of the coating throughout an experiment, TEER measurement was used as a fast and simple method. This method is particularly used to control the integrity of cell monolayers. A decrease of the TEER value is associated with a loss of barrier integrity. Furthermore, in previous work the d/p-system was complemented with a tool for online TEER measurement [34], which makes this approach favorable for the evaluation also of the integrity of lipid-based artificial permeation barriers.
2) As basic and well-established methods, light microscopy as well as scanning electron microscopy (SEM) were utilized for the characterization of the membrane and the coating. Especially SEM requires previous sample preparation, such as cutting the coated membrane which could lead to disruption of the coating integrity due to shear stress. A possibility to circumvent this risk is the use of confocal fluorescence microscopy. This technique necessitates labeling of the membrane and the lipid to discriminate between the two components, which could cause artifacts and changes in the coating. Flaten et al. has used this technique to visualize lipid-filled pores in an artificial membrane model [52].
3) As optical discrimination of the lipid coating and the membrane is limited by nearly the same color of the two components, a non-destructive, label-free and chemically selective technique appeared favorable for the

characterization of the lipid-coated membrane. Therefore for further characterization, confocal Raman microscopy was selected. It is a complementary technique to the well-established infrared spectroscopy relying on light scattering. In pharmaceutical research it has a broad variety of applications and has already been used for the investigation of drug distribution, drug release in solid dosage forms and implants, as well as for lipid detection [77-81].

The lipid-coated membrane shows a highly structured and rough surface due to the coating procedure. Therefore, the surface characterization by confocal Raman microscopy is hindered as spectra are recorded from the focal plane and the surface would crisscross numerous focal planes. Circumventing this limitation, optical profilometry as an additional technique to confocal Raman microscopy was performed. Optical profilometry is based on scattering of white light. The white light is focused on the sample by a probe, which also collects the backscattered photons. White light is composed of different wavelengths, each representing a unique color and a specific distance. Through a pinhole only the color in focus is detected. Therefore, exact information about the distance between sample and probe is given at a defined position of the sample. Subsequently, this information can be translated into topographic height differences leading to a profilometric image of the surface. This technique has already been used for diverse applications in surface analysis [82-84] and can be adapted for pharmaceutical research [85, 86].

The characterization using confocal Raman microscopy was performed in cooperation with Birthe Kann and Maike Windbergs. The experiments were conducted by Birthe Kann.

4.2 Materials and methods

4.2.1 Materials

DOPC (dioleoylphopsphatidylcholine) and Lipoid E 80 (egg phospholipids with 80 % phosphatidylcholine) were purchased from Lipoid GmbH (Ludwigshafen, Germany). Propranolol HCl and furosemide (Synopharm GmbH & Co KG,

Barsbuettel, Germany), atenolol and sodium fluorescein (Sigma-Aldrich, Steinheim, Germany) served as test model substances. All reagents for HPLC quantification were obtained from Sigma-Aldrich (Steinheim, Germany) and were of HPLC gradient grade. High purity water was prepared by a Millipore Milli-Q Synthesis system (Merck Millipore, Darmstadt, Germany). Transwells® type 3460 were purchased from Corning Inc. (Acton, MA, USA). All buffer reagents were purchased from Sigma-Aldrich (Steinheim, Germany) and were of cell culture tested grade. KRB was prepared as decribed in Chapter 2.2.4.

4.2.2 Simulated intestinal fluid

FaSSIF and FeSSIF were prepared using Phares SIF powder (Muttenz, Switzerland) dissolved in the appropriate buffer. The composition of both media can be found in Table 4.1.

Table 4.1. Composition of simulated intestinal fluids.

	FaSSIF (1 l)	FeSSIF (1 l)
Buffer:		
NaOH	0.348 g	4.04 g
$NaH_2PO_4*H_2O$	3.954 g	-
NaCl	6.186 g	11.874 g
Glacial acetic acid	-	8.65 g
SIF Powder	2.24 g	11.2 g
Equals:		
Sodium taurocholate	3 mM	15 mM
Lecithin	0.75 mM	3.75 mM
pH	6.5	5.0

4.2.3 Pretest setups for the selection of a lipid and a coating procedure

As a first step for the development of the lipid-coated membrane, different pretests were performed to select a lipid, as well as a coating procedure which would lead

to a robust and stable coating. Therefore, the setups listed in Table 4.2 were tested for their suitability to obtain a dense coating which is resistant against media for a time period of about 18 h especially in the FTPC.

Table 4.2. Pretest setups for the selection of a lipid and a coating procedure

Setup	Lipid 1	Lipid 2	Coating method
1	DOPC (2 % w/v) dispersed in dodecane	-	A (Sedimentation)
2	DOPC (4 % w/v) dispersed in water	-	A (Sedimentation)
3	DOPC as liposomes	-	B (Centrifugation)
4	-	Lipoid E 80 as liposomes	B (Centrifugation)

Two coating methods were tested:

A: An amount of 100 µl lipid dispersion was added to the apical side of a Transwell®. After 30 min the dispersion was removed and the Transwell® was dried at 37 °C in an oven for approximately 20 min. The procedure was repeated several times in order to produce Transwells® with one, two, five, ten or 20 coating layers.

B: An amount of 100 µl lipid dispersion was added to the apical side of a Transwell®. Then the Transwell® was centrifuged (Centrifuge Universal 32R, Hettich, Tuttlingen, Germany) for four minutes at 2090 rpm (equal to 600 g). Subsequently, the supernatant was removed and the Transwell® was dried at 37 °C in an oven for approximately 20 min. The procedure was repeated several times. At the end Transwells® with one, five or ten coating layers were available.

4.2.4 Preparation of liposomes

DOPC liposomes as well as liposomes made of Lipoid E 80 were prepared using the film method. The respective lipid (1 g) was dissolved in a mixture of methanol and ethyl acetate (4:1 v/v, 6 ml) in a round bottom flask (250 ml). Under reduced

pressure (2 h: 200 mbar, 30 min: 40 mbar) the solvent was evaporated at 55 °C (Rotavapor R-205, BÜCHI Labortechnik GmbH, Essen, Germany). Phosphate buffered saline (PBS, 6 ml; composition: 129 mM NaCl, 2.5 mM KCl, 7.07 mM Na_2HPO_4 * 7 H_2O, 1.3 mM KH_2PO_4, pH 7.4) was used to rehydrate the phospholipid film. The dispersion was filtered 10 times through a polycarbonate filter (pore size 800 nm, Millipore) to obtain a narrow size distribution of liposomes.

4.2.5 Characterization of liposomes

Hydrodynamic diameter was measured using dynamic light scattering (DLS) (Zetasizer Nano ZS, Malvern Instruments, UK) and zeta potential was determined using laser doppler micro-electrophoresis (Zetasizer Nano ZS, Malvern Instruments, UK).

4.2.6 TEER measurement

TEER was determined as described in Chapter 2.2.3.

4.2.7 Light microscopy

Light microscopy images were recorded with a Zeiss Axio Vert.A1 microscope (Carl Zeiss AG, Oberkochen, Germany) connected with an AxioCam ERc5s camera running on ZEN 2011 software. The system was equipped with a 32-fold magnifying objective (Zeiss N.A. = 0.45).

4.2.8 Scanning electron microscopy

For characterization of the liposomes, the lipid dispersion was diluted with water and dried at room temperature. For characterization of the (lipid-coated) membrane, the membrane was cut out of the Transwell® holder. Afterwards, all samples were sputter coated with gold.
Images were recorded by scanning electron microscopy (Zeiss EVO HD 15, Carl Zeiss AG, Oberkochen, Germany) at an accelerating voltage of 5 kV.

4.2.9 Raman microscopy

A confocal Raman microscope WITec alpha 300R+ (WITec GmbH, Ulm, Germany) equipped with 50-fold magnifying objectives (Zeiss N.A. = 0.8; Olympus N.A. = 0.35) was used to collect Raman spectra at an excitation wavelength of 532 nm (10 mW, Nd:YAG Laser) or 785 nm (diode laser, Toptica) without further sample preparation. The diode laser power was set to 50 mW (xz – scans) or 65 mW (xy – scans). The respective integration times and resolutions as well as the directions of record are summarized in Table 4.3 for each characterization purpose.

Table 4.3. Summary of imaging settings for the different purposes

Purpose	Direction of record	Integration time	Resolution
Pore morphology (cross section)	x- and z-axis	0.3 s	0.5 µm
Stacked images of pores	x- and y-axis	0.15 s	0.2 µm per pixel 0.5 µm between focal planes
Coating procedure (entire surface)	x- and y-axis	4 s	100 µm² per pixel
Coating thickness (cross section)	x- and z-axis	0.7 s / 0.5 s	5 µm² per pixel 100 µm² per pixel (entire cross section)

Interpretation and differentiation of the recorded data was done with complete spectra without selecting only specific peaks. Using the software WITec Project Plus, the recorded Raman spectra were converted into false color images. The lipid Lipoid E 80 is represented in blue, whereas the polyester membrane is depicted in red color.

For the evaluation of pore morphology, pores were selected randomly and were distributed equally across the membrane. At least three individual Transwells® were investigated.

4.2.10 Optical profilometry

Surface topography profiles were acquired by optical profilometry using a WITec alpha 300R+ without any sample preparation. The integration time was set to 0.02 s. Topography profiles have the same geometric dimension as respective Raman images and a concordant image point resolution of 100 µm x 100 µm.

4.2.11 Classical static transport experiments

To test the membranes for suitability in permeation experiments, classical static transport experiments were done with a high permeability marker (propranolol 100 µg/ml) and low permeability markers (furosemide 400 µg/ml, sodium fluorescein 5 µg/ml and atenolol 1.33 µg/ml). The general conditions for the classical static transport experiments were the same as described in Chapter 2.2.5, with Caco-2 cells as permeation barrier being replaced by lipid-coated Transwells® without pre-incubation prior to the experiment.

4.2.12 Stability test in medium

The stability of the coating in the presence of medium was tested with KRB, FaSSIF or FeSSIF in the FTPC. Flow rate was adjusted to 1.0 ml/min and experiments were performed for 18 h or 5 h.

4.2.13 Quantification of drug substances

The concentration of substance in the basolateral compartment at each sampling time point was determined via HPLC or fluorescence measurement in a plate reader. For further details of the quantification method see Chapter 10.1 in the annexes.

4.2.14 Data treatment

The P_{app} values were calculated as described in Chapter 2.2.8.
For statistical analysis t-tests ($p < 0.05$) were performed using SigmaStat integrated in SigmaPlot version 11.0 (Systat Software GmbH, Erkrath, Germany).

4.3 Results and discussion of the pretests

4.3.1 Setup 1: Coating with DOPC dispersed in dodecane using method A (sedimentation)

It was found that the estimated drying time of approximately 20 min was not sufficient for this setup. An extension of the drying time to 2-4 h for each coating step was necessary. Furthermore, it was not possible to measure the TEER value in the FTPC as the value was off-scale and so too high for the measuring instrument. Due to the long drying time and the impossibility of monitoring the barrier integrity the first setup was not examined further.

4.3.2 Setup 2: Coating with DOPC dispersed in water using method A (sedimentation)

For this setup approximately 20 min were sufficient to dry the coating. Classical static transport experiments were carried out with DOPC coated Transwells® using method A for a first estimation of the barrier properties. The permeated mass after three hours was nearly the same using a 10 or 20 times coated Transwell®. Furthermore, the change of P_{app} values of propranolol and sodium fluorescein was minimal between a 10 and 20 times coated Transwell® in comparison to the difference from a blank one. Therefore, coating the Transwell® ten times should be sufficient. As a consequence, experiments with furosemide and atenolol were performed only with a blank and a 10 times coated Transwell®. A decrease of permeated mass per area by a factor of 2.85, 25.9, 2.37 and 24.34 was reached for propranolol, sodium fluorescein, furosemide and atenolol, respectively with 10 times coated Transwells® as compared to blank Transwells®. Figure 4.1 shows the change of the P_{app} value with increasing numbers of coating steps. The P_{app} values of sodium fluorescein and atenolol decrease to a greater extent with an increase in the number of coating steps than the values of propranolol and furosemide. In light of this observation, the used substances can be divided into two groups. Propranolol and furosemide show less of a decrease of permeated mass and P_{app} values, whereas sodium fluorescein and atenolol show a greater decrease. Especially for atenolol and propranolol it can be explained by the different

hydrophobicity. According to the logP value, especially atenolol is more hydrophilic and so an increasing lipid barrier leads to slower permeation.

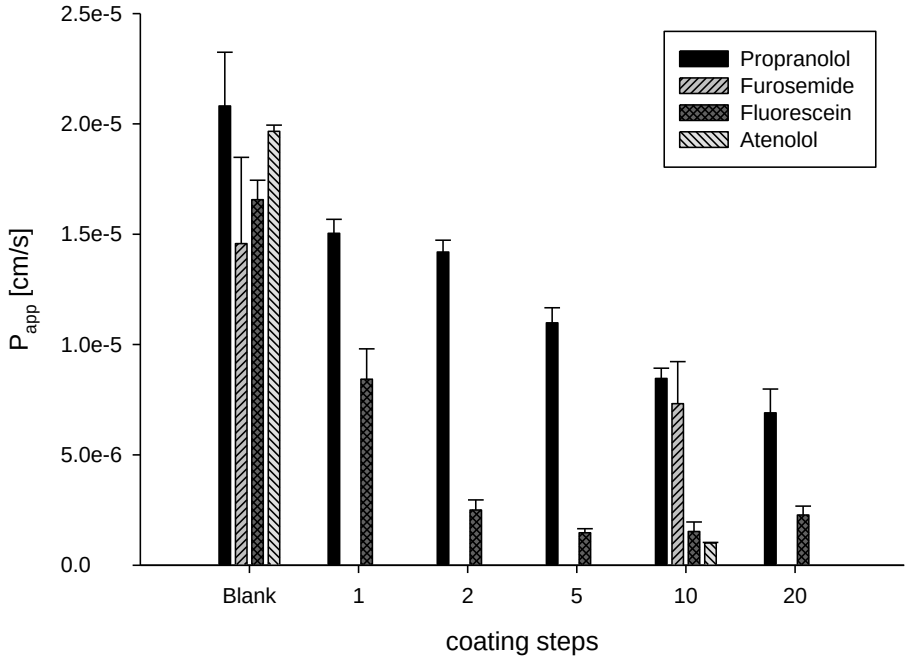

Figure 4.1. Comparison of P_{app} values of Transwells® with varying numbers of coating step in a classical static setup. Transwells® were coated with DOPC dispersed in water using method A (sedimentation). Data are presented as mean ± SD (n ≥ 3).

Before and after the classical static transport experiments (duration 180 min) the TEER of the Transwell® was measured. Table 4.4 gives an overview of the TEER values. The TEER value of Transwells® that were coated ten times was seen to be higher relative to blank Transwells® being in accordance with the P_{app} values. Surprisingly, the TEER value of 20 times coated Transwells® was lower as compared to 10 times coated Transwells®. One reason might be that the coating lost adhesion to the underlying membrane throughout the preparation.

Table 4.4. TEER values of coated Transwells® (DOPC, method A) before and after a classical static transport experiment. Data are presented as mean ± SD (n = 6).

Coating Steps	TEER before experiment [Ω*cm²]	TEER after experiment [Ω*cm²]
0 (Blank)	162 ± 7	162 ± 7
1	227 ± 16	220 ± 17
2	354 ± 20	267 ± 21
5	496 ± 95	369 ± 67
10	774 ± 19	452 ± 25
20	467 ± 79	327 ± 21

The decrease of the TEER after 180 min is probably caused by a loss of lipid on the membrane. The lipid is washed away from the Transwell® membrane, which could also be seen in agglomeration of lipid in the middle of the Transwell® during the experiment (Figure 4.2). The results indicate instability of the coating against the used medium in a classical static setup.

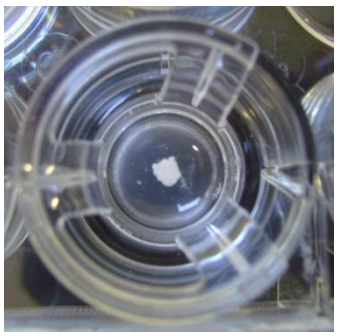

Figure 4.2. Agglomeration of lipid on a Transwell® coated with DOPC (method A) after a classical static transport experiment (180 min).

For DOPC and coating method A ten coating steps appeared to be the best considering the TEER values derived from the classical static experiments as well as the change of the P_{app} values. Therefore, the next step was to test the stability of this coating under dynamic flow conditions in the FTPC. Figure 4.3 shows the TEER value measured online in the FTPC. The TEER value decreased consistently over 9 h. Furthermore, areas without lipid coating on the membrane could be seen following the experiment by visual inspection. One reason for the

decreasing TEER value could be a slow detaching of the coating from the membrane as well as a washing off. A reason for the instability of the lipid coating in the FTPC could be the vertical orientation of the Transwell® or the constant flow of media. Therefore, the experiments were repeated without media flow and with a horizontal orientation of the Transwell®. The course of the TEER value is depicted in Figure 4.4. All conditions show a comparable course of the value with a decrease in the first hour. Neither the flow nor the orientation had an influence on the TEER value or correspondingly, on the stability of the coating. Therefore, the coating method using sedimentation in combination with the lipid DOPC did not qualify for further investigations and use in the FTPC.

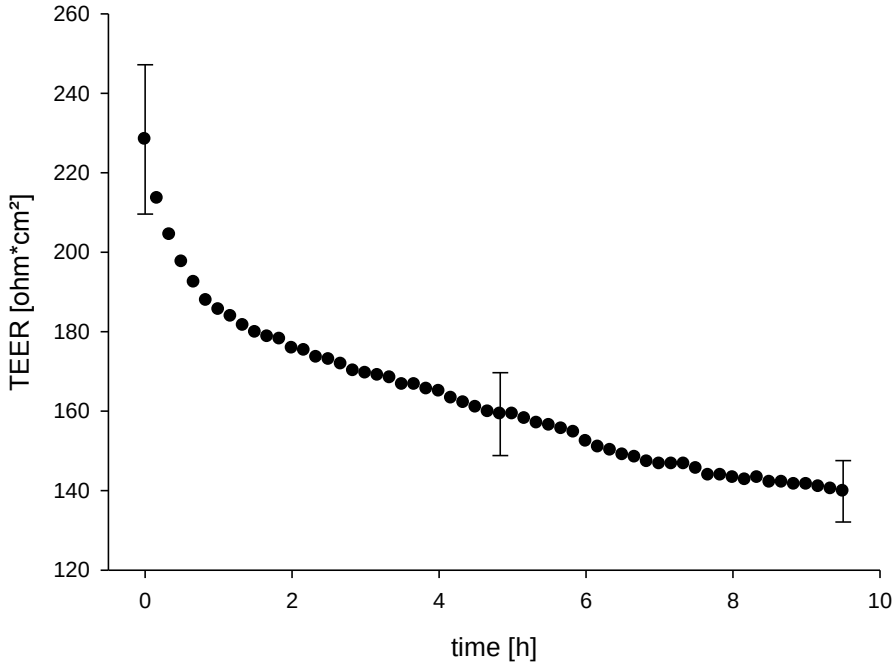

Figure 4.3. TEER value of a lipid-coated Transwell® (DOPC, method A, 10 times) in the FTPC. For the sake of clarity, only every tenth data point is presented as mean ± SE (for the starting and end point, n = 5).

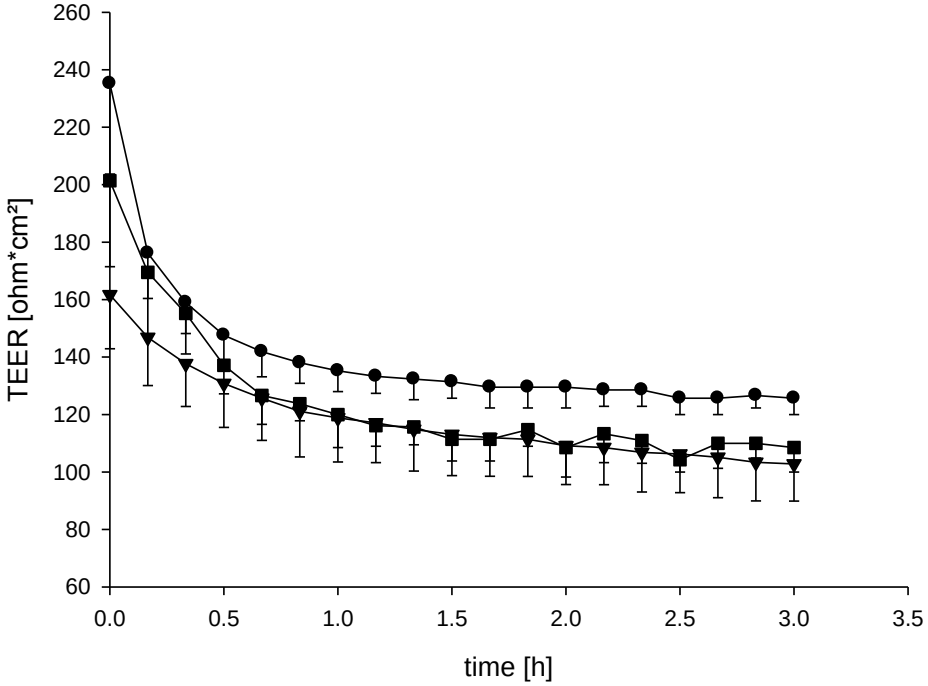

Figure 4.4. TEER value of a lipid-coated Transwell® (DOPC, method A, ten times) in the FTPC with media flow (●) and without media flow in a vertical orientation (▼), and without flow in horizontal orientation (■). For the sake of clarity, only every tenth data point is presented as mean ± SE (n ≥ 3).

4.3.3 Setup 3 and 4: Coating with DOPC or Lipoid E 80 using method B (centrifugation)

Since coating method A (sedimentation) with DOPC showed stability problems in the FTPC, a second method and lipid was tested for its suitability. The centrifugation method was based on a publication by Flaten et al. [51] and was performed in a simplified version.

As a first pretest, classical static permeation experiments were performed with propranolol and sodium fluorescein. Comparing the P_{app} values of the different methods one can see that the values for DOPC are comparable independent from number of repetitions (Figure 4.5) and also in comparison to method A. As the values for sodium fluorescein does not differ the experiments with propranolol were only carried out with 5 times coated Transwells®. In comparison to Transwells® coated 5 times with Lipoid E 80, the P_{app} values for both substances, sodium fluorescein and propranolol, are significantly different from DOPC results

(t-test, $p < 0.05$). Especially for sodium fluorescein, the permeability coefficient is closer to values obtained with Caco-2 cells ($P_{app} = 0.80 * 10^{-6}$ cm/s) using Lipoid E 80 coating. Furthermore, the TEER value of a Transwell® coated according to setup 4 did not show a rapid decrease within 3 h in the FTPC as it was found for setup 2 and 3. Therefore for the next experiments the lipid Lipoid E 80 and the coating procedure of 5 times centrifugation should be used.

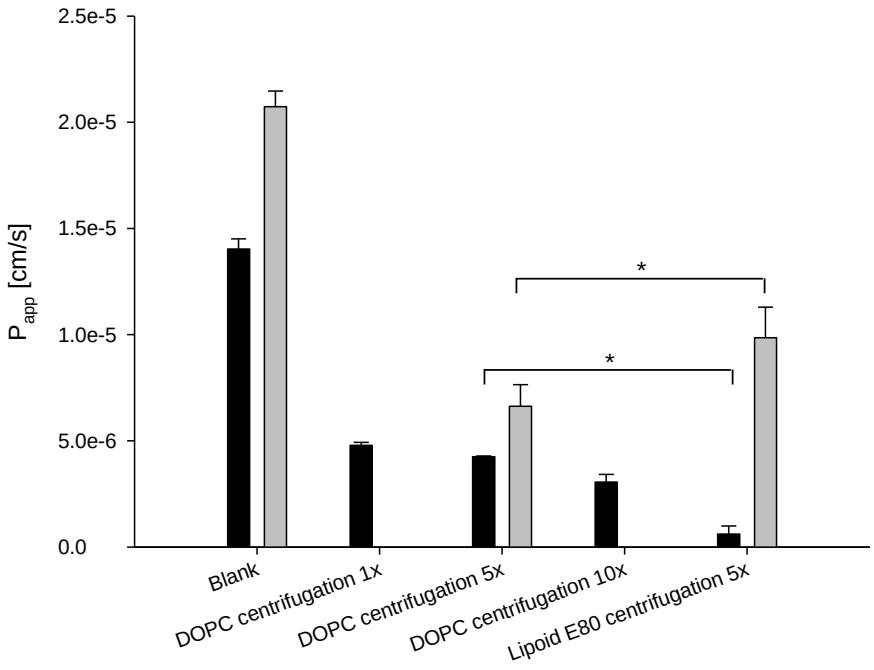

Figure 4.5. Comparison of P_{app} values of sodium fluorescein (black bars) and propranolol (grey bars) using different coated Transwells® in a classical static setup. Data presented as mean ± SD ($n \geq 3$). Bars marked with * are significantly different from P_{app} values without TPGS (t-test, $p \leq 0.05$).

In conclusion, the fourth setup using Lipoid E 80 centrifuged on the Transwell® membrane was favored as the best setup as a result of the performed pretests. In contrast to the sedimentation method, the centrifugation method is also far less time-consuming.

4.3.4 Characterization of Lipoid E 80 liposomes

Liposomes showed a main size peak at 656.7 ± 41.9 nm (95.6 % light scattering based intensity) and a second peak at 102.6 ± 88.9 nm (4.4 % light scattering

based intensity) measured in PBS. After dilution with water liposomes had a zeta potential of -18.6 ± 0.15 mV (pH 6.7).

For further characterization of the liposomes SEM images were recorded (Figure 4.6). In contrast to the data obtained via DLS a size range of liposomes of approximately 350 nm to 600 nm was found. The differences in size may be a direct result of the different techniques themselves. Size determination by DLS is partly influenced by the hydrodynamic diameter, and the hydration of the liposomes leads to larger particles. In contrast, the samples for SEM characterization are dried, thus excluding hydration effects. Furthermore, DLS is more sensitive to the presence of large particles resulting in a potential overprediction of mean size [87].

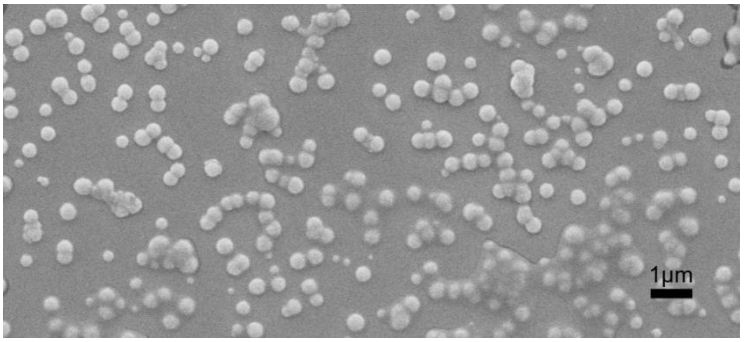

Figure 4.6. Scanning electron microscopic image of Lipoid E 80 liposomes.

4.4 Results and discussion of the characterization of the final coating

All the following characterization techniques were only performed with Transwells® which were coated with Lipoid E 80 five times using the centrifugation method. In the following chapters they are only called lipid-coated Transwells® or lipid-coated membranes without the addition of the used lipid (Lipoid E 80).

4.4.1 Monitoring of TEER value

An intact barrier layer is essential for reliable transport experiments, as changes in barrier properties during the study consequently lead to varying permeability data. It has to be guaranteed that the coating remains intact during the experiment despite the application of mechanical stress due to the flowing medium within the

FTPC. Therefore in a first attempt, the stability of the final coating under dynamic conditions was tested by means of TEER measurement every minute throughout the experiments.

Preliminary experiments have shown that pre-incubation with KRB prior to the experiments could minimize a steep increase of the TEER value during the first hour of the experiment and shorten the time until a constant TEER value level is reached (Figure 4.7). This might be due to a hydration of the barrier, which was described in a comparable way by Kanzer et al. [58]. Therefore, Transwells® were pre-incubated for 30 min before every experiment to reach the TEER plateau faster in the following experiments.

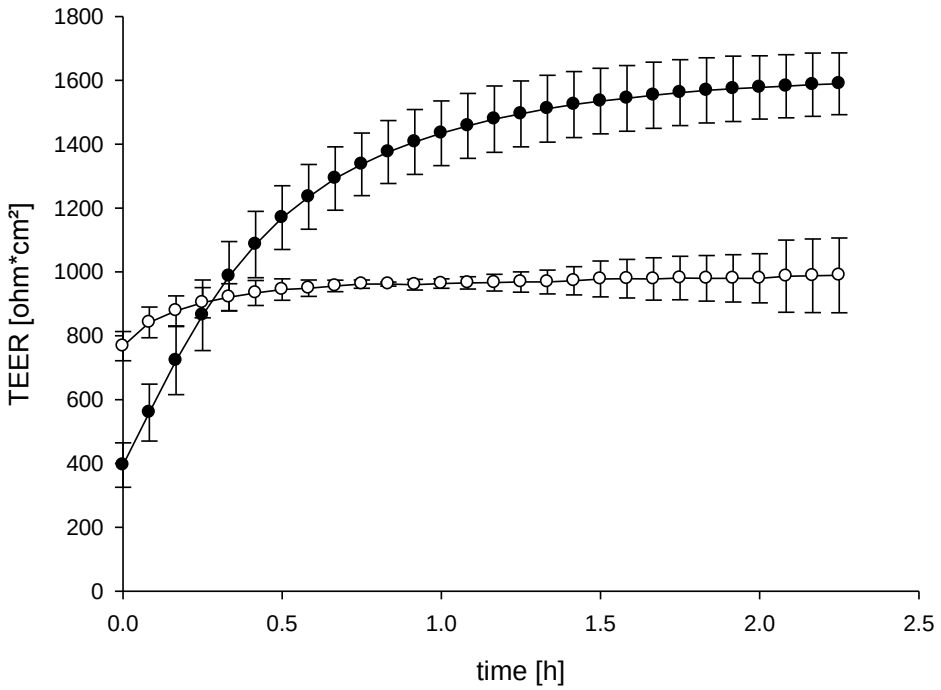

Figure 4.7. Comparative TEER values under dynamic flow conditions in the FTPC. Representative data of lipid-coated Transwells® without pre-incubation (●) and with 30 min pre-incubation (○) prior to the experiment. For the sake of clarity, only every fifth data point is presented as mean ± SD (n ≥ 3).

Figure 4.8 shows an example of the TEER value of a blank uncoated Transwell® compared to lipid-coated Transwells® of different batches. As a consequence of the equilibration to the flow conditions, the TEER value still increased during the first 30 min after mounting the Transwell® in the FTPC. The TEER values reached a constant plateau roughly 1.5 h after inserting in the FTPC and were above the

critical values of 300 Ω*cm² [34, 88]. The five batches showed some differences in the absolute TEER values but the TEER values remained over 600 Ω*cm² for at least 18 h for all batches. Consequnetly, the coating is stable under dynamic flow conditions over the entire time course of a transport experiment. Therefore, the lipid based model is suitable for transport studies under dynamic flow conditions for at least 18 h.

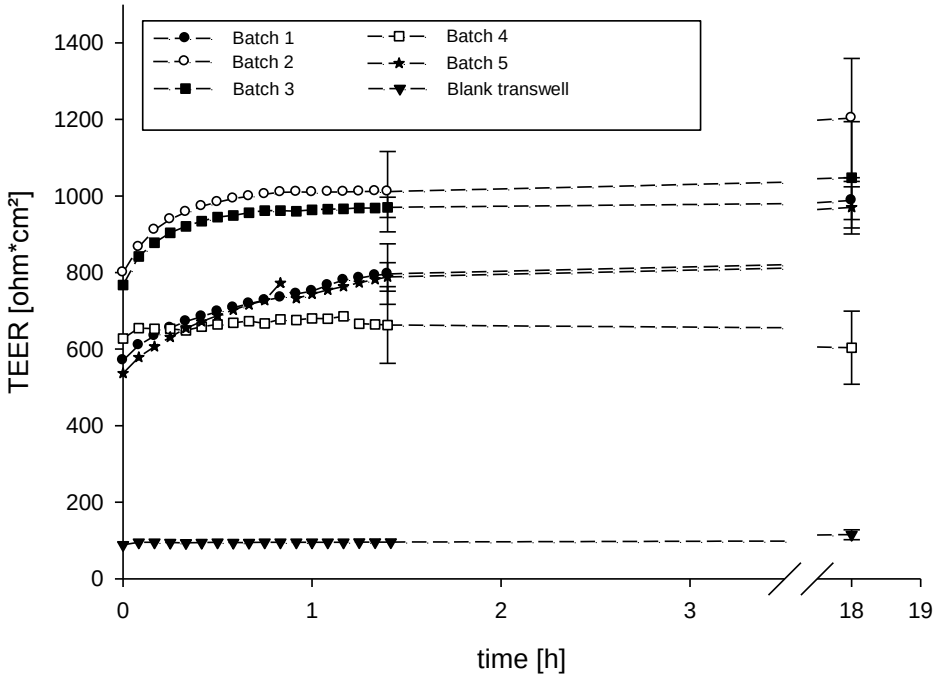

Figure 4.8. Comparative TEER values under dynamic flow conditions in the FTPC. Representative data of blank Transwells® and lipid-coated Transwells® of five different batches are presented. For the sake of clarity, only every fifth data point is presented as mean ± SE (for 1.5 h and 18 h) (n ≥ 3).

4.4.2 Light and scanning electron microscopy

Light microscopy and SEM were utilized for the analysis of the lipid-coated membrane in comparison to a blank one. Figure 4.9 a shows an overhead view of the blank membrane using SEM, whereas Figure 4.9 b displays the corresponding light microscopy image. Random distribution of the pores over the blank membrane is visualized in both images. Furthermore, coated Transwells® were analyzed using SEM and light microscopy. Figure 4.9 c depicts a top view SEM image of a Transwell®, which was coated five times with liposomes. As no pores

can be seen, it can be inferred that the entire surface of the membrane is covered with lipid. However, electron microscopy does not enable a distinct chemical discrimination between the two materials, namely the polyester membrane of the Transwell® and the phospholipid of the liposomes. Similarly, the light microscopic image appeared to show a coating of the entire membrane (Figure 4.9 d). While neither technique enabled a distinction between membrane and lipid, both images indicated a structured surface of the lipid coating.

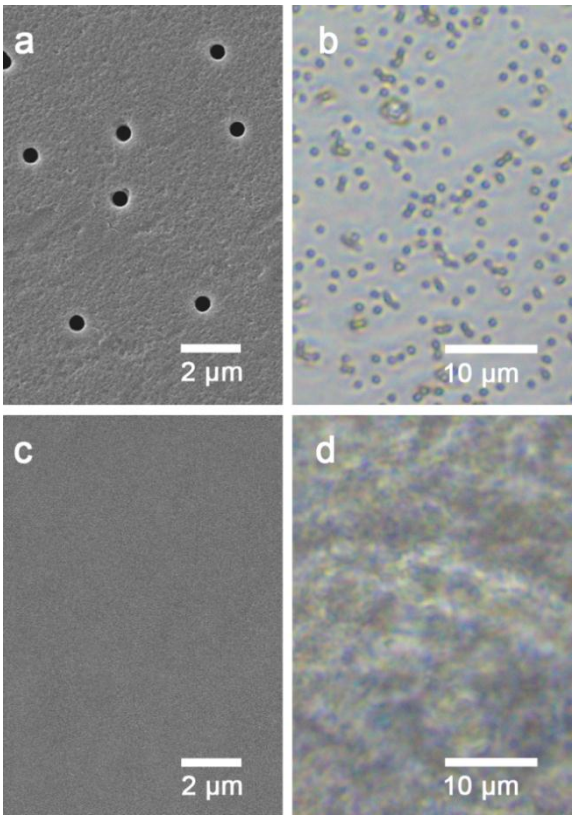

Figure 4.9. Electron (a, c) and light (b, d) microscopy images of the blank membrane (a, b) showing pore distribution, and of the lipid-coated membrane (b, d).

In summary, both techniques enabled a rough estimation of the surface and coating properties. A deeper investigation of the pores filled with lipid requires a cross section of the membrane. Due to the flexible and thin design of the membrane physical cutting without disruption of the sample was not possible. Different methods such as cryocutting or embedding in Tissue-Tek® OCT compound (Sakura, Staufen, Germany) were tested to obtain a cross section of the coated membrane. None of these techniques were successful. Therefore, Raman microscopy was used for further characterization.

4.4.3 Raman spectra

The blank polyester membrane as well as the pure lipid was tested for its Raman activity. Raman spectra of both substances were recorded separately. Figure 4.10 shows the spectra of the membrane and the lipid. The spectra show characteristic peaks for each substance, allowing for differentiation between membrane and lipid. Thus, it was deemed that Raman microscopy could be used for further characterization of the lipid-coated membrane.

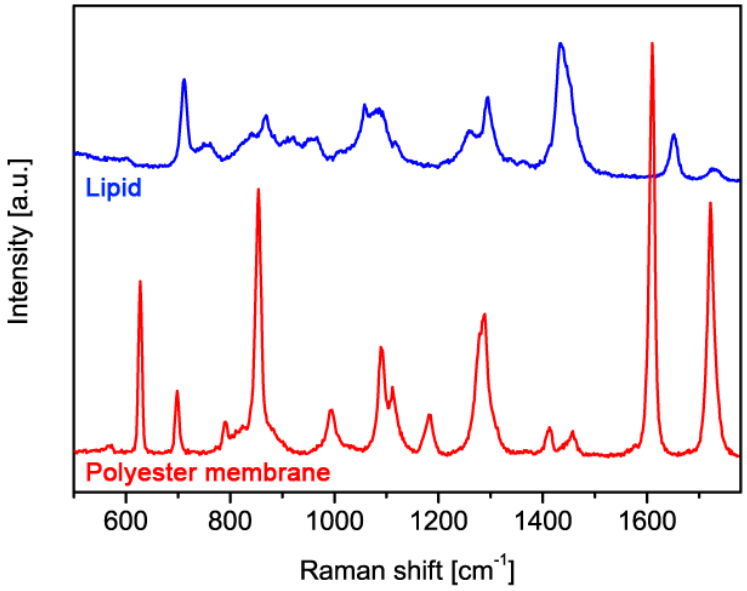

Figure 4.10. Raman spectra of polyester Transwell® membrane (red) and lipid Lipoid E 80 (blue).

4.4.4 Analysis of the blank membrane using Raman microscopy

As a first step, the blank membrane was thoroughly examined. The recording and conversion of Raman spectra along the xz-axes of a pore resulted in a two dimensional optical cross section of the pore (Figure 4.11 a). The morphology of all examined pores was found to be similar. The pores are characterized by a cone shape at the surface of the membrane fading into a channel-like structure. This form can be explained by the production of the pores by means of a track-etching process. In the images the boundaries are sharp, straight and distinct. As it is possible that the pore was not struck exactly in the center, due to the manual setting of the focal plane, a three dimensional image would be desirable in order to

add a higher degree of certainty to the results. Figure 4.11 b therefore shows a stacked image of a pore confirming the results of the optical cross sections.

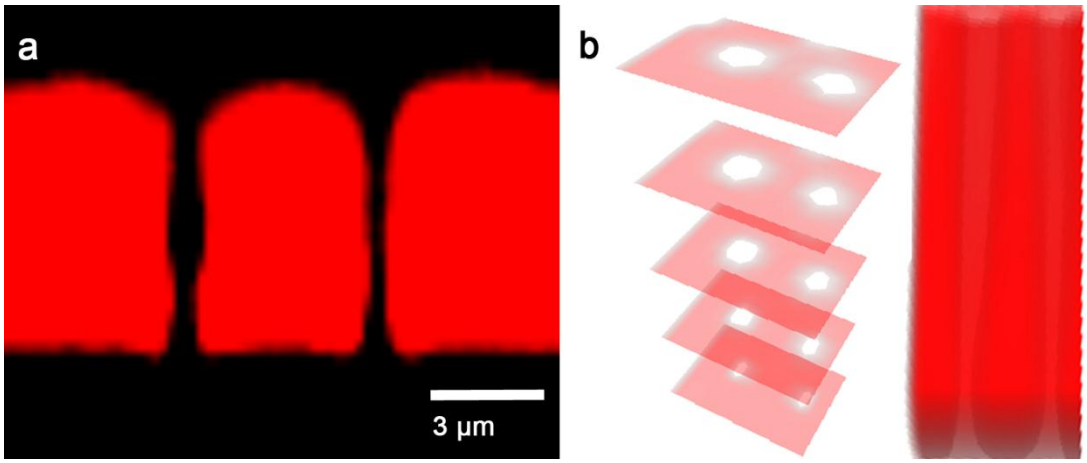

Figure 4.11. Characterization of the blank membrane. a) False color image of pore morphology derived from optical Raman cross sectioning of the membrane. b) Images derived from vertically adjacent focal planes are stacked visualizing the entire pore morphology.

4.4.5 Evaluation of coating procedure by Raman microscopy and optical profilometry

To get a deeper insight in the coating mechanism, the membranes were inspected after each coating step. Therefore, topography profiles were recorded after each coating step (Figure 4.12).

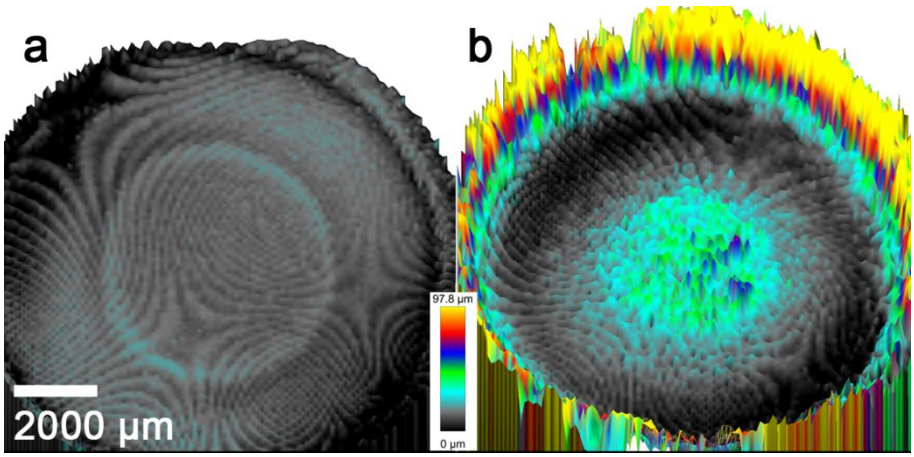

Figure 4.12. Exemplary topography profiles of a blank membrane (left) and a membrane after three coating steps (right) using optical profilometry.

Compared to the blank membrane the coated membrane shows a more structured surface with elevated areas in the center and at the edge of the membrane. For further characterization, the surface height information was used as a reference for subsequent guided Raman spectra acquisition of the same area. Figure 4.13 shows the Raman images of a blank membrane and a coated membrane after each individual coating step. A concentric circle of lipid as well as a lipid circle at the outer boundaries of the membrane was deposited after the first coating step. The lipid-covered area on the membrane increased until a full coating was obtained after three coating steps. The remaining two steps only added lipid to stabilize the coating.

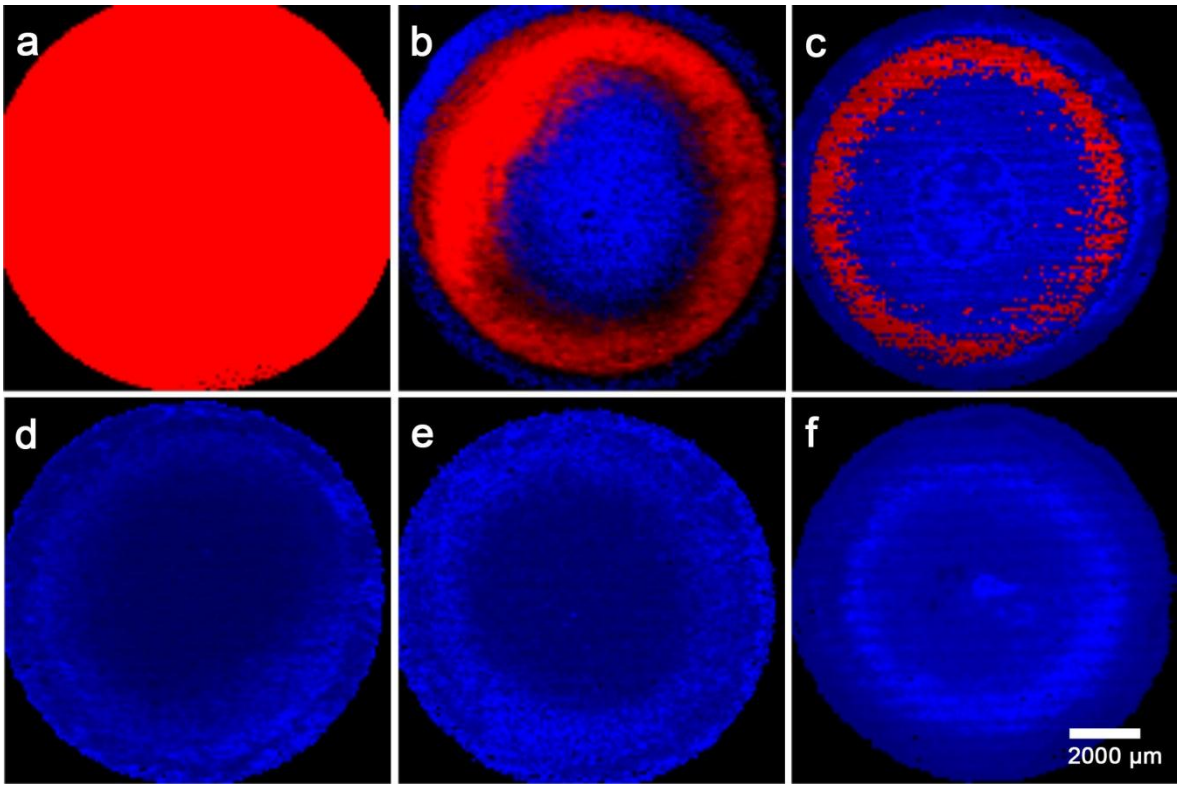

Figure 4.13. Topography images overlaid with recorded Raman data visualizing the successive increase of lipid coverage on the membrane from blank membrane (a) and subsequent coating steps 1 to 4 (b–e) up to the final lipid-coated membrane after 5 coating steps (f). Raman spectra assigned to the polyester membrane are depicted in red, lipid spectra are represented in blue.

The topography profiles assume that the coating thickness varies across the diameter of the Transwell®. Therefore, Raman cross sectioning was performed for each coating step (Figure 4.14) in order to verify this assumption.

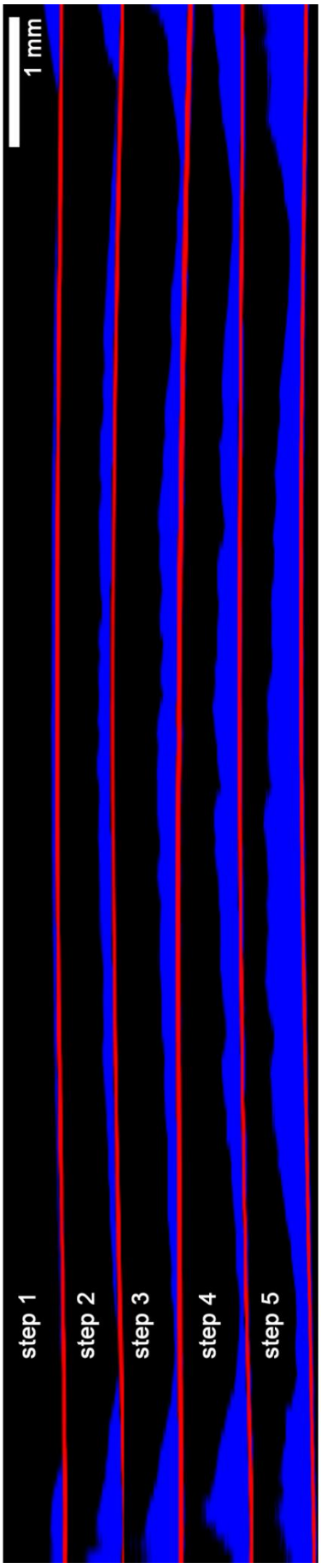

Figure 4.14. Raman cross section images of the entire membrane diameter showing gradual lipid assembly (blue) on the supportive membrane (red) after each coating step. Due to the image size the free aspect ratio is deregulated.

The cross section after the first coating step shows blank membrane as well as areas with a thin lipid coating. Lipid is localized in the middle and at the edge of the membrane. After the second step, the coating can be seen to spread over the membrane in a thin layer, a confluent layer is achieved after five coating steps. In addition, the results gained from the topography profiles (Figure 4.13) correlate well with the xz-images of the thickness investigation (Figure 4.14). The wavelike pattern of the lipid coating is a reproducible structure affirming a reproducible and controlled coating procedure.

In a next step it should be clarified if the pores are also filled with lipid as they are the supposed pathway for drug substances across the membrane. Furthermore, a filling of the pores would result in an anchoring of the lipid layer in the membrane.

4.4.6 Analysis of the pore morphology within the coated membrane

Figure 4.15 a shows a representative example of the complete filling of the pores with lipid without any areas filled with air, which could affect the permeation. Again, the pore boundaries are sharp and lipid can be precisely distinguished from the membrane. The conical shape of the pore may facilitate the soaking of the pores with lipid during the coating procedure. An image stack of a lipid filled pore is depicted in Figure 4.15 b. In addition, separate images of the lipid filling and the membrane pore are displayed for a better spatial understanding. The results from three dimensional imaging confirm the findings noted from two dimensional imaging.

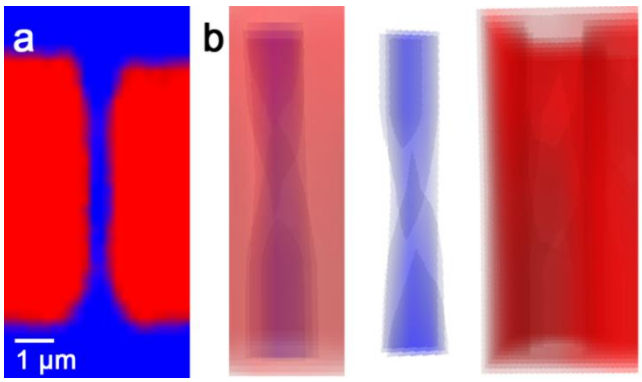

Figure 4.15. Pore morphology within the lipid-coated membrane a) False color image of membrane (red) pores filled with lipid (blue) derived from Raman cross sections. b) Three dimensional image stack visualizing the entire filled pore. For depicting chemically selective identification of the two components and a better spatial understanding, the stack is split into two individual images.

4.4.7 Coating integrity in the classical static setup

As the lipid coating should serve as the permeation barrier, it has to withstand exposure to media throughout transport experiments. If the coating is washed off the membrane, the barrier breaks down, falsifying the permeation results. Therefore, it was of vital importance to prove coating integrity after exposure to media under experimental circumstances. Transwells® were removed from the media after 6 and 24 h and were dried at room temperature. Figure 4.16 shows an optical Raman cross section of lipid-coated Transwells® before and after exposure to KRB under classical static transport conditions. Neither cross section image taken after 6 h nor 24 h exposure time reveals any uncovered membrane areas. Furthermore, the wavelike pattern remained during the exposure to media. Therefore, permeation experiments up to 24 h can be conducted with the lipid-coated membrane in the classical static setup without any deficiency in the integrity of the coating.

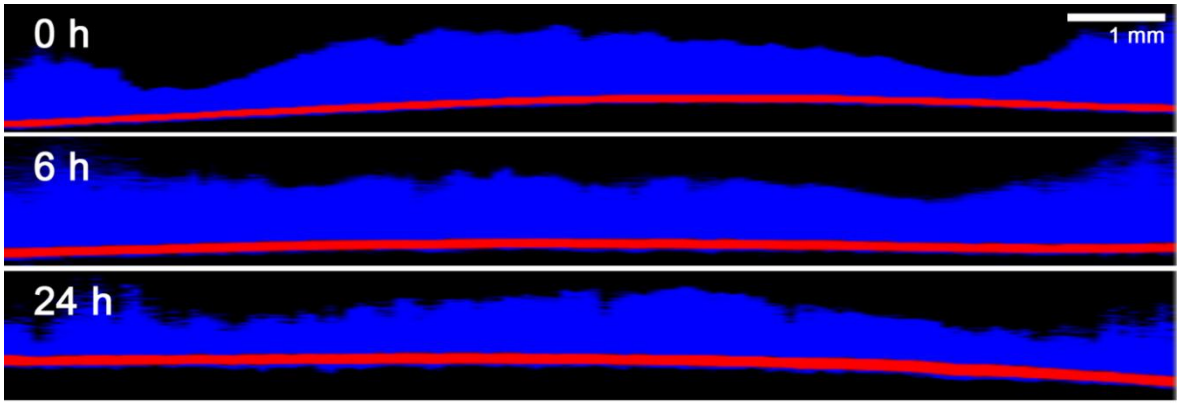

Figure 4.16. Optical Raman cross sections from edge to edge of lipid-coated Transwells®. Initial lipid layer (blue) on Transwell® membrane (red) before, after 6 h and after 24 h of classical static experiment with medium. Due to the image size the free aspect ratio is deregulated.

4.4.8 Coating integrity in the dynamic setup

Beside the evaluation of the coating integrity under classical static transport conditions also the stability under dynamic flow conditions was analyzed using confocal Raman microscopy and optical topography. Transwells® were removed from the FTPC after 6 h and 18 h and were dried at room temperature. Figure 4.17 depicts representative optical cross sections of the coated membrane before the

experiment and after 6 h and 18 h within the FTPC, respectively. At each investigated time point, the coating has a comparable wavelike pattern due to the coating procedure.

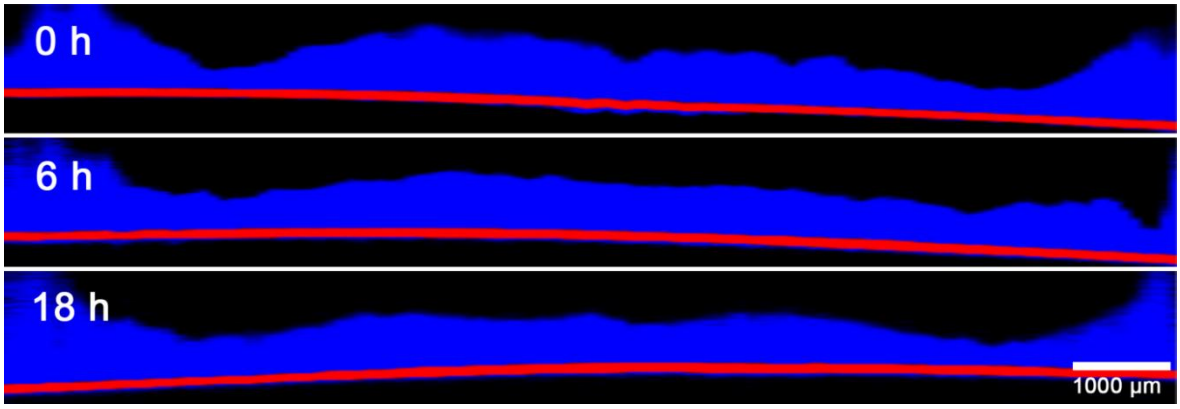

Figure 4.17. Optical Raman cross sections from edge to edge of lipid-coated Transwells®. Initial lipid layer (blue) on Transwell® membrane (red) before, after 6 h and after 18 h of experiment in the FTPC with medium. Due to the image size the free aspect ratio is deregulated.

To ensure lipid coverage of the entire membrane area at every time point and therefore intact barrier properties, top view images were recorded in addition to the optical cross sections. Figure 4.18 a and b show representative topography profiles of the coated Transwell® before and after 18 h of experiment under dynamic flow conditions as well as an overlay with Raman spectra (Figure 4.18 c, d). The surface of the coating showed structural differences indicating that KRB led to changes throughout the experiment. As no lipid-free areas were revealed, the images clarify that no defects were washed into the coating during the use in the FTPC. This verifies the results of the TEER measurement and the stability of the coating against KRB under dynamic flow conditions in the FTPC.

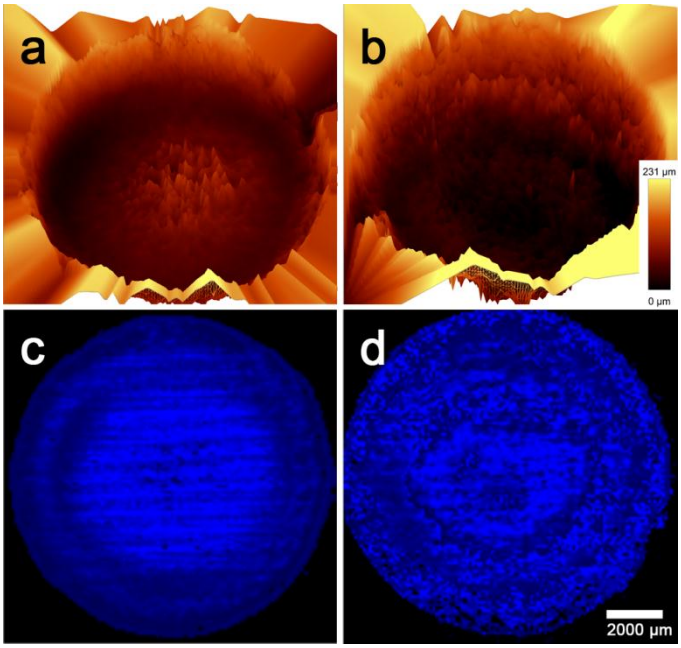

Figure 4.18. Topography profile (a, b) overlaid with Raman spectra (c, d) visualizing the complete lipid (blue) coverage of the Transwell® membrane (red) before (a,c) and after a dynamic transport experiment (18 h; b,d).

4.4.9 Stability against simulated intestinal fluid

As a preliminary test for the stability of the lipid coating in the presence of simulated intestinal fluid, the TEER value was recorded over 5 h in the FTPC. Figure 4.19 shows the course of the TEER value of a membrane expose to simulated intestinal fluid in comparison to KRB. For both, FaSSIF and FeSSIF, the TEER value decreased rapidly in the first minutes. Afterwards, the value stayed at a constant level of about 350 Ω*cm² for FaSSIF. This is close to the limit of 300 Ω*cm², which is the critical value for the integrity of Caco-2 cell monolayers. Using FeSSIF the TEER value fell below that limit reaching the same value as a blank Transwell® after 2 h (55 Ω*cm²).

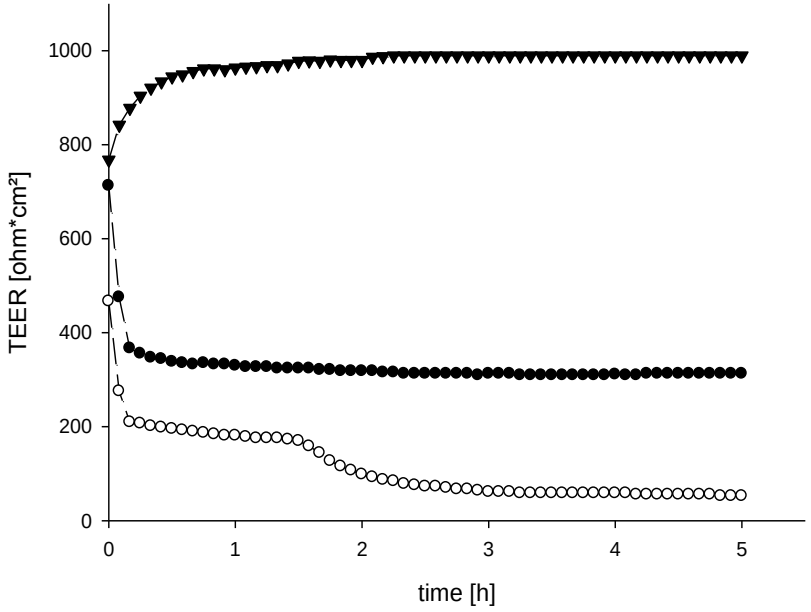

Figure 4.19. Comparative TEER values under dynamic flow conditions in the FTPC. Preliminary data for a lipid-coated Transwell® using KRB (▼), FaSSIF (●) and FeSSIF (○) as medium. For the sake of clarity only every fifth data point is presented (n = 1).

Visual inspection of the Transwell® after 5 h showed a complete washing off of the lipid coating. Due to the high concentration of lecithin and sodium taurocholate the lipid layer was solved and washed away with the constant medium flow. These first results indicate the instability of the coating against FeSSIF under dynamic flow conditions. Therefore, the lipid-coated membrane cannot be used for experiments with FeSSIF and only in a limited way with FaSSIF. Nevertheless, these results have to be confirmed with further experiments and a change of the lipid composition, e.g. addition of cholesterol, could be considered as a possibility to stabilize the coating.

4.5 Conclusion

The pretests have shown that the use of lipid Lipoid E 80 and centrifugation (5 times) as the coating method lead to better results compared to DOPC and sedimentation as coating method. The final coating was successfully characterized regarding its reproducibility and its stepwise buildup on the Transwell®. Furthermore, the stability of the coating was confirmed under classical static as

well as under dynamic flow conditions using KRB. Therefore, the lipid-coated membrane can be used for further characterization especially with respect to its permeation properties, which is described in the following chapter. Previous results showed that the use of simulated intestinal fluid especially FaSSIF is limited possible whereas FeSSIF cannot be used with the here described lipid-coated membranes. Further investigations are necessary.

5 Comparison of a lipid-coated membrane with Caco-2 cell monolayers using drug solutions

Parts of this chapter are prepared for submission as journal article:

"Characterization and evaluation of lipid-coated membranes in comparison to Caco-2 cell monolayers for combined dissolution and permeation testing"

Statement of authorship contribution:

The following author contributed to this chapter:
Sandra P. Gantzsch, Ulrich F. Schaefer, Claus-Michael Lehr, Co-operation partners from Sanofi-Aventis
The author of the thesis made the following contribution to this chapter.

1. Design of the project including formulation of problems to be tested and design of individual experiments:
   Contributed significantly

2. Planning of experiments and design of methods to answer the problems posed under # 1 including choice and development of the methods:
   Contributed significantly

3. Performance of experiments and data analysis:
   Essentially performed this study independently

4. Presentation, interpretation and discussion of the results obtained in article form:
   Essentially performed this study independently

5.1 Introduction

After successful characterization of the coating process and the stability of the coating against KRB, the next step was to evaluate the permeation properties of the lipid-coated membrane as it is intended for use as permeation barrier. Therefore, permeation experiments were performed under classical static conditions as well as under dynamic flow conditions in direct comparison to the well-established Caco-2 cell model using drug solutions. The permeability of different marker substances including highly and lowly permeable substances as well as efflux transporter substrates was investigated.

5.2 Materials and methods

5.2.1 Materials

Atenolol, rhodamine 123 and sodium fluorescein (Sigma-Aldrich, Steinheim, Germany), domperidone and domperidone maleate (Transo-Pharm, Siek, Germany), furosemide and propranolol HCl (Synopharm GmbH & Co KG, Barsbuettel, Germany) and talinolol (extracted from Cordanum tablets, AWD.pharma, Radebeul, Germany) served as model drugs. Lipoid E 80 (egg phospholipids with 80 % phosphatidylcholine) was a kind gift of Lipoid GmbH (Ludwigshafen, Germany). All buffer reagents were purchased from Sigma-Aldrich (Steinheim, Germany) and were of cell culture tested grade. All reagents for HPLC quantification were obtained from Sigma-Aldrich (Steinheim, Germany) and were of HPLC gradient grade. High purity water was prepared by a Millipore Milli-Q Synthesis system (Merck Millipore, Darmstadt, Germany). KRB was prepared as decribed in Chapter 2.2.4.

5.2.2 Cell culture

Cell culture conditions were the same as described in Chapter 2.2.2.

5.2.3 Coating procedure

The coating procedure was performed as described in Chapter 4.2.3 and 4.2.4 (5 times centrifugation of Lipoid E 80 liposomes).

5.2.4 TEER measurement

TEER was monitored as described in Chapter 2.2.3.

5.2.5 Classical static transport experiments

The general conditions for classical static transport experiments were the same as described in Chapter 2.2.5 with Caco-2 cell monolayers and were the same for lipid-coated Transwells®. Concentrations of drug solutions are listed in Table 5.1.

Table 5.1. Properties and concentrations of the drugs. Molecular weight (MW) and xlogP3 value according to PubChem database [89]. Substances marked with [1] are P-gp substrates.

Substance	Concentration	MW [g/mol]	xlogP3	Permeability according to BCS [62], [90]
Atenolol	5 µM = 1.33 µg/ml	266.3	0.2	Low
Domperidone[1]	23.5 µM = 10 µg/ml	425.9	3.9	High
Domperidone maleate[1]	23.5 µM = 12.7 µg/ml	542.0	-	High
Furosemide[1]	1209.5 µM = 400 µg/ml	330.7	2	Low
Propranolol HCl	385.7 µM = 100 µg/ml	259.3	3	High
Rhodamine 123[1]	15 µM = 5.77 µg/ml	380.8	2.5	Low
Sodium fluorescein	14 µM = 5 µg/ml	376.3	3.4 (without Na)	Low
Talinolol[1]	27.5 µM = 10 µg/ml	363.5	2.6	High

5.2.6 Dynamic transport experiments

Dynamic transport experiments in the FTPC were performed as described in Chapter 2.2.6 with Caco-2 cell monolayers and were the same for lipid-coated Transwells®. Concentrations of drug solutions are listed in Table 5.1.

5.2.7 Quantification of drug substances

The concentration of substance in the basolateral compartment at each sampling time point was determined via HPLC or fluorescence measurement in a plate reader. For further details of the quantification method see Chapter 10.1 in the annexes.

5.2.8 Data treatment

The P_{app} values were calculated as described in Chapter 2.2.8.
For statistical analysis t-tests ($p < 0.05$) were performed using SigmaStat integrated in SigmaPlot version 11.0 (Systat Software GmbH, Erkrath, Germany).

5.3 Results and Discussion

5.3.1 Monitoring of the TEER value

As already described in Chapter 4.4.1, the TEER value of the lipid-coated membrane remained over 600 Ω*cm² for 18 h. In comparison, TEER values for Caco-2 cell monolayers remained above 300 Ω*cm² only for about 3 h (Figure 5.1).
Based on the principle that high, stable measurements of electrical resistance indicate an intact, stable barrier, it follows that decreasing TEER values indicate a less dense permeation barrier. This may for instance be caused by an opening of tight junctions of the cell monolayer [15] which may in turn result in higher amounts of drug permeating across the layer and consequently in inaccurate P_{app} values. For Caco-2 cell monolayers, TEER values above 300 Ω*cm² are considered to be appropriate for permeation experiments [15], which was uphold for about 3 h in the FTPC. In contrast, the TEER values of the lipid-coated membrane do not decrease below 300 Ω*cm². These results highlight the long term coating stability in comparison to Caco-2 cell monolayers, as the breakdown of barrier integrity of the cellular system after 2-3 h is obvious.
Compared to Caco-2 cells, the artificial membrane model is therefore advantageous regarding the possible experiment duration. Ultimately, long term transport studies are an option with this artificial permeation model in contrast to

Caco-2 cells. Therefore, the lipid-coated membrane bears the potential to analyze controlled release formulations.

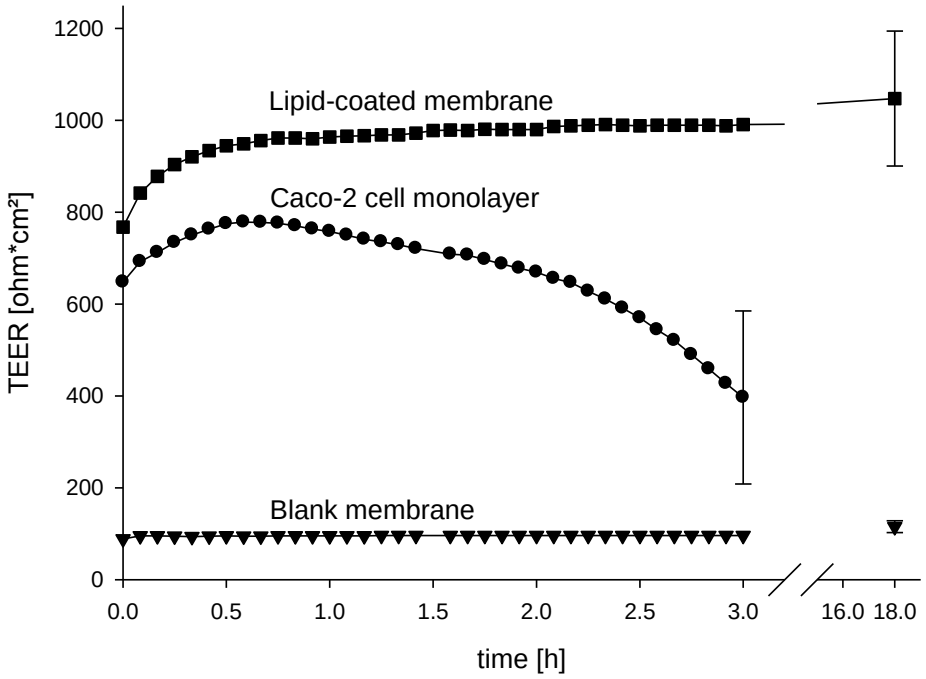

Figure 5.1. Comparative TEER values under dynamic flow conditions in the FTPC. Representative data of blank Transwell® (▼), Caco-2 cell monolayer (●) and lipid-coated Transwell® (■) are presented. For the sake of clarity, only every fifth data point is presented as mean ± SE (for the last time point, n ≥ 3).

5.3.2 Comparison of classical and dynamic setup

During development the FTPC was validated with the highly permeable substance propranolol and the lowly permeable marker sodium fluorescein for Caco-2 cells [32]. These experiments showed that due to the different permeation conditions the obtained P_{app} values differed in a certain range compared to data from classical transport experiments. Although these differences were already known, comparative experiments with Caco-2 cell monolayers in the classical as well as in the dynamic setup were performed to gain a broader understanding of the permeability behavior for each examined drug. Four of the model drugs showed higher permeability values in the FTPC using a Caco-2 cell monolayer than in the classical static setup (Table 5.2).

Table 5.2. Overview of P_{app} values. Data presented as mean ± SD (n ≥ 3).

Substance	P_{app} Caco-2 cells (classical setup) [* 10^{-6} cm/s]	P_{app} Caco-2 cells (dynamic setup) [* 10^{-6} cm/s]	P_{app} lipid-coated membrane (classical setup) [* 10^{-6} cm/s]	P_{app} lipid-coated membrane (dynamic setup) [* 10^{-6} cm/s]
Propranolol HCl	14.6 ± 1.7	25.00 ± 5.20 [32]	1.54 ± 0.17	13.30 ± 2.40
Domperidone	4.21 ± 0.46	6.08 ± 0.52	0.59 ± 0.09	5.18 ± 0.77
Domperidone maleate	2.28 ± 0.62	8.11 ± 2.19	0.68 ± 0.03	8.60 ± 1.30
Rhodamine 123	1.84 ± 0.67	1.60 ± 0.23	0.65 ± 0.18	1.61 ± 0.43
Sodium fluorescein	0.80 ± 0.07	0.34 ± 0.08	0.43 ± 0.02	0.16 ± 0.07
Talinolol	0.45 ± 0.13	1.50 ± 0.42	1.42 ± 0.36	3.72 ± 0.56
Furosemide	0.26 ± 0.07	0.18 ± 0.02	0.84 ± 0.0001	1.41 ± 0.64
Atenolol	0.25 ± 0.04	0.44 ± 0.20	0.28 ± 0.09	0.52 ± 0.13

In a further step, the transport experiments were repeated with the lipid-coated membrane. Here, higher P_{app} values were also found under dynamic flow conditions compared to the classical setup (Table 5.2) except for sodium fluorescein. Therefore, by comparing the two transport experiment conditions of classical static and dynamic flow, the same tendency of P_{app} values was found independent of the barrier employed. One essential difference between the classical setup and the FTPC is the fluid dynamic condition at the membrane. While in the classical setup the whole system is gently shaken and therefore, more or less similar conditions are provided at the apical and basolateral side, the situation in the FTPC is different. Here, at the apical side the donor solution is continuously moved over the membrane whereas the basolateral side is mixed with a stirrer. These differences result in different shear stress at the membrane, and therefore a different influence on the unstirred water layers (UWL) within the apical and basolateral compartments. As UWLs can act as additional permeation barriers, different influences on UWLs in classical static and dynamic flow setups might be the reason for observed deviations in P_{app} values under these two conditions. The transport of lipophilic substances in particular can be influenced by manipulation of the UWL [40]. Among the substances used in the current study, propranolol and domperidone have the highest lipophilicity. Therefore, the greatest

differences between the P_{app} values of the classical and dynamic setup should be found for these substances. This can successfully be confirmed by comparing the results using the lipid-coated membrane.

In comparison to the results of Flaten et al. [51], the P_{app} values of the presented modified lipid-coated membrane are in the same range. For example, atenolol with a P_{app} value of 0.28 * 10^{-6} cm/s shows reasonably similar values in the classical static setup compared to the result from Flaten et al. (0.22 * 10^{-6} cm/s) [51].

5.3.3 Permeation experiment under dynamic flow conditions – comparing Caco-2 cell monolayers and lipid-coated membranes

For evaluation of the permeation properties of the lipid-coated membrane, transport experiments with different drugs were conducted and the P_{app} values were compared with filter grown Caco-2 cell monolayers. Permeation experiments with Caco-2 cell monolayers and lipid-coated Transwells® were performed in the FTPC for 3 h or 18 h, respectively. Donor solutions of each drug were pumped into the apical compartment of the permeation cell. The calculated P_{app} values are summarized in Table 5.2. It can be seen that in the FTPC the lipid-coated membrane provides comparable permeability data to that obtained using the Caco-2 cells. Furthermore, the standard deviation of such data is rather low indicating reliable reproducibility. Both models can distinguish between highly and lowly permeable substances. Compared to use in a Caco-2 cell-based setup, atenolol, talinolol, furosemide and domperidone maleate had P_{app} values which were higher by factors of 1.2, 2.5, 7.8 or 1.1, respectively, using lipid-coated Transwells®. Sodium fluorescein and propranolol showed a 0.5-fold lower P_{app} value for the lipid-coated Transwells® compared to Caco-2 cells.

For better comparison, the substances were put in order according to increasing P_{app} values obtained with Caco-2 cell monolayers. The ranking of the substances leads to a comparable pattern when using the lipid-coated membrane (Figure 5.2). From low to high P_{app} values the ranking for Caco-2 cells is the following: Furosemide, sodium fluorescein, atenolol, talinolol, rhodamine 123, domperidone maleate and propranolol HCl. Using lipid-coated Transwells® a comparable ranking

was found. Only furosemide and talinolol rank at different positions with the non-cellular model. Nevertheless, using the non-cellular model it is still possible to classify all the substances according to their permeability into highly, medially and lowly permeable substances.

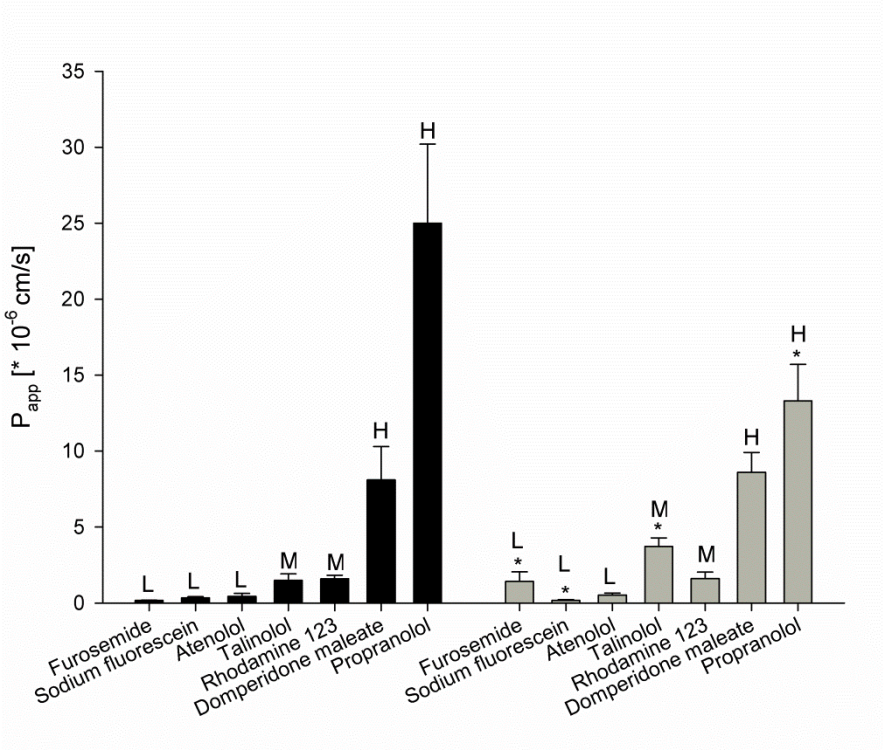

Figure 5.2. Ranking of apparent permeability (P_{app}) values for Caco-2 cell monolayers (black bars) and for lipid-coated membranes (grey bars) under dynamic flow conditions. Lowly permeable substances are indicated with L, medium with M and highly permeable with H. Data are presented as mean ± SD (n ≥ 3). Bars marked with * are significantly different from Caco-2 cell data (t-test, $p \leq 0.05$).

As expected, the permeation data differ in a certain range between cellular and non-cellular models due to the individual transport pathways across the different barriers. Besides passive diffusion, being the only pathway possible for transport in the artificial membrane model, Caco-2 cells also exhibit influx and efflux transporters which influence drug permeation. For example, permeation of talinolol across Caco-2 cells is affected by the efflux transporter P-gp [62, 71]. In contrast, non-cellular permeation models such as the presented lipid-coated membrane do not possess such transporters. However, in this approach only the absorptive transport (apical to basolateral) can be determined, for which the ratio of transport rates across Caco-2 cell monolayers in absence or in presence of a p-gp inhibitor

(0.01 % TPGS), resp., for all the drugs studied was between 0.94 and 1.54 in the d/p-system (see Chapter 2.3.6). Consequently, differences between cellular and non-cellular systems are low.

Even though transport proteins are missing in the non-cellular model it represents a suitable model for permeation studies, as passive diffusion is the main route for drug uptake *in vivo* [91].

5.3.4 Correlation of Caco-2 cell monolayer and lipid-coated membrane in classical and dynamic setup

For deeper evaluation of this lipid-coated membrane as a potential surrogate for Caco-2 cells, log P_{app} values obtained in each setup were plotted together in a single figure. Figure 5.3 illustrates the correlation between log P_{app} values obtained using Caco-2 cell monolayers and lipid-coated membranes for the two setups. Under classical static transport conditions, data points deviate from the line of identity (y = x) to a greater extent compared to dynamic flow conditions, where they are closer to the line of identity. Therefore, substitution of Caco-2 cell monolayers by the lipid-coated membrane appears not reasonable for the classical transport setup. In contrast, in the FTPC, a good correlation between Caco-2 cells and the artificial membrane was found. The use of the developed artificial membrane may therefore be meaningful in this setup.

Again, different fluid dynamic conditions in the classical setup and the FTPC can be found resulting in different UWLs. For PAMPA thicker UWLs were reported in an unstirred setup compared to Caco-2 cells [92]. Therefore, drug permeation in the classical static setup may be influenced by an UWL to a greater extent for this lipid-coated membrane than for Caco-2 cells. In contrast, Flaten et al. [53] reported that the importance of decreased UWLs on permeability in a lipid-coated membrane model is less. In the here presented dynamic flow experiments this was not observed.

As already shown in the comparative ranking of P_{app} values, two outliers, namely furosemide and talinolol, were found in the correlation plot. Again, divergence of data points for these two substances can be explained by an additional transport mechanism, namely the P-gp efflux transporter, which is only present in cellular models.

Other reports using the classical static setup reported a good correlation between the permeability over a liposome-based model and the extent of absorption in humans [51]. A direct correlation to Caco-2 cells was not performed in that report. By plotting these results from Flaten et al. (marked with F in Figure 5.3, top) in a similar way as in Figure Figure 5.3, a comparable pattern for the classical setup can be found, where the currently obtained results fit completely. This supports the comparability of the presented modified version of the lipid-coated membrane. Moreover, the results and the good correlation to Caco-2 cells under dynamic flow conditions confirm the specific application of the presented lipid-coated membrane for the combined dissolution and permeation system. In contrast to others [49, 51], the presented lipid-coated membranes are made of commercially available Transwells®, which are also used for Caco-2 cell culture. The coating can be done without the need of freeze-thaw cycles, in a high reproducible manner, which distinguishes the current setup from other approaches.

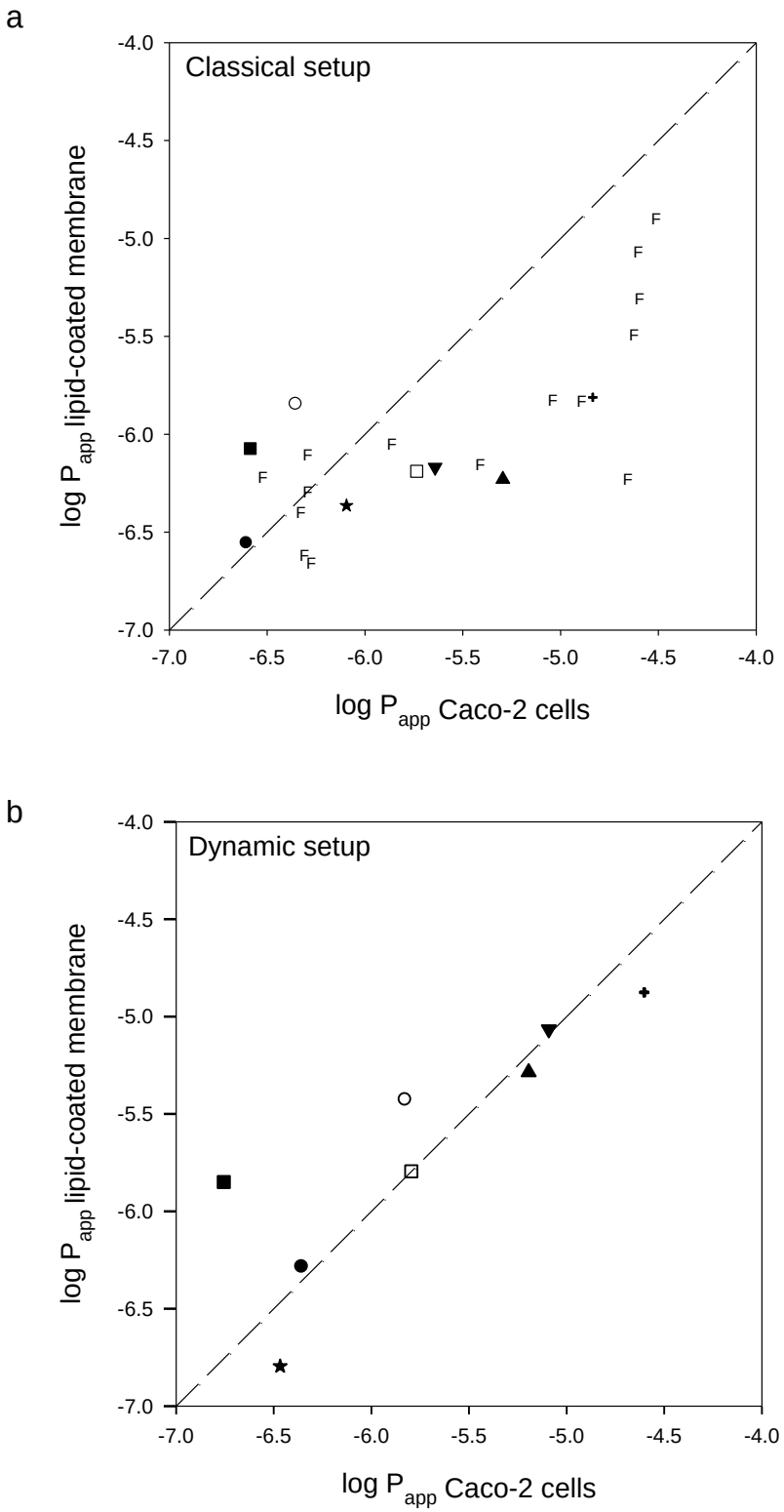

Figure 5.3. Correlation between Caco-2 cells and lipid-coated membranes. Permeability data determined in classical static setup (a) and under dynamic flow conditions (b) for atenolol (●), domperidone (▲), domperidone maleate (▼), sodium fluorescein (*), furosemide (■), propranolol (+), rhodamine 123 (□) and talinolol (○). Data taken from Flaten et al. [51] are marked with F. Dashed line represents line of identity.

5.4 Conclusion

A lipid-coated membrane for the use under dynamic flow conditions in a combined dissolution and permeation apparatus was successfully evaluated. The lipid coating is stable under the used flow conditions and the integrity of the lipid barrier is guaranteed. Compared to a Caco-2 cell monolayer, the lipid-coated membrane shows similar permeation results under constant flow and stirring. Therefore, it bears the potential to be implemented for the classification of new drugs according to their permeability. The potential influence of cellular transporter systems can of course not be taken into account. For further studies, an implementation of transporter proteins in the lipid coating could be considered.

As an alternative for Caco-2 cells, the presented lipid-coated membrane facilitates fast permeation testing without the need to grow cells, yet, being close to real human conditions particularly enabled by the application of dynamic flow conditions. In addition to drug solutions, the system bears the potential to analyze drug formulations like tablets without previous dispersion in buffer which will be examined in the following chapter. Due to the high stability of the lipid-coated membrane over time, the experimental time frame to investigate dissolution and permeation simultaneously can be extended beyond the limit of Caco-2 cell monolayers offering the possibility to investigate extended release formulations over a relevant period of time.

6 Suitability of a lipid-coated membrane to analyze tablets

Parts of this chapter are prepared for submission as journal article:

“Characterization and evaluation of lipid-coated membranes in comparison to Caco-2 cell monolayers for combined dissolution and permeation testing”

Statement of authorship contribution:

The following author contributed to this chapter:
Sandra P. Gantzsch, Ulrich F. Schaefer, Claus-Michael Lehr, Co-operation partners from Sanofi-Aventis
The author of the thesis made the following contribution to this chapter.

1. Design of the project including formulation of problems to be tested and design of individual experiments:
   Contributed significantly

2. Planning of experiments and design of methods to answer the problems posed under # 1 including choice and development of the methods:
   Contributed significantly

3. Performance of experiments and data analysis:
   Essentially performed this study independently

4. Presentation, interpretation and discussion of the results obtained in article form:
   Essentially performed this study independently

6.1 Introduction

The permeation experiments with solutions of different drug substances, as described in Chapter 5, showed a good correlation between the P_{app} values of the lipid-coated membrane and the Caco-2 cell monolayer. Furthermore, the results pointed out the particular qualification of this artificial membrane for the use under dynamic flow conditions. Therefore, the next step was to test the suitability of the lipid-coated membrane for the measurement of the dissolution and permeation of solid oral dosage forms. In this study it was of particular interest to clarify if the lipid-coated membrane is applicable for the testing of tablets.

6.2 Materials and methods

6.2.1 Materials

Domperidone maleate was purchased from Transo-Pharm (Siek, Germany) and Kolliphor TPGS was from BASF (Ludwigshafen, Germany). CapsuLac® 60 was a kind gift from Meggle (Wasserburg, Germany), Microcell MC-102 was a kind gift from Lehmann & Voss & Co (Hamburg, Germany), Kollidon CL was from BASF (Ludwigshafen, Germany), Aerosil 200 was from Degussa (Frankfurt, Germany) and Mg-stearate was from Fagron (Barsbuettel, Germany). All tablet excipients were of Ph. Eur. grade. Propranolol tablets were were prepared according to Motz et al. [32]. Lipoid E 80 (egg phospholipids with 80 % phosphatidylcholine) was a kind gift of Lipoid GmbH (Ludwigshafen, Germany). All reagents for HPLC quantification were obtained from Sigma-Aldrich (Steinheim, Germany) and were of HPLC gradient grade. High purity water was prepared by a Millipore Milli-Q Synthesis system (Merck Millipore, Darmstadt, Germany). All buffer reagents were purchased from Sigma-Aldrich (Steinheim, Germany) and were of cell culture tested grade. KRB was prepared as described in Chapter 2.2.4.

6.2.2 Cell culture

Cell culture conditions were the same as described in Chapter 2.2.2.

6.2.3 Coating procedure

The coating procedure was performed as described in Chapter 4.2.3 and 4.2.4 (5 times centrifugation of Lipoid E 80 liposomes).

6.2.4 TEER measurement

TEER was monitored as described in Chapter 2.2.3.

6.2.5 Preparation and characterization of tablets

Immediate release tablets (IR tablets) with 10 mg propranolol and extended release tablets (ER tablets) with 10 mg propranolol and 4 % Eudragit® were prepared according to Motz et al. [32]. Composition can be found in Table 6.1.

Table 6.1. Composition of propranolol tablets according to Motz et al. [32]

	Immediate release	Extended release
Propranolol	10 %	10 %
Eudragit® NE 30 D	-	4 %
Avicel PH 102	70 %	55 %
Lactose EP type D20	17 %	29 %
Water	-	q. s.
PVP insol.	1 %	-
Aerosil 200	1 %	1 %
Mg-stearate	1 %	1 %

The content of tablets was retested by dissolving a tablet in 100.0 ml KRB by means of ultrasonication. The resulting solution was filtered through a cellulose acetate filter (pore size 0.2 µm) and the filtrate was diluted with KRB (1:62.5). The concentration was determined via HPLC. For each release property, three tablets were tested.

Domperidone maleate tablets with and without TPGS were prepared and characterized as described in Chapter 3.2.4 and 3.2.5.

6.2.6 Combined dissolution and permeation experiment in the d/p-system

Combined dissolution and permeation experiments with propranolol and domperidone maleate tablets (2 tablets at a time) were performed in the d/p-system as described in Chapter 3.2.6 with Caco-2 cell monolayers and were the same for lipid-coated membranes.

6.2.7 Extraction of propranolol from lipid coating

For the measurement of propranolol accumulation in the lipid coating during an experiment with tablets, Transwells® were removed from the FTPC after 1.7 h, 5 h and 8 h, dried at room temperature and subsequently extracted. A mixture of 45 % (v/v) water, 22 % (v/v) acetonitrile, 33 % (v/v) methanol, 0.033 % (v/v) triethylamine and 0.044 % (v/v) phosphoric acid (mobile phase of HPLC method) was used as an extraction agent. Transwells® were shaken with 5 ml extraction agent on an orbital shaker for 18 h.

6.2.8 Quantification of drug substances

The concentration of substance at sampling ports D and A was determined by online detection. Fluorometric detection of propranolol was performed with the FIAlab fluorescence detector PMT-FL. Scan rate was adjusted to 4 Hz and integration time was set to 80 msec. UV absorbance at 285 nm was used for the online detection of domperidone maleate.
The concentration of substance in the basolateral compartment at each sampling time point was determined via HPLC. For further details of the quantification method see Chapter 10.1 in the annexes.

6.2.9 Comparison of dissolution profiles

Dissolution profiles at sampling ports D and A were compared using classical equivalence parameters [93]. The area under the curve (AUC) was calculated using the trapezoidal rule. Furthermore, the release profiles in cumulative form from the setup with the Caco-2 cell monolayers (reference batch R) were compared to the profiles from the setup with lipid-coated membranes (test batch

T). Comparisons were performed by calculating the f_2 similarity factor (eq. 4) [94] and by employing the Tolerated Difference Test (TDT) [95].

$$f_2 = 50\, x\, Log \left\{ \left[1 + \frac{1}{n} \sum_{t=1}^{n} w_t (R_t - T_t)^2 \right]^{-0.5} x\, 100 \right\} \qquad \text{(eq. 4)}$$

R_t is the mean percent of the dissolved drug from the reference batch at time t, T_t is the mean percent of the drug dissolved from the test batch at time t, n is the number of time points and w_t is a weight factor that can be used to enhance the influence of particular time points. If the calculation yields f_2 ≥ 50, similarity of R and T is declared.

A tolerated difference (δ) in dissolution between two tablets is the basis of TDT. At each time point the differences between test sample and reference are statistically proved for exceedance of the predetermined δ performing $n_{Reference}$ * n_{Test} comparisons. The number (D_d) of greater differences is counted (eq. 5), where D_i is the sum of differences greater than δ at the ith time point.

$$D_d = \frac{1}{n} \sum_{i=1}^{n} D_i \qquad \text{(eq. 5)}$$

TDT can also be used to determine the critical (maximum) δ, at which the profiles are considered not similar and are interpreted as the typical difference in percentage between the two profiles.

The main difference of both tests is that f_2 is an empirical method and TDT is a statistic one. In comparison to f_2, TDT has the advantage of performing customized comparisons of different formulations and distinction of different similarity levels. Furthermore, because the exact distribution of the random variable D_d is known, rejection values at any specified type I error (0.05 in this case) can be calculated and compared with the calculated statistic using the TDT.

For further statistical analysis an Anova (Holm-Sidak, $p < 0.05$) were performed using SigmaStat integrated in SigmaPlot version 11.0 (Systat Software GmbH, Erkrath, Germany).

6.3 Results and discussion

6.3.1 Characterization of propranolol tablets

Table 6.2 shows the results of the retest of propranolol tablets. For the IR tablets the retested content fits to the described content of 9.70 ± 0.25 mg by Motz et al. [32]. The content of the ER formulation is significantly different from the described content of 9.80 ± 0.35 mg. Nevertheless, the contents are still within the accepted limit of 90-110 %.

Table 6.2. Content of propranolol tablets. Data are presented as mean ± SD (n = 3).

	IR tablet	ER tablet
Set content	10 mg	10 mg
Real content	9.78 ± 0.3 mg	9.16 ± 0.5 mg

6.3.2 Monitoring of TEER value

The TEER values for Caco-2 cell monolayers and for lipid-coated membranes were at a level indicating an intact permeation barrier.

6.3.3 Assessment of dissolution and drug permeability of propranolol

As a first step, the dissolution profiles at sampling ports D and A for each formulation were compared. The concentration time trends for each barrier and formulation are shown in Figure 6.1 and Figure 6.2. The dissolution profiles showed a pattern as expected for immediate and extended release, respectively. Compared to immediate release tablets the extended release formulation yielded a flattened and broader dissolution profile. As further expected aspects of this release kinetic, the maximum dissolution peak was lower for the extended release formulation and dissolution was finished at a later time. Furthermore, the concentration determined at the apical side of the FTPC led to the same shape of peak compared to the sampling port dissolution. However, the apically determined peak showed a small time shift and was flattened. This can be explained by the

setup of the d/p-system, especially by the action of the stream splitter and the considerable tubing length between the dissolution cell and the FTPC [32].

According to the standard f_2-test, the release profiles of the IR and the ER tablet are different (Table 6.3) as expected.

Table 6.3. Similarity test of dissolution between immediate and extended release tablets for Caco-2 cells and lipid-coated membrane. Data marked with * indicate non-similarity.

Parameter	Dissolution	
	Caco-2 cells	Lipid-coated membrane
Original time points	19	25.3
f_2	24.26	27.66
TDT (d = 5)	P < 0.0005*	P < 0.0005*
TDT (d = 10)	P < 0.0005*	P < 0.0005*
Critical δ	31.2	27.4

Due to the spatial separation of dissolution and permeation testing in two different modules, the permeation barrier should have no impact on the dissolution of the tablet. As expected, there were no dramatic differences in dissolution between Caco-2 cell monolayers and lipid-coated membranes.

A comparison of typical parameters used for the evaluation in equivalence studies such as the area under the curve (AUC) and the maximum drug concentration (C_{max}) are listed in Table 6.4 for the apical compartment. The AUCs of IR tablets did not show a significant difference between Caco-2 cell monolayers and lipid-coated membranes. The same was found for the ER formulation and for the comparison of IR and ER tablets. In contrast as expected, C_{max} and t_{max} values were significantly different between the IR and the ER formulation, independent of the permeation barrier used. However, C_{max} and t_{max} were not significantly different between the Caco-2 cell monolayer and the lipid-coated membrane for every individual release kinetic. These results confirm the independence of the dissolution from the used permeation barrier.

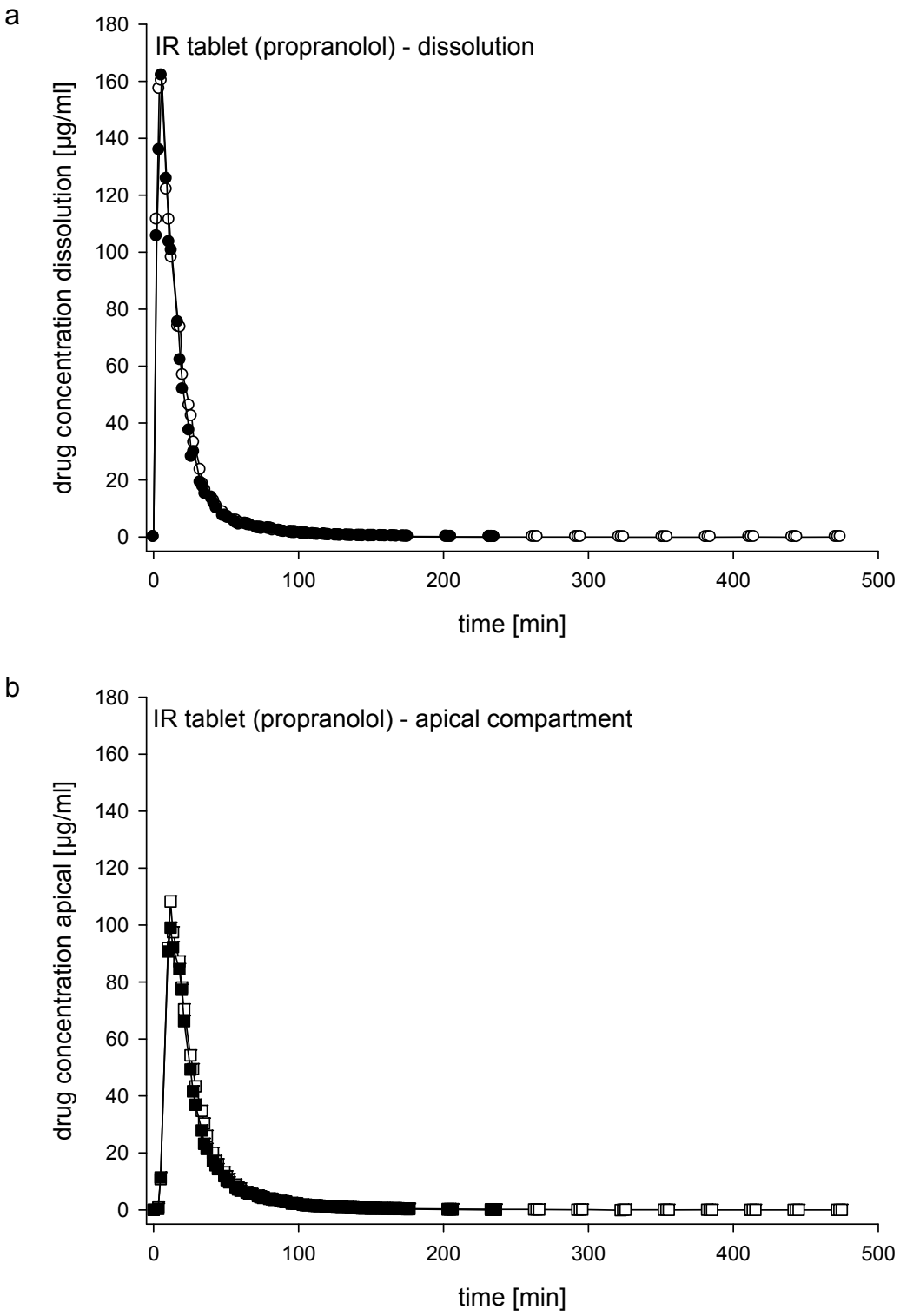

Figure 6.1. Concentration time trends for immediate release tablets at sampling port D (a) and A (b). Closed symbols (●, ■) represent the Caco-2 cell monolayer and open symbols (○, □) represent the lipid-coated membrane. For the sake of clarity, data are presented as mean (n ≥ 3) without SD.

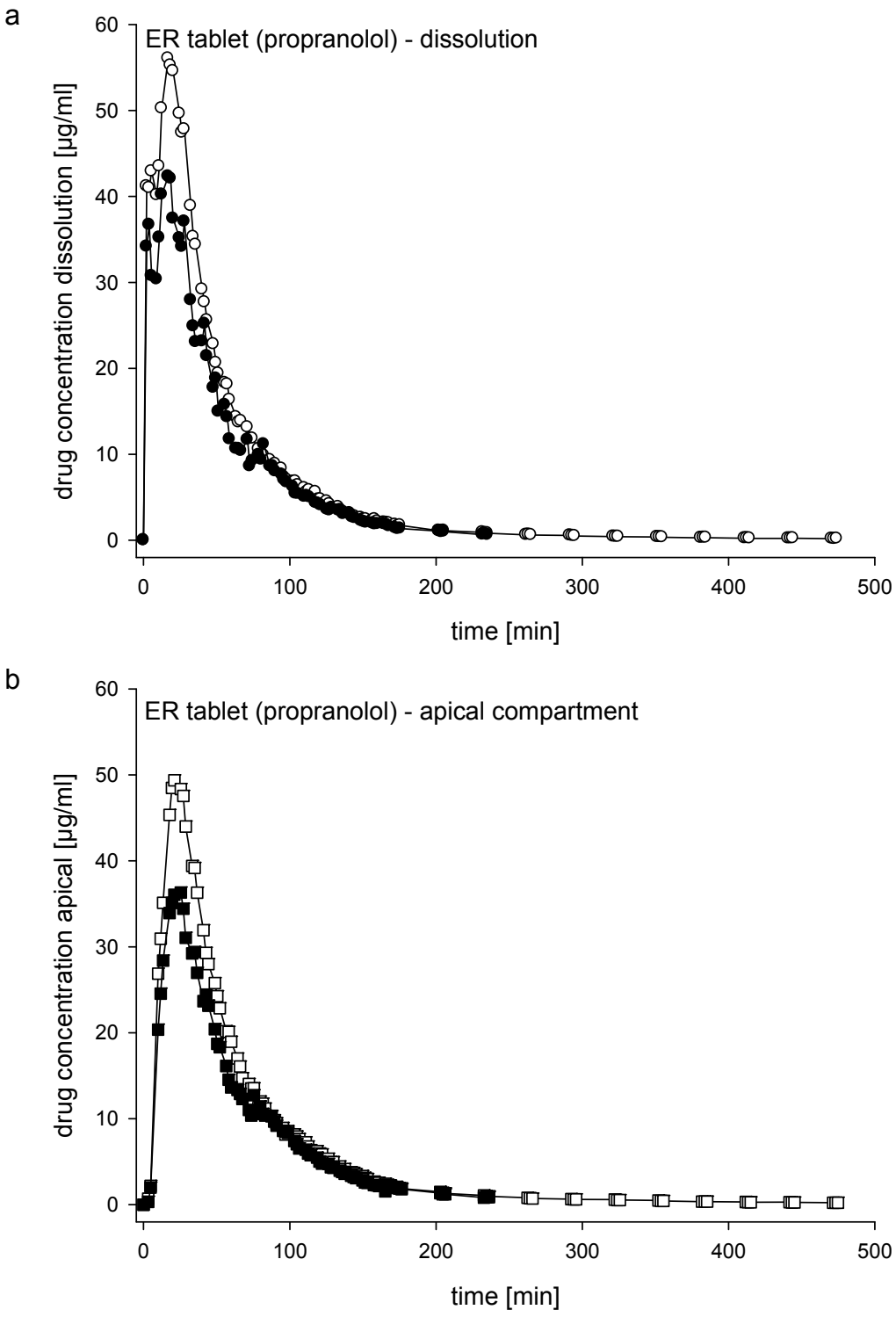

Figure 6.2. Concentration time trends for extended release tablets at sampling port D (a) and A (b). Closed symbols (●, ■) represent the Caco-2 cell monolayer and open symbols (○, □) represent the lipid-coated membrane. For the sake of clarity, data are presented as mean (n ≥ 3) without SD.

Table 6.4. Comparison of equivalence parameters in the apical compartment for different release kinetics and permeation barriers. Data are presented as mean ± SD (n ≥ 3). Data marked with * are significantly different from IR formulation using the same permeation barrier (ANOVA, Holm-Sidak, $p \leq 0.05$).

Parameter	IR tablet	ER tablet
AUC (Caco-2 cells)	2384.3 ± 187.7	2194.6 ± 640.7
AUC (lipid-coated membrane)	2582.2 ± 305.7	2715.6 ± 354.4
C_{max} (Caco-2 cells)	104.0 ± 7.1 µg/ml	39.1 ± 13.3 µg/ml*
C_{max} (lipid-coated membrane)	115.7 ± 33.3 µg/ml	52.7 ± 7.6 µg/ml*
t_{max} (Caco-2 cells)	13.2 ± 3.3 min	23.7 ± 3.1 min*
t_{max} (lipid-coated membrane)	12.9 ± 2.5 min	23.0 ± 3.3 min*

For further comparison, the dissolution profiles were tested for similarity using the f_2 factor and the TDT. The results are summarized in Table 6.5. The profiles obtained at sampling port D as well as at port A show similarity between the used permeation barriers. For both IR and ER tablets, the f_2 factor is greater than 50, indicating similarity. Furthermore, the critical δ is low. These results confirm the comparison using equivalence parameters. Nevertheless, the similarity values at sampling port D are higher than at sampling port A suggesting an influence of the permeation barrier on the measured concentration in the apical compartment. Also, using lipid-coated membranes the C_{max} in the apical compartment is higher than with Caco-2 cell monolayers. Looking at the permeation profiles one can see that the permeation over Caco-2 cells is faster. Therefore, the concentration at the apical compartment decreases faster in this case than with lipid-coated membranes. Due to the construction of the FTPC and the sampling position the permeation of propranolol has an influence on the measured apical concentration. However, for propranolol it is not as serious as it is highly permeable.

Table 6.5. Similarity test between Caco-2 cell monolayer and lipid-coated membrane for propranolol tablets. Data marked with * indicate non-similarity.

Parameter	Dissolution		Apical compartment	
	IR	ER	IR	ER
Original time points	15	40	57	61
f_2	82.39	59.18	57.41	58.89
TDT (d = 5)	P = 0.045*	P = 0.35	P < 0.0005*	P < 0.0005*
TDT (d = 10)	P > 0.5	P > 0.5	P > 0.5	P > 0.5
Critical δ	5	4.3	7.3	6.3

As a second step, the permeation profiles of each formulation were compared. Surprisingly in contrast to the dissolution profiles, the permeation profiles of the two release kinetics show no statistically significant difference. This was observed for both Caco-2 cell monolayer and lipid-coated membrane (Figure 6.5). Thus, the differences as observed in the dissolution profiles are obviously not strong enough to affect the permeation data underlining the advantage of a combined dissolution and permeation system.

In relation to the present concentration at the apical side of the permeation barrier, the permeation across the Caco-2 cell monolayer showed an appropriate profile for each formulation (Figure 6.3 and Figure 6.5). Although the permeated amount within the first 100 min did not show a significant difference at all time points between the two formulations, a clear trend and delay can be seen for the ER tablet. This is in accordance with the slower increase of drug available at the apical side. So, the concentration at the apical side controls the occurrence of propranolol at the basolateral side as is expected for a highly permeable compound. As both formulations showed a complete release of drug, the apical concentration decreased to almost zero for the IR and the ER tablet after approximately 100 min and 180 min, respectively. With a certain time delay the permeation also reached a steady-state. Correlating well with the AUCs, the permeated mass also did not show a significant difference between the two formulations at the end of the experiment.

The permeation profile obtained with lipid-coated membranes showed a longer lag time until the onset of permeation in the case of both formulations (Figure 6.4 and

Figure 6.5). Nevertheless, the permeation profiles have a comparable course to those obtained using Caco-2 cell monolayers. Again the ER tablet showed a delayed but not significantly different permeation at the beginning and after 180 min the curves are aligned, ending in a plateau. Here again, the permeated mass at the end of the experiment did not show a significant difference between IR and ER tablets, which fits to the AUCs. Furthermore, the total amount of propranolol permeated over the lipid-coated membrane is 2-fold lower than in the case of Caco-2 cell monolayers.

The differences between Caco-2 cell monolayer and lipid-coated membrane permeation are related mainly to a delayed onset and longer duration as well as to the total permeated drug amount. These effects can be explained by different factors. Firstly, Caco-2 cell monolayers have a thickness of approximately 5 to 10 µm, whereas the average thickness of the lipid coating goes up to 83 µm as can be seen in Figure 4.14 (Chapter 4.4.5). Therefore, the longer diffusion from the apical to the basolateral side resulted in a time shift of the permeation. Secondly, the lipid coating may also act as a depot, which is filled at the beginning and continues to empty even when the drug concentration at the apical side is almost zero. To verify this, the determination of the drug concentration inside the lipid coating at different times during the experiment appears beneficial (see Chapter 6.3.5). Thirdly, previous experiments with drug solutions of propranolol led to P_{app} values differing by a factor of 2 (Chapter 5.3.2 Table 5.2). As lower P_{app} values indicate less permeability, this explains the lower permeated amount when using lipid-coated membranes.

Although the permeation profiles showed some differences depending on the used permeation barrier, the results confirm the suitability of the lipid-coated membrane for tablet testing in a combined dissolution and permeation system.

The integration of a lipid-coated membrane in a combined dissolution and permeation system as described here enables the testing of intact tablets without the necessity to disintegrate the formulation prior to the experiment, as described previously [58].

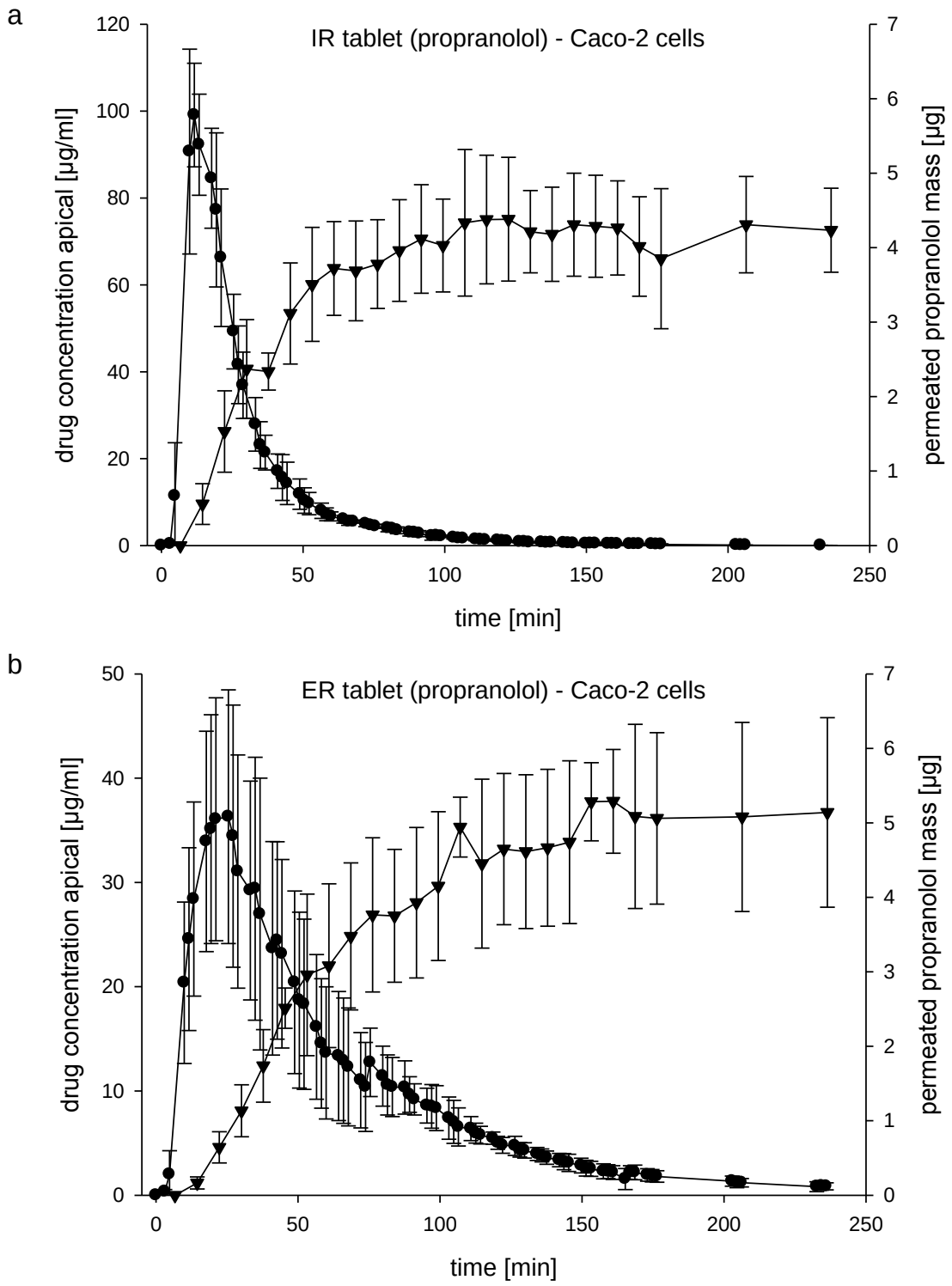

Figure 6.3. Concentration time trends for immediate release tablets (a) and extended release tablets (b) using Caco-2 cells. Circles (●) represent the apical side of the FTPC and triangles (▼) represent the basolateral side. Data are presented as mean ± SD (n ≥ 3).

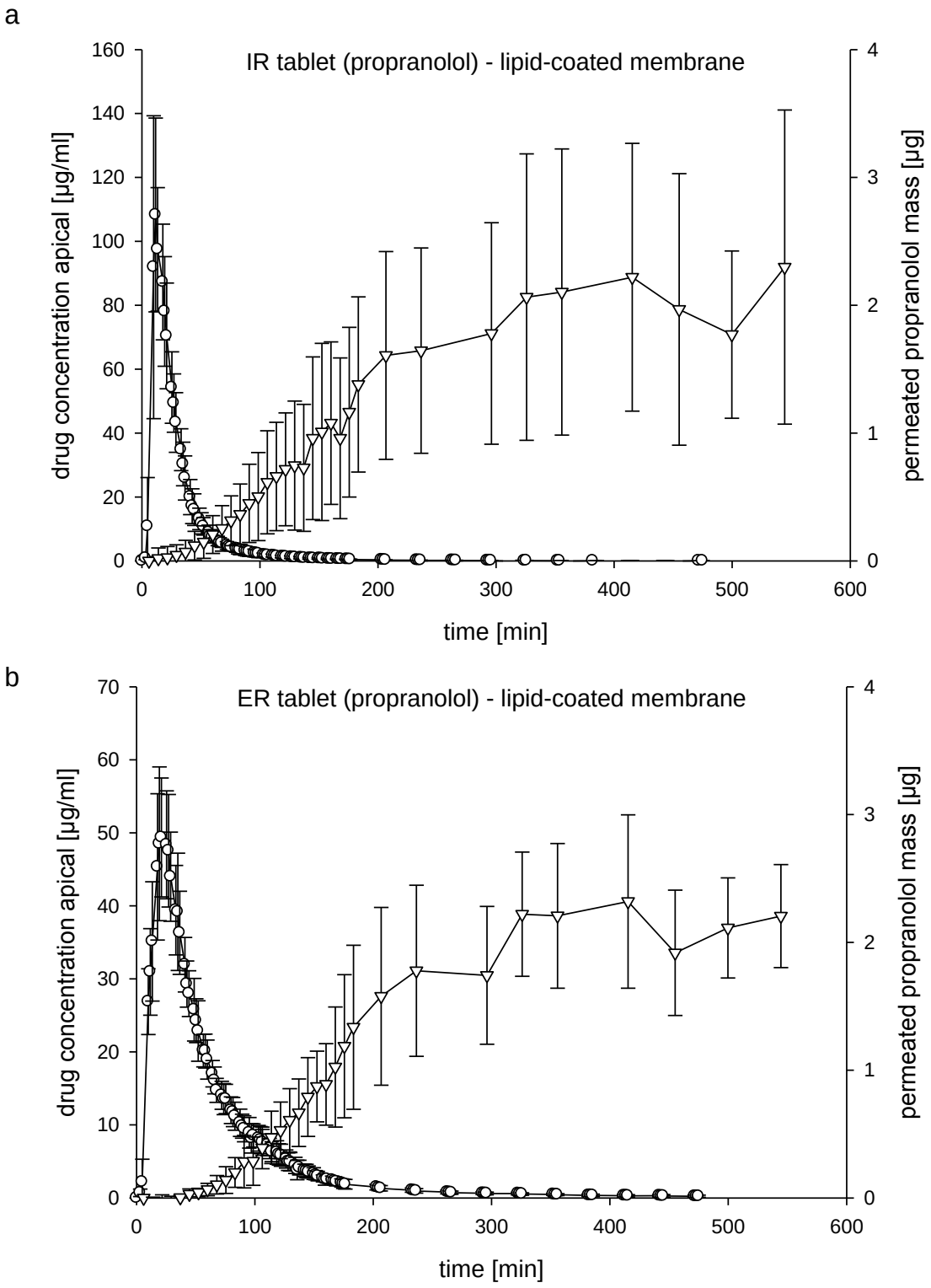

Figure 6.4. Concentration time trends for immediate release tablets (a) and extended release tablets (b) using lipid-coated membranes. Circles (○) represent the apical side of the FTPC and triangles (▽) represent the basolateral side. Data are presented as mean ± SD (n ≥ 3).

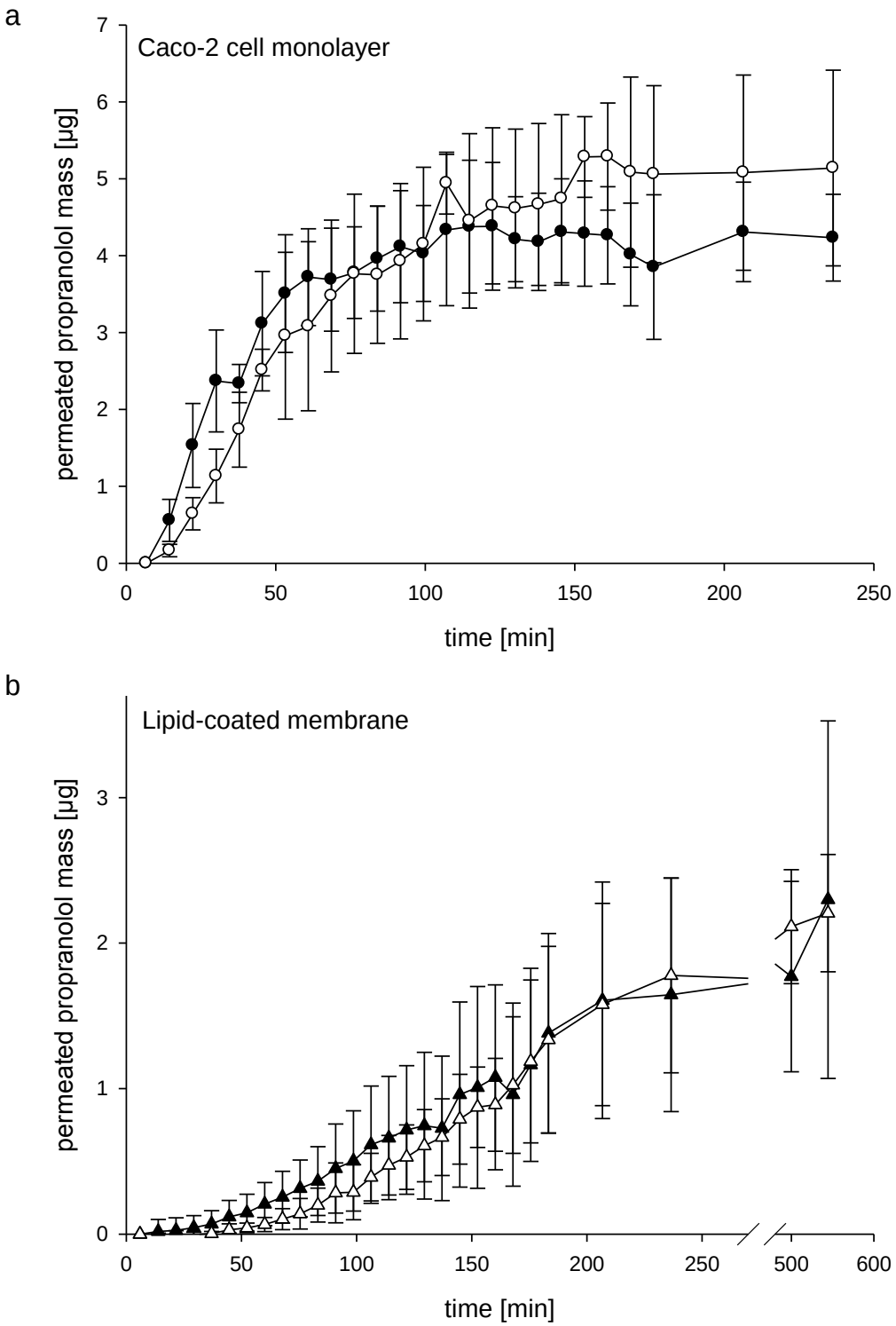

Figure 6.5. Permeated amount calculated from the drug concentration assessed at sampling port B for Caco-2 cell monolayers (a) and lipid-coated membranes (b). Closed symbols (●, ▲) represent immediate release tablets and open symbols (○, ∆) represent extended release tablets. Data are presented as mean ± SD (n ≥ 3).

6.3.4 Validation of extraction of propranolol from lipid coating

For a deeper evaluation of the function of the lipid coating and its behavior during the permeation process, the amount of propranolol in the lipid coating should be determined. For this purpose, a suitable extraction method was essential. As an extraction agent the mobile phase of the HPLC method for propranolol was chosen. In comparison to KRB as solvent, the determined concentrations for different stock solutions were similar with the mobile phase as solvent. Furthermore, the addition of Lipoid E 80 liposomes to the stock solution did not cause any differences in the determined concentrations and did not result in the introduction of additional peaks in the HPLC chromatogram. Therefore, a separation of liposomes after the extraction by means of ultracentrifugation was not mandatory. To check the extraction potential of the mobile phase a defined amount of propranolol was placed on the lipid-coated membrane. Afterwards, the complete Transwell® was subjected to the extraction process for 18 h. The recovery of propranolol was 107.4 ± 5.2 % of the applied amount. Thus, the extraction process was suitable for further investigation of the lipid coating.

6.3.5 Extraction of propranolol from lipid-coated membrane

For both release kinetic formulations the extracted mass of propranolol from the lipid coating shows a decrease over the time of experiment (Figure 6.6). After 1.7 h, the extracted mass is larger compared to the later time points. Furthermore, the mass found in the lipid coating when applying the IR tablet is higher than for the ER tablet at the first time point, but is not significantly different. This correlates well with the faster release and the therefore higher concentrations of propranolol present at the apical side of the permeation barrier. Moreover, the different extracted amounts reflect the differences in the permeated mass within the first two hours of experiments. After 5 h the extracted mass is almost similar for both formulations. Again, this can be linked well to the permeation profiles.

In addition, the total amount that can be extracted from the coating after 8 h is relatively high compared to the permeated amount (appr. 2 µg). This can also explain the lower permeated amounts of propranolol in comparison to Caco-2 cells. An extension of the experimental time may lead to higher permeated amounts due to an emptying of the depot. In addition, a greater back diffusion into

the apical compartment has also to be taken into consideration as the presence of a drug depot within the lipid coating leads to the creation of a concentration gradient in this direction. Further experiments should clarify and confirm this.

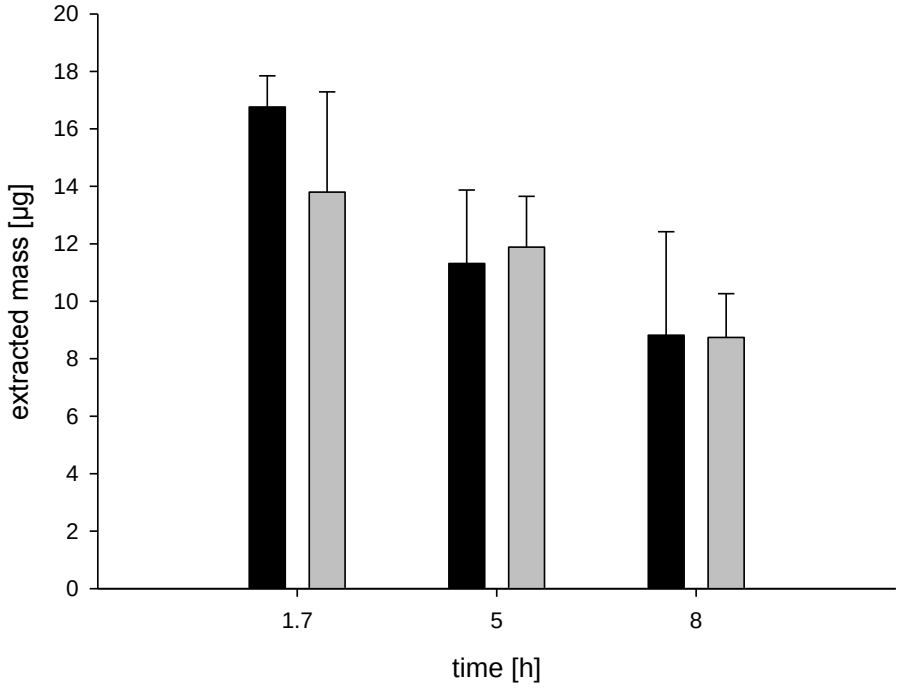

Figure 6.6. Extracted mass of propranolol from lipid-coated Transwells® after different time points in the d/p-system. Black bars represent experiments with immediate release tablets and grey bars with extended release tablets. Data are presented as mean ± SD (n = 3).

6.3.6 Assessment of dissolution and drug permeability of domperidone maleate

To prove the results obtained with propranolol tablets, the combined dissolution and permeation experiments were done with domperidone maleate tablets with and without TPGS.

As for the propranolol tablets, the dissolution profiles at sampling ports D and A for each formulation were first compared. The concentration time trends for each barrier and formulation are shown in Figure 6.7 and Figure 6.8. The apical peak is flatten and broadened as it was also found for propranolol tablets.

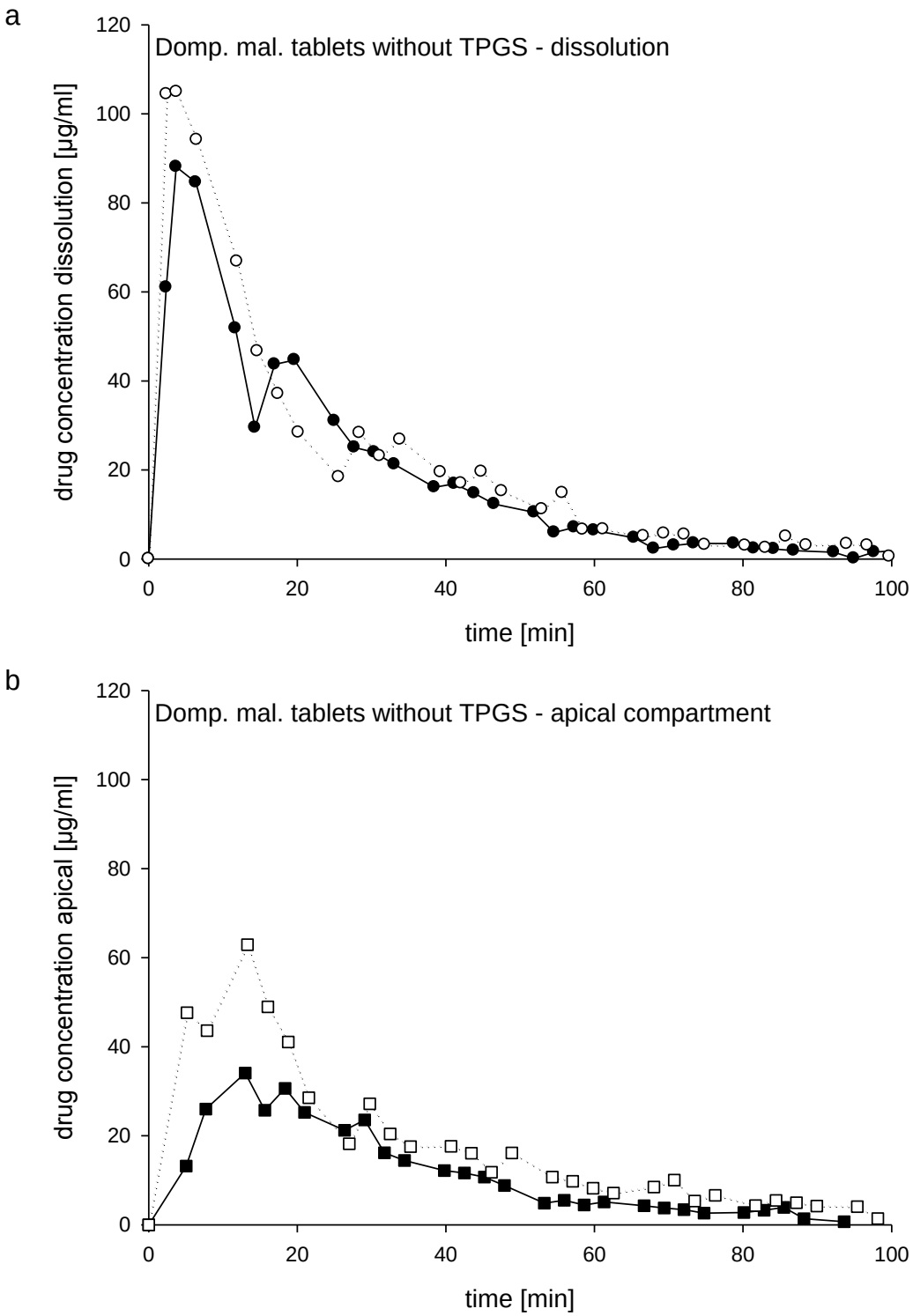

Figure 6.7. Concentration time trends for domperidone maleate tablets without TPGS at sampling port D (a) and A (b). Closed symbols (●, ■) represent the Caco-2 cell monolayer and open symbols (○, □) represent the lipid-coated membrane. For the sake of clarity, data are presented as mean (n ≥ 3) without SD.

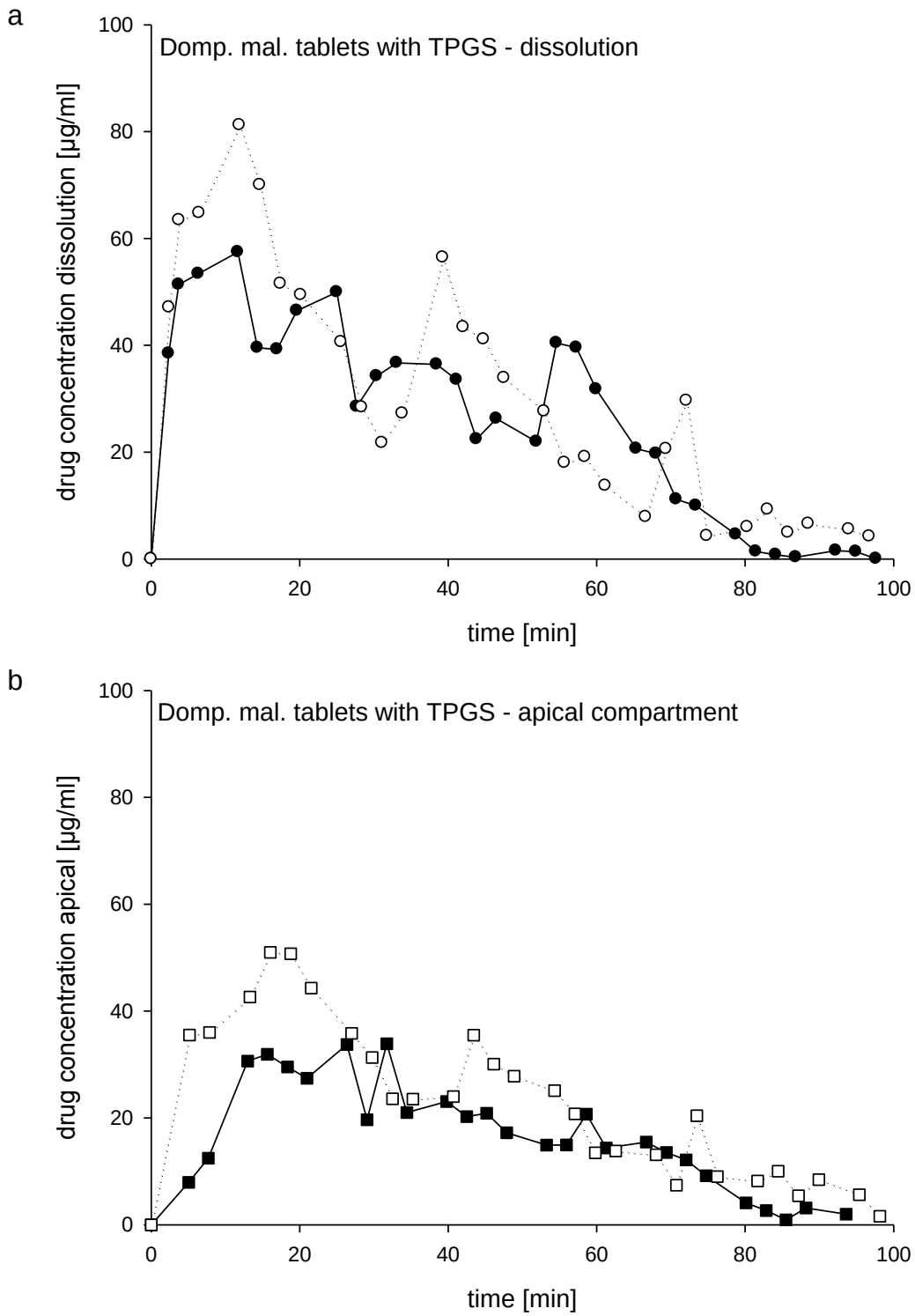

Figure 6.8. Concentration time trends for domperidone maleate tablets with TPGS at sampling port D (a) and A (b). Closed symbols (●, ■) represent the Caco-2 cell monolayer and open symbols (○, □) represent the lipid-coated membrane. For the sake of clarity, data are presented as mean (n ≥ 3) without SD.

Table 6.6 summarizes a comparison of typical equivalence parameters calculated for the apical side of the FTPC. Independent of the used permeation barrier and the dosage form the AUC, C_{max} and t_{max} do not show significant differences (ANOVA, $p \leq 0.05$) when considering each parameter. This confirms the independence of the dissolution from the used permeation barrier on the one hand and the similarity of the two formulations on the other hand. Only the AUC for tablets with TPGS shows a significant difference (t-test, $p \leq 0.001$) between Caco-2 cell monolayers and lipid-coated membranes. This can be also substantiated by the less controlled and reproducible release of domperidone maleate from tablets containing TPGS, as was already mentioned in Chapter 3.3.2, and associated differences in the total released amounts.

Table 6.6. Comparison of equivalence parameters in the apical compartment for different release kinetics and permeation barriers. Data are presented as mean ± SD ($n \geq 3$).

Parameter	Tablet without TPGS	Tablet with TPGS
AUC (Caco-2 cells)	1078.3 567.9	1424.9 ± 86.8
AUC (lipid-coated membrane)	1804.8 ± 601.5	2199.9 ± 129.2
C_{max} (Caco-2 cells)	48.8 30.6 µg/ml	36.8 ± 6.6 µg/ml
C_{max} (lipid-coated membrane)	74.7 ± 20.3 µg/ml	59.8 ± 24.1 µg/ml
t_{max} (Caco-2 cells)	13.0 5.3 min	19.2 ± 6.2 min
t_{max} (lipid-coated membrane)	8.5 ± 3.4 min	12.4 ± 6.9 min

For further comparison, the dissolution profiles were tested for similarity using the f_2 factor and the TDT. The results are summarized in Table 6.7. The profiles obtained at sampling port D show similarity between the used permeation barriers. For both tablets without and with TPGS the f_2 factor is greater than 50. Furthermore, the critical δ is low. These results confirm the comparison using equivalence parameters. However, the values for sampling port A indicate non-similarity between Caco-2 cell monolayers and lipid-coated membranes. The f_2 factor is below 50 and the critical δ is also high. This assumes an influence of the permeation barrier on the measured concentration in the apical compartment.

Using lipid-coated membranes also the C_{max} in the apical compartment is higher than with Caco-2 cell monolayers. Looking at the permeation profiles one can see that the permeation over Caco-2 cells is faster. Therefore, the concentration at the apical compartment decreases faster. Due to the construction of the FTPC and the sampling position the permeation of domperidone maleate has an influence on the measured apical concentration. As the lag time of the permeation using lipid-coated membranes is quite high, the change of concentration in the apical compartment is lower than for Caco-2 cell monolayers as less API is permeated. Hence, the permeation barrier has a great impact on the apical concentration of domperidone maleate resulting in non-similar concentration time trends. To avoid this, the position of sampling port A should be changed. A sampling directly before the FTPC and not after appears more reasonable and should lead to similar curves. This has to be verified in further experiments.

In comparison to propranolol, the lag time of the permeation is approximately two times higher using the lipid-coated membrane. So, the influence is more substantial for domperidone maleate, which is reflected in the similarity test results.

Table 6.7. Similarity test between Caco-2 cell monolayer and lipid-coated membrane for domperidone maleate tablets. Data marked with * indicate non-similarity.

Parameter	Dissolution		Apical compartment	
	Without TPGS	With TPGS	Without TPGS	With TPGS
Original time points	22	34	34	34
f_2	68.98	58.70	48.19*	41.81*
TDT (d = 5)	P > 0.5	P < 0.0005*	P < 0.0005*	P < 0.0005*
TDT (d = 10)	P > 0.5	P > 0.5	0.1	P < 0.0005*
Critical δ	2.9	5.8	9.1	12.5

The permeation profiles obtained with Caco-2 cell monolayers and lipid-coated membranes do not show a comparable pattern (Figure 6.9). The permeation of domperidone maleate released from TPGS-containing tablets showed a delay and

smaller permeated amounts at the end of the experiments using lipid-coated membranes. For the lipid-coated membrane one would expect that the permeation profiles do not differ between both domperidone formulations. The difference may be caused by the retention of domperidone in the lipid coating by TPGS. Furthermore, the affinity of domperidone to the lipid coating could be hindered by an inclusion into TPGS micelles. In general, the addition of TPGS could have, independently from efflux transporter effects, an influence on the partition coefficient as well as on the diffusion coefficient and thereby an effect on the permeability of domperidone maleate. The impact could vary between Caco-2 cell monolayers and lipid-coated membranes possibly explaining the different permeation profiles.

Furthermore, the permeation over the lipid-coated membrane shows a certain lag time at the beginning of the permeation process and a lower total permeated drug amount, as was the case for propranolol. Again, this can be explained by the thicker permeation barrier and the therefore longer diffusion pathway. In contrast to propranolol, the result could not be confirmed by different P_{app} values. In previous experiments with stock solutions, the permeability coefficient was almost the same for Caco-2 cell monolayers and lipid-coated membranes.

6.4 Conclusion

In comparison to Caco-2 cell monolayers, the lipid-coated membrane shows comparable results when analyzing solid oral dosage forms containing BCS class I substances. Differences were only detectable for the onset time of permeation, correlating with the thicker permeation barrier. Therefore, the lipid-coated membrane is suitable for analyzing tablets without previous disintegration and is a valuable alternative to Caco-2 cells. However, the evaluation of effects of excipients is not possible with the lipid-coated membrane and additional effects such as micellar inclusion may hamper the analysis. For deeper understanding and validation further investigations with different dosage forms should be carried out. In addition, the experiments with domperidone maleate demonstrate that the position of sampling port A is not optimal, which may lead to inaccurate results.

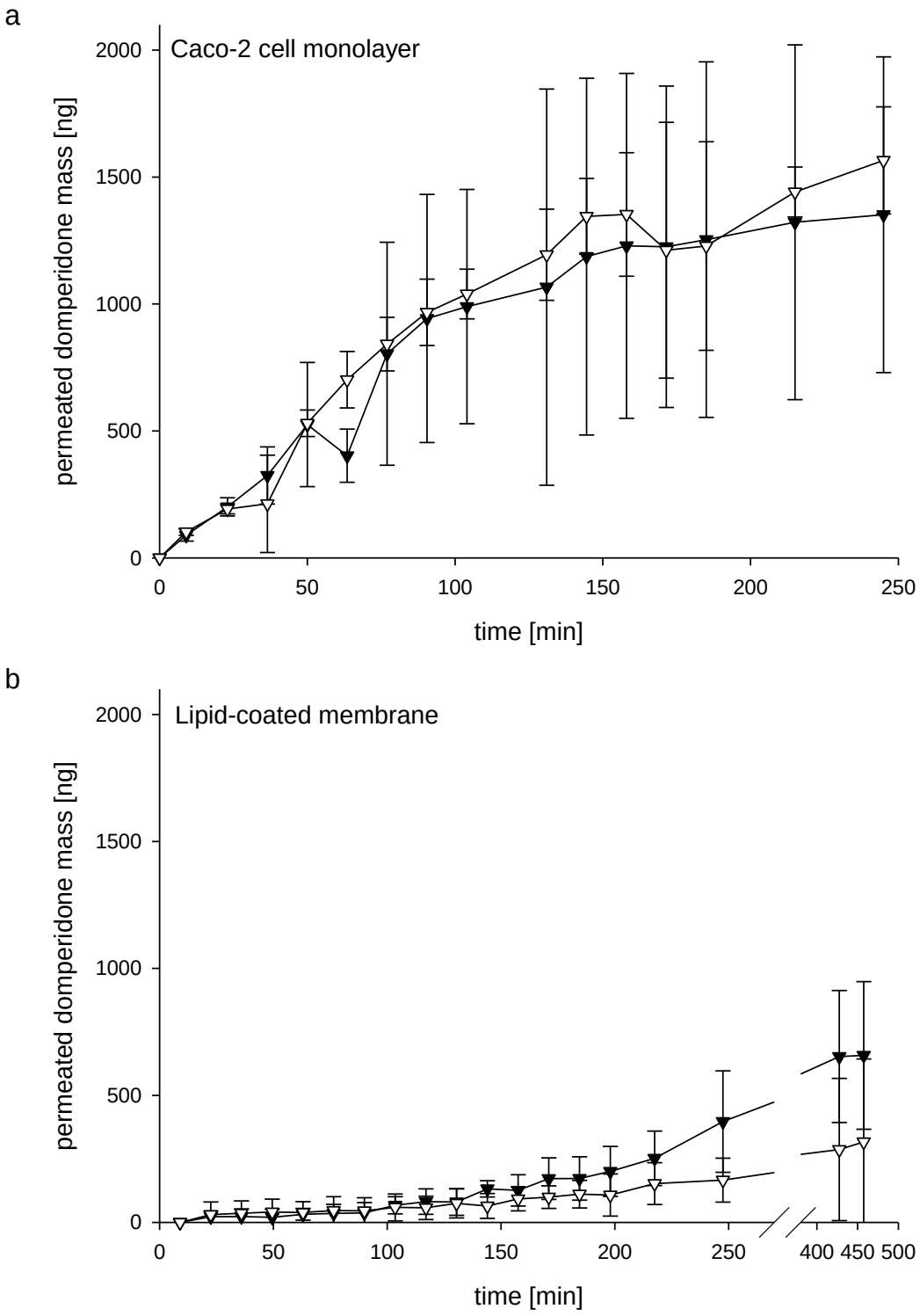

Figure 6.9. Permeated amount calculated from the drug concentration assessed at sampling port B for Caco-2 cell monolayers (a) and lipid-coated membranes (b). Closed symbols (●, ▲) represent tablets without TPGS and open symbols (○, Δ) represent tablets with TPGS. Data are presented as mean ± SD (n ≥ 3).

7 Mathematical modeling of the d/p-system

Statement of authorship contribution:

The following author contributed to this chapter:
Sandra P. Gantzsch, Dominik Selzer, José David Gómez-Mantilla, Ulrich F. Schaefer, Claus-Michael Lehr
The author of the thesis made the following contribution to this chapter.

1. Design of the project including formulation of problems to be tested and design of individual experiments:
   Contributed significantly

2. Planning of experiments and design of methods to answer the problems posed under # 1 including choice and development of the methods:
   Contributed significantly

3. Performance of experiments and data analysis:
   Contributed significantly

4. Presentation, interpretation and discussion of the results obtained in article form:
   Contributed significantly

7.1 Introduction

An in-depth understanding of the processes at the permeation barrier is missing. Consequently, a mathematical modeling of the permeation step appears to be a possibility to gain knowledge of the transport processes at the permeation barrier. Therefore, the dissolution step should be mathematically linked with the permeation step in a model. Such a model could then possibly be used to predict the permeation of e. g. ER formulations based on experimental data obtained from IR formulations. Thus, an adequate mathematical description of the system could also minimize the number of experiments which have to be performed. For this purpose in a first attempt, modeling of the dissolution as well as the permeation step was tested in the below described way.

7.2 Methods

Dissolution and permeation data of IR and ER tablets obtained with Caco-2 cells as described in Chapter 6 were used for the following fittings.

As a first step, dissolution data (D) was fitted to the Weibull function [96] with scale parameter k_1, shape parameter k_2 and applied dose M_{inf} according to equation 6 using a nonlinear least square fit. The applied dose was considered unknown due to the variability of propranolol content in the tablets.

$$D(t) = \left(1 - e^{-(k_1 * t)^{k_2}}\right) * M_{inf} \qquad \text{(eq. 6)}$$

Afterwards, a pharmacokinetic model of the d/p-system was set up based on three compartments as depicted in Figure 7.1. The following processes were modeled:

a) The dissolution and the flow from the dissolution cell to the sampling port D was the first part.
b) The transfer from D to the apical compartment including the stream splitter was modeled assuming a delay of approximately 3 min.
c) The transport from the apical to the basolateral compartment was modeled according to a first order kinetic with a constant rate.

d) Furthermore, the flow into the waste from the dissolution and the apical compartment was considered.

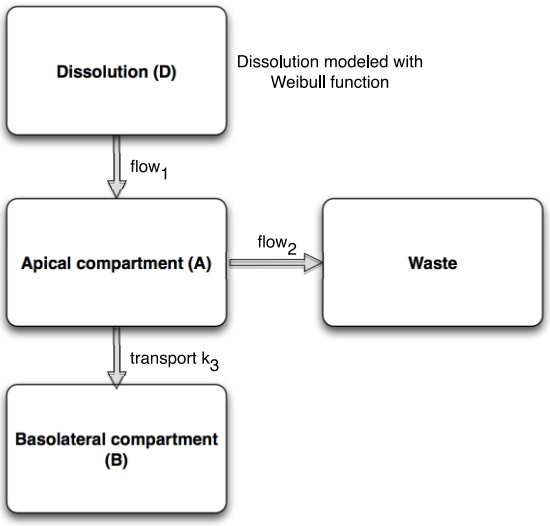

Figure 7.1. Simple illustration of the pharmacokinetic compartment model of the d/p-system.

The model resulted in the following three equations for dissolution (D, equation 5), the apical compartment (A, equation 6) and the basolateral compartment (B, equation 7). The parameters k_1, k_2 and M_{inf} are the Weibull parameters determined as described above. The flow rates between the compartments were entered in the formulas with 6.5 ml/min ($flow_1$) and 1.0 ml/min ($flow_2$). Furthermore, the volume of each compartment is described with V_D for the dissolution and V_A for the apical part. The transport parameter k_3 was determined by nonlinear least square fitting. When it comes to least squares, the basolateral masses were weighted with the average mass of the apical compartment for the fitting procedure to emphasize the impact of these data in comparison to the apical data.

$$\frac{dD}{dt} = k_1^{k_2} * k_2 * t^{(k_2-1)} * e^{-(k_1*t)^{k_2}} * M_{inf} - D * \frac{flow_1}{V_D} \qquad \text{(eq. 7)}$$

$$\frac{dA}{dt} = \frac{1}{6.5} * D * \frac{flow_1}{V_D} - A * k_3 - A * \frac{flow_2}{V_A} \qquad \text{(eq. 8)}$$

$$\frac{dB}{dt} = A * k_3 \qquad \text{(eq. 9)}$$

This set of differential equations (eq. 7-9) was solved numerically with a Runge-Kutta 4th order method.

In order to get insight into the potential to predict the permeation of API released from an ER formulation based on experiments with IR formulations, the Weibull parameters from the dissolution of the ER tablets and the transfer parameter k_3 of the IR tablets fitting were used.

7.3 Results and discussion

Fitting of the dissolution data resulted in the Weibull parameters k_1 and k_2 listed in Table 7.1. P-values for all parameters were below 0.001. As expected due to the different release kinetics, the scale parameter k_1 differs between the IR and the ER tablet by a factor of approximately 3. The shape parameter and the applied dose were comparable. The corresponding plots of the fits and the experimental data are shown in Figure 7.2.

Table 7.1. Overview of Weibull parameters. Data are presented as mean ± SE (n ≥ 3).

	IR tablet	ER tablet
K_1	5.722 ± 0.08 * 10^{-2}	2.03 ± 0.02 * 10^{-2}
K_2	1.13 ± 0.02	1.13 ± 0.01
M_{inf}	1.84 ± 0.004 * 10^4 µg	1.85 ± 0.006 * 10^4 µg

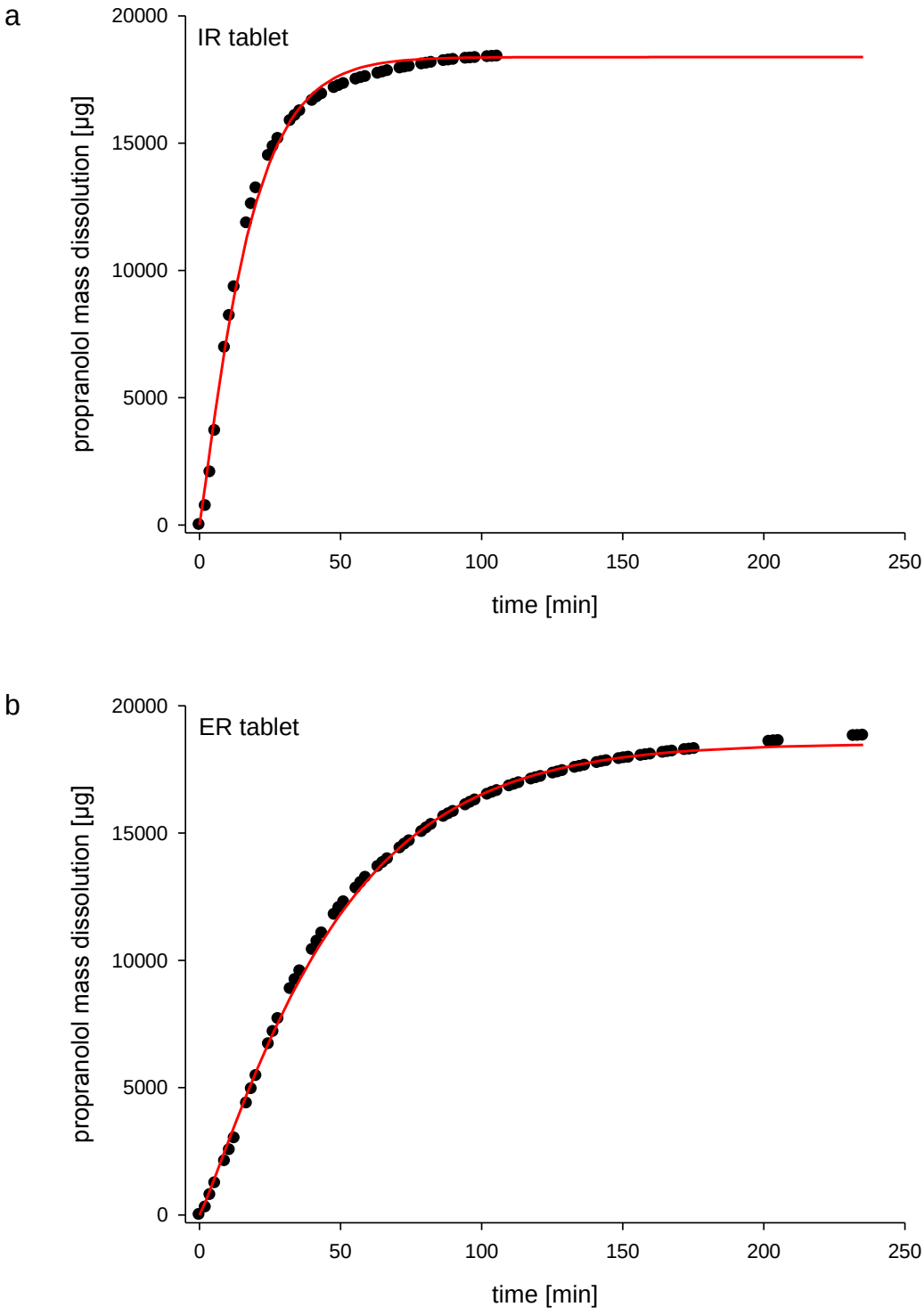

Figure 7.2. Experimental data of dissolved cumulative mass (●) for an IR formulation (a) and an ER formulation (b) and the corresponding fits of the Weibull function (solid lines).

Both experimental and fitted data matched well together for IR as well as ER tablets. The fitted k_3 values for the IR tablet was $2.49 \pm 0.31 * 10^{-4}$ and for the ER tablet $3.10 \pm 0.22 * 10^{-4}$. As expected, only minor differences between the two k_3 values could be observed. Therefore, using k_3 from experiments with the IR formulation showed the potential to predict the permeation of an ER formulation (Figure 7.3). On the one hand, as depicted in Figure 7.3 a the amount of substance in the apical compartment was slightly overpredicted for later time points. On the other hand, for late times the permeation was slightly underpredicted (see Figure 7.3 b). It seems meaningful to use a greater amount of experimental data to improve the predictive capacities of the model. Furthermore, diffusion processes in the tubings could be included besides the transport, which was only taken into consideration in this attempt.

7.4 Conclusion

In this first attempt, a mathematically modeling of the processes in the d/p-system was successfully performed and employment of a three compartment model was successfully achieved. A prediction of the permeation of API released from an ER formulation based on IR data was possible. However, the results should be confirmed and the model should be improved. This comprises further collection and inclusion of experimental data as well as a profound analysis of possible predictive capabilities. The behavior of critical points like the splitter should be carefully investigated from a modeling perspective. Furthermore, a variability analysis of the fitted parameters should be performed to estimate the predictive power of the model.

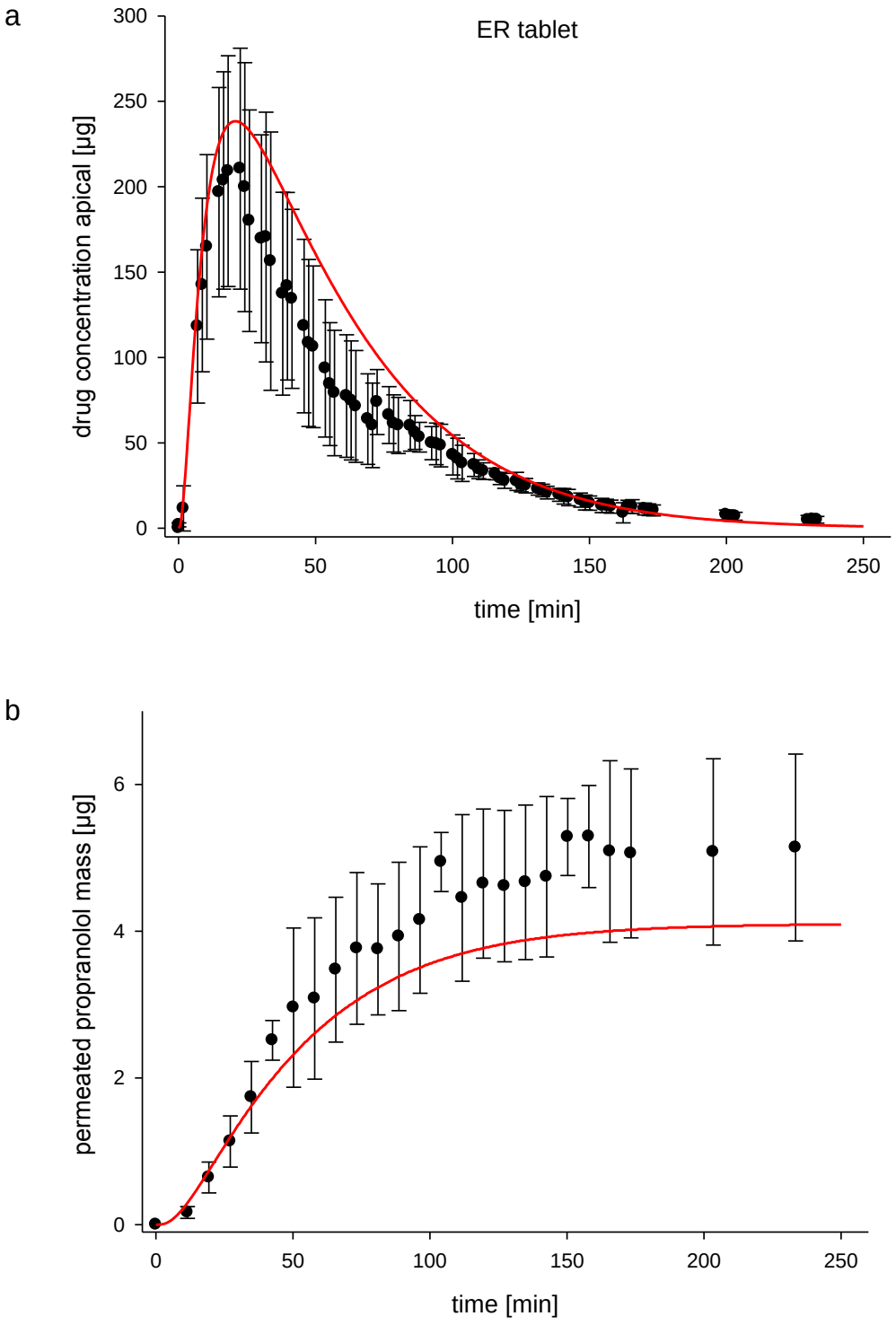

Figure 7.3. Experimental data (●) of the concentration in the apical compartment (a) and the permeated mass (b) for an ER formulation corresponding predictions (solid lines). Data presented as mean ± SD (n ≥ 3).

8 Summary and outlook

Bioavailability of solid oral dosage forms is mainly influenced by the liberation and absorption of the drug. As surrogate for these *in vivo* parameters mostly two *in vitro* assays are performed: dissolution testing quantifying liberation of the drug, and *in vitro* permeability assays based on cell cultures, especially the cell line Caco-2 resembling features of the intestinal epithelium. Although these assays are well-established and considered as standard methods, they are conducted separately. Therefore, they do not allow for drawing of direct correlations between dissolution and permeation parameters. To overcome this problem, a system combining both assays was developed in our laboratory by Motz [97] and further improved by Muendoerfer [98]. The aim of the present work was to evaluate further application fields for this d/p-system.

In the first part of this thesis, the suitability of the d/p-system to analyze effects of excipients was tested with drug solutions as well as with solid oral dosage forms. Here, the main focus was on the inhibition of P-gp with TPGS. Inhibiting P-gp in the FTPC, a trend to higher permeated amounts and P_{app} values was found, even though a significant difference could not be detected for all investigated substances. Considering only the absorptive transport direction, which is rather important for the *in vivo* situation, an inhibition ratio of 0.9 to 1.5 was found under dynamic flow conditions in comparison to a ratio of 1.6 to 3.1 under classical static conditions using drug solutions. The smaller ratios under dynamic conditions are likely resulting from greater standard deviations blurring the inhibitory effect. Although it was possible to detect an effect using domperidone solutions, this could not be found in the first attempts with tablets without and with TPGS. Dissolutions profiles of both formulations were different but the permeation profiles did not show a difference. Therefore, at that point it cannot be stated clearly if the d/p-system is suitable for testing of effects of excipients. These results have to be confirmed by additional studies modifying the dosage form and the test conditions.

Even though Caco-2 cells represent a well-established and validated model for the performance of *in vitro* permeability testing, they are associated with significant disadvantages including long cultivation time or compatibility with dissolution

media like FaSSIF or FeSSIF. Therefore as the second part of this work, a non-cellular alternative permeation barrier suitable for use in the FTPC was developed and characterized. For this purpose, cell culture inserts were coated with lipid using a centrifugation method. As suitable lipid Lipoid E 80, mainly consisting of egg phosphatidylcholine, was applied to the membrane as liposomes.

The stability against permeation medium as well as the coating procedure was tested using different techniques such as TEER measurement, light microscopy, scanning electron microscopy and Raman microscopy. Constant levels of the TEER value were monitored online over 18 h confirming the long term stability of the coating under experimental conditions. Furthermore, Raman images visualize the complete pore filling with lipid and verified the stability of the lipid coating. Moreover, first experiments showed the stability of the lipid coating against FaSSIF but not against FeSSIF. This needs further investigation in order to overcome the limited ability to use simulated intestinal fluid in the developed model.

After successful characterization of the lipid coating, the applicability for transport experiments was tested under classical static and dynamic flow conditions in direct comparison to Caco-2 cells with drug solutions. Both barriers were able to distinguish between highly, medially and lowly permeable substances. Especially under dynamic flow conditions, the lipid-coated membrane showed a good correlation to Caco-2 cells, confirming the specific suitability for this purpose. Furthermore, also the suitability for tablet testing was analyzed. For propranolol IR and ER tablets, dissolution as well as permeation profiles were comparable to Caco-2 cells. However, with domperidone maleate the result was not as clear as for propranolol requiring further investigation. The results of the applicability test of the artificial membrane for the assessment of tablets seemed promising as a basis for further studies.

In summary, a simple and reproducible coating procedure was found which resulted in the production of a stable and robust lipid coating. In comparison to Caco-2 cell monolayers the lipid-coated membranes showed a good correlation with regard to the permeability using different drug solutions as well as solid oral dosage forms. Therefore, this non-cellular model holds the potential for versatile applications for solid dosage form testing in the d/p-system including extended

release formulations and it has some advantages over Caco-2 cell monolayers such as the possibility of long term studies.
Besides the above mentioned points, dissolution and permeation experiments evaluating the influence of food are of interest for further studies using the lipid-coated membrane and FaSSIF as dissolution medium.

Furthermore, an in-depth understanding of the processes occuring at the permeation barrier is missing. Consequently, mathematical modeling of the permeation step appears a possibility to gain knowledge of the processes at the permeation barrier. In a first attempt the modeling of the d/p-system was tested using a three compartment model and was successfully implemented. With such a model prediction of permeation is possible. Further investigations such as increasing the number of experimental data are necessary to improve the predictive power of the model.

For research as well as industrial applications the d/p-system with Caco-2 cells and lipid-coated membranes could be a valuable addition to standard methods of dissolution and permeation testing especially with respect to possible interactions of both parameters. For further rating and potentially improvement of the benefit of the d/p-system one of the most important parameters which has to be clarified in following experiments is the evaluation of an *in vitro in vivo* correlation. Different formulations having a clear effect on the permeation of the API in *in vivo* experiments should be tested in the combined system.

9 Zusammenfassung und Ausblick

Die Bioverfügbarkeit von festen oralen Arzneiformen wird hauptsächlich durch die Freisetzung und die Absorption des Wirkstoffes beeinflusst. Als Surrogat für diese *in vivo* Parameter werden meist zwei *in vitro* Assays verwendet: Dissolutionstest in Bezug auf die Freisetzung des Wirkstoffes und *in vitro* Permeabilitätstests basierend auf Zellkulturen insbesondere die Caco-2 Zelllinie, welche den Eigenschaften des Darms ähnlich ist. Auch wenn diese Testmethoden gut etabliert sind und als Standardmethoden angesehen werden, werden sie separat durchgeführt. Um dieses Problem zu umgehen wurde in unserem Labor durch Motz [97] ein System entwickelt, welches beide Parameter kombiniert, und durch Mündörfer [98] weiter verbessert. Das Ziel dieser Arbeit war es weitere Anwendungsmöglichkeiten dieses d/p-Systems zu untersuchen.

Im ersten Teil dieser Arbeit wurde mit Wirkstofflösungen als auch mit festen oralen Arzneiformen die Eignung des d/p-Systems zur Analyse von Hilfsstoffeffekten getestet. Dabei lag der Hauptfokus auf der Hemmung des P-Glykoproteins (P-gp) durch TPGS. In der FTPC kann ein Trend zu höheren permeierten Mengen und P_{app} Werten unter P-gp-Hemmung gefunden werden, auch wenn nicht für alle untersuchten Substanzen ein statistisch signifikanter Unterschied bestimmt werden konnte. Unter alleiniger Berücksichtigung der absorptiven Transportrichtung, welche für die *in vivo* Situation eher wichtig ist, wurde bei Verwendung von Wirkstofflösungen unter dynamischen Flussbedingungen ein Hemmverhältnis von 0,9 bis 1,5 gefunden im Vergleich zu einem Verhältnis von 1,6 bis 3,1 unter klassischen statischen Bedingungen. Die geringeren Verhältnisse unter dynamischen Bedingungen resultieren wahrscheinlich aus den größeren Standardabweichungen, welche einen inhibitorischen Effekt verschleiern. Obwohl es mit Domperidonlösungen möglich war einen Hemmeffekt zu bestimmen, konnte dies in ersten Versuchen mit Tabletten, welche TPGS enthalten oder nicht enthalten, nicht gefunden werden. Die Freisetzungsprofile beider Formulierungen waren unterschiedlich, aber die Permeationsprofile zeigten keine Unterschiede. Daher kann an diesem Punkt nicht genau festgelegt werden, ob das d/p-System zur Analyse von Hilfsstoffeffekten geeignet ist. Die Ergebnisse müssen in

zusätzlichen Untersuchungen mit modifizierten Arzneiformen und Testbedingungen bestätigt werden.

Obgleich Caco-2 Zellen ein gut etabliertes und validiertes Model zur Durchführung von *in vitro* Permeationstests darstellen, haben sie einige Nachteile wie lange Kultivierungszeiten und Verträglichkeit von Dissolutionsmedien wie FaSSIF und FeSSIF. Aus diesem Grund sollte im zweiten Teil dieser Arbeit eine nicht zelluläre Alternative, welche für den Einsatz in der FTPC geeignet ist, entwickelt und charakterisiert werden. Zu diesem Zweck wurden Zellkultureinsätze mit einem Lipid mittels Zentrifugation beschichtet. Als geeignetes Lipid wurde Lipoid E 80, welches hauptsächlich aus Eiphosphatidylcholin besteht, in Form von Liposomen auf die Membrane aufgetragen.
Die Stabilität gegenüber Permeationsmedien wie auch das Beschichtungsverfahren wurde mittels verschiedener Methoden wie der TEER-Messung, Licht-, Elektronen- und Raman-Mikroskopie untersucht. Konstante TEER-Wert-Level wurden über 18 h unter experimentellen Bedingungen aufgezeichnet, welche die Langzeitstabilität der Beschichtung bestätigen. Weiterhin machten Raman-Bilder eine komplette Füllung der Membranporen mit Lipid sichtbar und verifizierten die Stabilität der Lipidbeschichtung. Darüber hinaus zeigten erste Versuche, dass die Beschichtung gegenüber FaSSIF stabil ist nicht jedoch gegenüber FeSSIF. Dies bedarf weiterer Untersuchungen um den eingeschränkten Einsatz von künstlichen Darmflüssigkeiten zu beseitigen.
Nach erfolgreicher Charakterisierung der Lipidbeschichtung wurde die Anwendbarkeit für Transportversuche unter klassischen statischen und dynamischen Flussbedingungen im direkten Vergleich zu Caco-2 Zellen unter Nutzung von Wirkstofflösungen getestet. Mit beiden Barrieren war es möglich zwischen schnell, mittel und langsam permeierenden Substanzen zu unterscheiden. Insbesondere unter dynamischen Flussbedingungen zeigte die lipid-beschichte Membran eine gute Korrelation zu Caco-2 Zellen, welches die spezielle Eignung für diesen Zweck bestätigt. Des Weiteren wurde die Anwendbarkeit zur Analyse von Tabletten untersucht. Sowohl die Dissolutions- als auch die Permeationsprofile von schnell und langsam freisetzenden Propranololtabletten waren vergleichbar mit Caco-2 Zellen. Dieses Ergebnis war

jedoch bei Domperidontabletten nicht genauso eindeutig, was weitere Untersuchungen erfordert.
Zusammenfassend wurde ein einfaches und reproduzierbares Beschichtungsverfahren gefunden, welches in stabilen und robusten Lipidbeschichtungen resultiert. Im Vergleich zu Caco-2-Zell Monoschichten zeigten die lipid-beschichteten Membranen in Bezug auf die Permeabilität eine gute Korrelation sowohl unter Verwendung von Wirkstofflösungen als auch von festen oralen Arzneiformen. Daher hat dieses nicht zellulare Model das Potential für eine vielseitige Anwendung in Bezug auf Analyse fester Arzneiformen im d/p-System, darin eingeschlossen langsam freisetzende Formulierungen, und es hat einige Vorteile gegenüber Caco-2 Zellen wie zum Beispiel die Möglichkeit von Langzeituntersuchungen.
Neben den oben genannten Punkten ist außerdem die Untersuchung des Einflusses von Nahrung auf die Dissolution und Permeation unter Nutzung der lipid-beschichteten Membrane und FaSSIF für weitere Studien von Interesse.

Des Weiteren fehlen bisher tiefergehende Erkenntnisse der Prozesse an der Permeationsbarriere. Folglich erscheint ein mathematisches Model des Permeationsschrittes als eine Möglichkeit um Wissen über diesen Prozess zu erlangen. In einem ersten Versuch wurde die Modellierung des d/p-Systems mit Hilfe eines drei Kompartimenten Models getestet und erfolgreich umgesetzt. Mittels solch eines Models ist die Vorhersage der Permeation möglich. Weiter Untersuchungen wie z. B. die Erhöhung der Anzahl experimenteller Daten ist notwendig um die Vorhersagekraft zu verbessern.

Für Forschungszwecke als auch für industrielle Anwendungen kann das d/p-System mit Caco-2 Zellen und lipid-beschichteten Membrane eine wertvolle Alternative zu den standardisierten Dissolutions- und Permeationstests darstellen, insbesondere in Hinblick auf mögliche Interaktionen zwischen beiden Parametern.
Um den Nutzen des d/p-systems weiter zu bewerten und möglicherweise zu verbessern einer der wichtigsten Parameter, der in folgenden Experimenten geklärt warden sollte, ist die Untersuchung von *in vitro in vivo* Korrelationen. Verschiedene Formulierungen, welche in *in vivo* Versuchen einen eindeutigen

Effekt auf die Permeation des Wirkstoffes zeigen, sollten in dem kombinierten System getested werden.

10 Annexes

10.1 Quantification of drug substances

Quantification of drug substances were performed according to already validated in-house protocols (furosemide, propranolol, rhodamine 123, sodium fluorescein) or were developed and validated partially based on methods described in literature (atenolol [99], domperidone [100], talinolol [101], TPGS [102]).
HPLC quantification was performed with a Dionex system (Thermo Fisher GmbH, Idstein, Germany) consisting of a Dionex ISO-3100A pump, a Dionex WPS-3000 TSL autosampler, a Dionex VWD-3400 variable wavelength detector, a Dionex TCC-3000 column compartment and a Dionex SRD-3200 solvent rack. The system ran on Chromeleon software version 6.80 SP2.

10.1.1 Quantification of atenolol

Quantification was performed with an RP-18 select B (LiChrospher® 60, Merck), 5 µm, 12.5 cm column. The mobile phase was composed of 90 % (v/v) acid water, 5 % (v/v) methanol and 5 % (v/v) acetonitrile. The oven temperature was 40 °C and the flow rate was set to 1.2 ml/min. Detection was performed with a fluorescence detector (L-2480, Merck Hitachi) at an excitation wavelength of 231 nm and an emission wavelength of 307 nm. Linearity ($R > 0.999$) was given between 4 ng/ml and 1 µg/ml. The retention time was 5.2 ± 0.1 min.

10.1.2 Quantification of domperidone (maleate)

Domperidone and domperidone maleate were quantified with an RP-18e (LiChrospher® 100, Merck), 5 µm, 12.5 cm column. The mobile phase consisted of 50 % (v/v) water and 50 % (v/v) phosphate buffer pH 2.3. The oven temperature was 40 °C and the flow rate was set to 1.0 ml/min. Detection was performed with UV at 285 nm. Linearity ($R > 0.9989$) was given between 20 ng/ml and 1000 ng/ml. The retention time was 2.6 ± 0.1 min.

10.1.3 Quantification of furosemide

Quantification of furosemide was performed with an RP-18 select B (LiChrospher® 60, Merck), 5 µm, 12.5 cm column. The mobile phase was composed of 60 % (v/v) water, 30 % (v/v) acetonitrile, 10 % (v/v) methanol, 0.033 % (v/v) triethylamine and 0.044 % (v/v) phosphoric acid. The oven temperature was 40 °C and the flow rate was set to 1.2 ml/min. Detection was performed with UV at 235 nm. Linearity (R > 0.999) was given between 25 ng/ml and 4000 ng/ml. The retention time was 3.0 ± 0.1 min.

10.1.4 Quantification of propranolol

Propranolol was quantified with an RP-18 (LiChrospher® 100, Merck), 5 µm, 12.5 cm column. The mobile phase was composed of 45 % (v/v) water, 22 % (v/v) acetonitrile, 33 % (v/v) methanol, 0.033 % (v/v) triethylamine and 0.044 % (v/v) phosphoric acid. The oven temperature was 40 °C and the flow rate was set to 1.2 ml/min. Detection was performed with UV at 215 nm. Linearity (R > 0.999) was given between 30 ng/ml and 100 µg/ml. The retention time was 3.0 ± 0.2 min.

10.1.5 Quantification of talinolol

Quantification of talinolol was performed with an RP-18 select B (LiChrospher® 60, Merck), 5 µm, 12.5 cm column. The mobile phase consisted of 77 % (v/v) triethylammonium phosphate (0.025 mol/l) and 23 % (v/v) acetonitrile. The oven temperature was 40 °C and the flow rate was set to 1.2 ml/min. Detection was performed with a fluorescence detector (L-2480, Merck Hitachi) (λ_{exc}= 252 nm, λ_{em}= 332 nm). Linearity (R > 0.999) was given between 3 ng/ml and 1000 ng/ml. Retention time was 5.7 ± 0.1 min.

10.1.6 Quantification of TPGS

Quantification of TPGS was performed with an RP-8 (LiChrospher® 100, Merck), 5 µm, 12.5 cm column. The mobile phase consisted of 90 % (v/v) of a 2-propanol/acetonitrile mixture (50:50) and 10 % (v/v) ammonium acetate (5 mM). The oven temperature was 40 °C and the flow rate was set to 1.0 ml/min.

Detection was performed with UV at 285 nm. Linearity (R > 0.999) was given between 1.25 µg/ml and 400 µg/ml. Retention time was 2.4 ± 0.1 min.

10.1.7 Quantification of rhodamine 123

Quantification of rhodamine 123 was performed using a fluorescence plate reader (TECAN infinite M200, Tecan GmbH, Crailsheim, Germany; λ_{exc} = 480 nm, λ_{em} = 530 nm). Linearity (R > 0.999) was given between 4 ng/ml and 200 ng/ml.

10.1.8 Quantification of sodium fluorescein

Quantification of sodium fluorescein was performed using a fluorescence plate reader (TECAN infinite M200, Tecan GmbH, Crailsheim, Germany; λ_{exc} = 485 nm, λ_{em} = 530 nm). Linearity (R > 0.999) was given between 5 ng/ml and 1000 ng/ml.

10.2 Programming codes for SIA automation

10.2.1 SIA programs for propranolol

Main routine propranolol

Delay (sec) 101
Insert File C:\Programme\WINFIA 5.0\Marco\Propranolol Programme\subroutinen\Probenzug dissolution 25- neuer Propenzug.fia
Insert File C:\Programme\WINFIA 5.0\Marco\Propranolol Programme\subroutinen\Probenzug apical 25- neuer Probenzug.fia
Insert File C:\Programme\WINFIA 5.0\Marco\Propranolol Programme\subroutinen\Probenzug dissolution 25- neuer Propenzug.fia
Insert File C:\Programme\WINFIA 5.0\Marco\Propranolol Programme\subroutinen\Probenzug apical 25- neuer Probenzug.fia
Insert File C:\Programme\WINFIA 5.0\Marco\Propranolol Programme\subroutinen\Probenzug dissolution 25- neuer Propenzug.fia

Variable Define New sampos
sampos = 1
Insert File C:\Programme\WINFIA 5.0\Marco\Propranolol Programme\subroutinen\Propranolol_basolateral_new_compartment_ new_valve.fia

Loop Start (#) 22
sampos += 1
Insert File C:\Programme\WINFIA 5.0\Marco\Propranolol Programme\subroutinen\Probenzug dissolution 25- neuer Propenzug.fia
Insert File C:\Programme\WINFIA 5.0\Marco\Propranolol Programme\subroutinen\Probenzug apical 25- neuer Probenzug.fia
Insert File C:\Programme\WINFIA 5.0\Marco\Propranolol Programme\subroutinen\Probenzug dissolution 25- neuer Propenzug.fia
Insert File C:\Programme\WINFIA 5.0\Marco\Propranolol Programme\subroutinen\Probenzug apical 25- neuer Probenzug.fia
Insert File C:\Programme\WINFIA 5.0\Marco\Propranolol Programme\subroutinen\Probenzug dissolution 25- neuer Propenzug.fia
Insert File C:\Programme\WINFIA 5.0\Marco\Propranolol Programme\subroutinen\Probenzug apical 25- neuer Probenzug.fia
Insert File C:\Programme\WINFIA 5.0\Marco\Propranolol Programme\subroutinen\Propranolol_basolateral_new_ compartment_ new_valve.fia

Loop End

Loop Start (#) 10
sampos += 1
Delay (sec) 1325
Insert File C:\Programme\WINFIA 5.0\Marco\Propranolol Programme\subroutinen\Probenzug dissolution 25- neuer Propenzug.fia
Insert File C:\Programme\WINFIA 5.0\Marco\Propranolol Programme\subroutinen\Probenzug apical 25- neuer Probenzug.fia
Insert File C:\Programme\WINFIA 5.0\Marco\Propranolol Programme\subroutinen\Probenzug dissolution 25- neuer Propenzug.fia
Insert File C:\Programme\WINFIA 5.0\Marco\Propranolol Programme\subroutinen\Probenzug apical 25- neuer Probenzug.fia
Insert File C:\Programme\WINFIA 5.0\Marco\Propranolol Programme\subroutinen\Probenzug dissolution 25- neuer Propenzug.fia
Insert File C:\Programme\WINFIA 5.0\Marco\Propranolol Programme\subroutinen\Probenzug apical 25- neuer Probenzug.fia
Insert File C:\Programme\WINFIA 5.0\Marco\Propranolol Programme\subroutinen\Propranolol_basolateral_new_ compartment_ new_valve.fia

Loop End

Subroutine for sampling port D (dissolution)

```
Syringe Pump Valve In
        Syringe Pump Flowrate (microliter/sec) 250
        Syringe Pump Aspirate (microliter) 1000
Multiposition Valve dissolution
        Syringe Pump Delay Until Done
Syringe Pump Valve Out
        Syringe Pump Flowrate (microliter/sec) 100
```

Syringe Pump Aspirate (microliter) 50
Syringe Pump Delay Until Done
Multiposition Valve waste
Syringe Pump Flowrate (microliter/sec) 200
Syringe Pump Dispense (microliter) 100
Syringe Pump Delay Until Done

Multiposition Valve dissolution
Syringe Pump Flowrate (microliter/sec) 25
Syringe Pump Aspirate (microliter) 25
Syringe Pump Delay Until Done

Multiposition Valve PMT-FL
Syringe Pump Flowrate (microliter/sec) 50
Syringe Pump Empty

Analyte New Sample
Analyte Name dissolution

PMT Start Scans
Syringe Pump Delay Until Done
PMT Stop Scans

Subroutine for sampling port A (apical)

Syringe Pump Valve In
Syringe Pump Flowrate (microliter/sec) 500
Syringe Pump Aspirate (microliter) 1000
Syringe Pump Delay Until Done
Syringe Pump Valve Out
Multiposition Valve apical
Syringe Pump Flowrate (microliter/sec) 15
Syringe Pump Aspirate (microliter) 100
Syringe Pump Delay Until Done
Multiposition Valve waste
Syringe Pump Flowrate (microliter/sec) 200
Syringe Pump Dispense (microliter) 200
Syringe Pump Delay Until Done

Multiposition Valve apical
Syringe Pump Flowrate (microliter/sec) 15
Syringe Pump Aspirate (microliter) 25
Syringe Pump Delay Until Done

Multiposition Valve PMT-FL
Syringe Pump Flowrate (microliter/sec) 50
Syringe Pump Empty

Analyte New Sample
Analyte Name apical

PMT Start Scans
Syringe Pump Delay Until Done
PMT Stop Scans

Subroutine for sampling port B (basolateral)

autosampler Command: Set Port 5

Basolateral Pump Valve In
Basolateral Pump Flowrate (microliter/sec) 50
Basolateral Pump Aspirate (microliter) 325
Basolateral Pump Delay Until Done
Basolateral Pump Valve Out
Basolateral Valve Akzeptorkompartiment
Basolateral Pump Flowrate (microliter/sec) 10
Basolateral Pump Aspirate (microliter) 100
Basolateral Pump Delay Until Done
Basolateral Valve Abfall
Basolateral Pump Dispense (microliter) 125
Basolateral Pump Delay Until Done
Basolateral Valve 6
autosampler Wash

```
        Basolateral Pump Flowrate (microliter/sec) 10
        Basolateral Pump Aspirate (microliter) 25
        Basolateral Pump Delay Until Done

Basolateral Valve Akzeptorkompartiment
        Basolateral Pump Aspirate (microliter) 100
        Basolateral Pump Delay Until Done

Basolateral Valve 6
        Basolateral Pump Aspirate (microliter) 25
        Basolateral Pump Delay Until Done

autosampler standard rack (sample #) 10
Delay (sec) 3
Basolateral Valve Probensammler
        Basolateral Pump Flowrate (microliter/sec) 20
        Basolateral Pump Dispense (microliter) 220
        Basolateral Pump Delay Until Done

autosampler RACK 2 (sample #) = sampos
Delay (sec) 3
        Basolateral Pump Dispense (microliter) 110
        Basolateral Pump Delay Until Done
autosampler standard rack (sample #) 10
Delay (sec) 3

Basolateral Pump Valve In
        Basolateral Pump Flowrate (microliter/sec) 50
        Basolateral Pump Fill
        Basolateral Pump Delay Until Done
Basolateral Pump Valve Out
        Basolateral Pump Empty
        Basolateral Pump Delay Until Done
Basolateral Pump Valve In
        Basolateral Pump Fill
        Basolateral Pump Delay Until Done
Basolateral Pump Valve Out
        Basolateral Pump Empty
        Basolateral Pump Delay Until Done
autosampler Wash
```

10.2.2 SIA programs for domperidone maleate

Main routine domperidone

```
Hardware Settings Wavelength 1 (nm) 286
Hardware Settings Wavelength 2 (nm) 285
Hardware Settings Wavelength 3 (nm) 344
Hardware Settings Wavelength 4 (nm) 360

autosampler Command: Set port 5

Spectrometer Reference Scan

Delay (sec) 101

Insert File C:\Programme\WINFIA 5.0\Marco\Furosemid Programme\subroutinen\dissolution_flowrate 10.fia
        Spectrometer Reference Scan
Insert File C:\Programme\WINFIA 5.0\Marco\Furosemid Programme\subroutinen\dissolution_flowrate 10.fia
        Spectrometer Reference Scan
Insert File C:\Programme\WINFIA 5.0\Marco\Furosemid Programme\subroutinen\apical_flowrate 10.fia
        Spectrometer Reference Scan
Insert File C:\Programme\WINFIA 5.0\Marco\Furosemid Programme\subroutinen\dissolution_flowrate 10.fia
        Spectrometer Reference Scan
Insert File C:\Programme\WINFIA 5.0\Marco\Furosemid Programme\subroutinen\apical_flowrate 10.fia
        Spectrometer Reference Scan

Variable Define New sampos
```

sampos = 1

Insert File C:\Programme\WINFIA 5.0\Marco\Furosemid Programme\subroutinen\basolateral_new_compartment_new_valve.fia

Loop Start (#) 40

sampos += 1

Insert File C:\Programme\WINFIA 5.0\Marco\Furosemid Programme\subroutinen\dissolution_flowrate 10.fia
Spectrometer Reference Scan
Insert File C:\Programme\WINFIA 5.0\Marco\Furosemid Programme\subroutinen\apical_flowrate 10.fia
Spectrometer Reference Scan
Insert File C:\Programme\WINFIA 5.0\Marco\Furosemid Programme\subroutinen\dissolution_flowrate 10.fia
Spectrometer Reference Scan
Insert File C:\Programme\WINFIA 5.0\Marco\Furosemid Programme\subroutinen\apical_flowrate 10.fia
Spectrometer Reference Scan
Insert File C:\Programme\WINFIA 5.0\Marco\Furosemid Programme\subroutinen\dissolution_flowrate 10.fia
Spectrometer Reference Scan
Insert File C:\Programme\WINFIA 5.0\Marco\Furosemid Programme\subroutinen\apical_flowrate 10.fia
Spectrometer Reference Scan
Insert File C:\Programme\WINFIA 5.0\Marco\Furosemid Programme\subroutinen\dissolution_flowrate 10.fia
Spectrometer Reference Scan
Insert File C:\Programme\WINFIA 5.0\Marco\Furosemid Programme\subroutinen\apical_flowrate 10.fia
Spectrometer Reference Scan
Insert File C:\Programme\WINFIA 5.0\Marco\Furosemid Programme\subroutinen\basolateral_new_compartment_new_valve.fia

Loop End

Subroutine for sampling port D (dissolution)

Syringe Pump Valve In
Syringe Pump Flowrate (microliter/sec) 500
Syringe Pump Aspirate (microliter) 750
Multiposition Valve dissolution
Syringe Pump Delay Until Done
Syringe Pump Valve Out
Syringe Pump Flowrate (microliter/sec) 50
Syringe Pump Aspirate (microliter) 100
Syringe Pump Delay Until Done
Multiposition Valve Waste
Syringe Pump Flowrate (microliter/sec) 100
Syringe Pump Dispense (microliter) 300
Syringe Pump Delay Until Done
Multiposition Valve dissolution
Syringe Pump Flowrate (microliter/sec) 10
Syringe Pump Aspirate (microliter) 50
Syringe Pump Delay Until Done

Delay (sec) 1

Multiposition Valve UV- detector
Syringe Pump Flowrate (microliter/sec) 10

Analyte New Sample
Analyte Name Dis

Spectrometer Absorbance Scanning

Delay (sec) 1
Syringe Pump Dispense (microliter) 300
Syringe Pump Delay Until Done

Spectrometer Stop Scanning

Syringe Pump Flowrate (microliter/sec) 50
Syringe Pump Empty
Syringe Pump Delay Until Done

Subroutine for sampling port A (apical)

Syringe Pump Valve In
    Syringe Pump Flowrate (microliter/sec) 500
    Syringe Pump Aspirate (microliter) 800
Multiposition Valve apical
    Syringe Pump Delay Until Done
Syringe Pump Valve Out
    Syringe Pump Flowrate (microliter/sec) 50
    Syringe Pump Aspirate (microliter) 150
    Syringe Pump Delay Until Done
Multiposition Valve Waste
    Syringe Pump Flowrate (microliter/sec) 100
    Syringe Pump Dispense (microliter) 400
    Syringe Pump Delay Until Done
Multiposition Valve apical
    Syringe Pump Flowrate (microliter/sec) 10
    Syringe Pump Aspirate (microliter) 50
    Syringe Pump Delay Until Done

Delay (sec) 1

Multiposition Valve UV- detector
    Syringe Pump Flowrate (microliter/sec) 10

Analyte New Sample
Analyte Name Api

Spectrometer Absorbance Scanning

  Delay (sec) 1
  Syringe Pump Dispense (microliter) 300
  Syringe Pump Delay Until Done

Spectrometer Stop Scanning

  Syringe Pump Flowrate (microliter/sec) 50
  Syringe Pump Empty
  Syringe Pump Delay Until Done

Subroutine for sampling port B (basolateral)

Basolateral Pump Valve In
    Basolateral Pump Flowrate (microliter/sec) 50
    Basolateral Pump Aspirate (microliter) 325
    Basolateral Pump Delay Until Done
Basolateral Pump Valve Out
    Basolateral Valve Akzeptorkompartiment
    Basolateral Pump Flowrate (microliter/sec) 10
    Basolateral Pump Aspirate (microliter) 100
    Basolateral Pump Delay Until Done
Basolateral Valve Abfall
    Basolateral Pump Dispense (microliter) 125
    Basolateral Pump Delay Until Done
Basolateral Valve 6
autosampler Wash
    Basolateral Pump Flowrate (microliter/sec) 10
    Basolateral Pump Aspirate (microliter) 25
    Basolateral Pump Delay Until Done
Basolateral Valve Akzeptorkompartiment
    Basolateral Pump Aspirate (microliter) 100
    Basolateral Pump Delay Until Done
Basolateral Valve 6
    Basolateral Pump Aspirate (microliter) 25
    Basolateral Pump Delay Until Done

autosampler standard rack (sample #) 10
Delay (sec) 3

Basolateral Valve Probensammler
    Basolateral Pump Flowrate (microliter/sec) 20
    Basolateral Pump Dispense (microliter) 220
    Basolateral Pump Delay Until Done

autosampler RACK 2 (sample #) = sampos
Delay (sec) 3

Basolateral Pump Dispense (microliter) 110
Basolateral Pump Delay Until Done

autosampler standard rack (sample #) 10
Delay (sec) 3

Basolateral Pump Valve In
    Basolateral Pump Flowrate (microliter/sec) 50
    Basolateral Pump Fill
    Basolateral Pump Delay Until Done
Basolateral Pump Valve Out
    Basolateral Pump Empty
    Basolateral Pump Delay Until Done
Basolateral Pump Valve In
    Basolateral Pump Fill
    Basolateral Pump Delay Until Done
Basolateral Pump Valve Out
    Basolateral Pump Empty
    Basolateral Pump Delay Until Done

autosampler Wash

10.2.3 SIA program for bottling in HPLC vials

Basolateral Pump Valve In
    Basolateral Pump Flowrate (microliter/sec) 50
    Basolateral Pump Aspirate (microliter) 325
    Basolateral Pump Delay Until Done
Basolateral Pump Valve Out
    Basolateral Valve Akzeptorkompartiment
    Basolateral Pump Flowrate (microliter/sec) 10
    Basolateral Pump Aspirate (microliter) 100
    Basolateral Pump Delay Until Done
Basolateral Valve Abfall
    Basolateral Pump Dispense (microliter) 125
    Basolateral Pump Delay Until Done
Basolateral Valve 6
autosampler Wash
    Basolateral Pump Flowrate (microliter/sec) 10
    Basolateral Pump Aspirate (microliter) 25
    Basolateral Pump Delay Until Done
Basolateral Valve Akzeptorkompartiment
    Basolateral Pump Aspirate (microliter) 100
    Basolateral Pump Delay Until Done
Basolateral Valve 6
    Basolateral Pump Aspirate (microliter) 25
    Basolateral Pump Delay Until Done

autosampler standard rack (sample #) 10
Delay (sec) 3

Basolateral Valve Probensammler
    Basolateral Pump Flowrate (microliter/sec) 20
    Basolateral Pump Dispense (microliter) 220
    Basolateral Pump Delay Until Done

autosampler RACK 2 (sample #) = sampos
Delay (sec) 3

Basolateral Pump Dispense (microliter) 110
Basolateral Pump Delay Until Done

autosampler standard rack (sample #) 10
Delay (sec) 3

Basolateral Pump Valve In
    Basolateral Pump Flowrate (microliter/sec) 50
    Basolateral Pump Fill
    Basolateral Pump Delay Until Done

Basolateral Pump Valve Out
    Basolateral Pump Empty
    Basolateral Pump Delay Until Done
Basolateral Pump Valve In
    Basolateral Pump Fill
    Basolateral Pump Delay Until Done
Basolateral Pump Valve Out
    Basolateral Pump Empty
    Basolateral Pump Delay Until Done

autosampler Wash

10.2.4 SIA program for filling in 96-well plate

Basolateral Pump Valve In
    Basolateral Pump Flowrate (microliter/sec) 50
    Basolateral Pump Aspirate (microliter) 325
    Basolateral Pump Delay Until Done
Basolateral Pump Valve Out
Basolateral Valve Akzeptorkompartiment
    Basolateral Pump Flowrate (microliter/sec) 10
    Basolateral Pump Aspirate (microliter) 100
    Basolateral Pump Delay Until Done
Basolateral Valve Abfall
    Basolateral Pump Dispense (microliter) 125
    Basolateral Pump Delay Until Done
Basolateral Valve 6
autosampler Wash
    Basolateral Pump Flowrate (microliter/sec) 10
    Basolateral Pump Aspirate (microliter) 25
    Basolateral Pump Delay Until Done
Basolateral Valve Akzeptorkompartiment
    Basolateral Pump Aspirate (microliter) 100
    Basolateral Pump Delay Until Done
Basolateral Valve 6
    Basolateral Pump Aspirate (microliter) 25
    Basolateral Pump Delay Until Done

autosampler standard rack (sample #) 10
Delay (sec) 3
Basolateral Valve Probensammler
    Basolateral Pump Flowrate (microliter/sec) 20
    Basolateral Pump Dispense (microliter) 220
    Basolateral Pump Delay Until Done

autosampler RACK 4 (sample #) = 1
Delay (sec) 3
Basolateral Pump Dispense (microliter) 110
Basolateral Pump Delay Until Done

autosampler standard rack (sample #) 10
Delay (sec) 3

Basolateral Pump Valve In
    Basolateral Pump Flowrate (microliter/sec) 50
    Basolateral Pump Fill
    Basolateral Pump Delay Until Done
Basolateral Pump Valve Out
    Basolateral Pump Empty
    Basolateral Pump Delay Until Done
Basolateral Pump Valve In
    Basolateral Pump Fill
    Basolateral Pump Delay Until Done
Basolateral Pump Valve Out
    Basolateral Pump Empty
    Basolateral Pump Delay Until Done

autosampler Wash

10.3 Allocation of the ports at the SIA valves

10.3.1 8-port valve

Port number	Port appelation
1	waste
2	UV-detector
3	PMT-FL
4	dissolution
5	apical
6	basolateral
7	KRB for replenishing
8	autosampler

10.3.2 6-port valve

Port number	Port appelation
1	Müll
2	Buffer
3	Akzeptorkompartiment
4	Probensammler
5	Abfall
6	6

10.4 List of abbreviations

ABC	ATP binding cassette
ADP	adenosine diphosphate
AFM	atomic force microscopy
API	active pharmaceutical ingredient
ATP	adenosine triphosphate
AUC	area under the curve
BCRP	breast cancer resistance protein
BCS	Biopharmaceutics Classification System
BDDCS	Biopharmaceutics Drug Disposition Classification System
CYP	cytochrome P
CysA	cyclosporine A
DLS	dynamic light scattering
DOPC	1,2-dioleoyl-sn-glycero-3-phosphocholine
d/p-system	combined dissolution and permeation system
ER	extended release
EVOM	epithelial volt ohm meter
FaSSIF	fasted state simulated intestinal fluid
FeSSIF	fed state simulated intestinal fluid
FTPC	flow through permeation cell
HEPES	N-2-hydroxyethylpiperazine-N'-2-ethane sulfonic acid
HPLC	high performance liquid chromatography
IR	immediate release
KRB	Krebs Ringer Buffer
MCC	microcrystalline cellulose
MCT1	monocarboxylate transporter 1
MDR1	multidrug resistance protein 1
MW	molecular weight
N.A.	numerical aperture
PAMPA	parallel artificial membrane permeability assay
P_{app}	apparent permeability coefficient
PBS	phosphate buffered saline
PepT1	peptide transporter 1

Ph. Eur.	European Pharmacopoeia
P-gp	P-glycoprotein
PMT-FL	photomultiplier tube for fluorescence detection
SD	standard deviation
SE	standard error
SEM	scanning electron microscopy
SIA	sequential injection analysis
TDT	tolerated difference test
TEER	transepithelial electrical resistance
TPGS	d-alpha tocopheryl polyethylene glycol 1000 succinate
USP	United States Pharmacopoeia
UV	ultra violet light
UWL	unstirred water layer

11 Curriculum vitae

personal information

name	Sandra Pia Gantzsch
date of birth	13.10.1985
place of birth:	Riesa, Germany

PhD thesis

February 2010 – July 2013	Department of Biopharmaceutics and Pharmaceutical Technology, Saarland University under supervision of Prof. Dr. Claus-Michael Lehr

undergraduate study

WS 2004/05 – WS 2008/09	Pharmacy, Universität Leipzig Diploma in Pharmacy (July 2009) Certification as Pharmacist (January 2010)

school

1996 – 2004	Secondary High School “Gymnasium Franziskaneum” Meißen. University entrance requirement

internships

May 2009 – October 2009	„Schlehen-Apotheke“, Leipzig (second part of the practical training for pharmacists)
November 2008 – April 2009	R&D Quality Unit, Sanofi-Aventis Deutschland GmbH, Frankfurt/Main, Germany (first part of the practical training for pharmacists)

12 List of publications

Publications:

Manuscript prepared for submission:
“Characterization and evaluation of lipid-coated membranes in comparison to Caco-2 cell monolayers for combined dissolution and permeation testing”

Conferences:

Posters:
S. Gantzsch, B. Kann, M. Windbergs, M. Ofer-Gläßgen, P. Loos, H. Berchtold, S. Balbach, T. Eichinger, U. F. Schaefer, C-M. Lehr. Evaluation of a lipid based permeation model for the use under dynamic conditions in a combined dissolution and permeation system, 2012 AAPS Annual Meeting and Exposition, October 14-18, 2012, Chicago, IL, USA

B. Kann, S. Gantzsch, C-M. Lehr, U. F. Schaefer, M. Windbergs
Chemically selective imaging of structured surfaces – a novel complementary analytical approach for pharmaceutical investigations, DPhG Jahrestagung 2012, October 11-13,2012, Greifswald, Germany

S. Gantzsch, U. F. Schaefer, P. Loos, H. Berchtold, S. Balbach, T. Eichinger, C-M. Lehr. Complex Characterization of Drug Formulation by means of combined Dissolution and Permeation Measurement, New Developments in Cell-Based In-Vitro Testing and 3rd Annual Quasi-Vivo® User Group Meeting, May 18-20, 2011, Saarbrücken, Deutschland

Oral presentation:
S. Gantzsch. Combined assessment of drug dissolution and epithelial permeability, Analytical Forum Sanofi, November 27, 2012, Frankfurt/Main, Deutschland

B. Kann, S. Gantzsch, C-M. Lehr, U. F. Schaefer and M. Windbergs. Confocal Raman microscopy as a novel approach for development and chemically resolved characterization of a drug permeation model, 39th Annual Meeting & Exposition of the Controlled Release Society, June 14-18, 2012, Québec City, Canada

13 Acknowledgement / Danksagung

An erster Stelle möchte ich mich herzlich bei Herrn Prof. Claus-Michael Lehr für die Überlassung des interessanten Themas und die sehr gute Betreuung meiner Doktorarbeit bedanken.
Herrn Jun.-Prof. Thorsten Lehr danke ich für die Anfertigung des Zweitgutachtens, sowie den anderen Mitgliedern der Prüfungskommission.

Mein ganz besonderer Dank gilt Herrn Prof. Ulrich Schäfer für die ausgezeichnete Betreuung meiner Arbeit auch über den Ruhestand hinaus. Nicht nur bei wissenschaftlichen Fragen sondern auch bei administrativen Problemen stand er mir mit hilfreichem Rat und Tat jederzeit zur Seite.

Bei der Sanofi-Aventis Deutschland GmbH möchte ich mich für die Finanzierung und Unterstützung dieser Arbeit bedanken. Insbesondere spreche ich meinen Dank Herrn Dr. Stefan Balbach, Herrn Dr. Harald Berchtold, Herrn Dr. Eichinger, Frau Dr. Petra Loos und Frau Dr. Ofer-Gläßgen aus, die durch gute Zusammenarbeit und wertvolle Diskussionen eine sehr gute Kooperation ermöglichten.

Für die gute Zusammenarbeit und Kooperation danke ich Birthe Kann und Maike Windbergs, die eine weitere Charakterisierung meiner Membranen mittels Raman-Mikroskopie ermöglicht haben.

Ich bedanke mich bei den Technikern unseres Institutes für ihre Hilfe. Vor allem danke ich Heike Stumpf und Petra König für ihre Unterstützung bei der Anzucht und Pflege meiner Caco-2 Zellen, welche mir das Leben nicht unwesentlich erleichterte. Peter Meiers danke ich für die Hilfe bei allen Problemen mit der HPLC-Analytik und Chiara de Rossi für die Aufnahme der SEM Bilder.

Dominik Selzer und José-David Gómez-Mantilla danke ich für die Unterstützung bei der Umsetzung des mathematischen Models und bei der Durchführung der f2- und TDT-Tests. (Thanks to JD for helping me to realize the mathematically model and the f2- and TDT-test.)

Julia Hahnemann und Elena Hoffmann danke ich für ihre experimentelle Hilfe als studentische Hilfskräfte.

Ich bedanke mich bei Sarah Gordon fürs Korrekturlesen dieser Arbeit. (Many thanks to Sarah Gordon for proofreading.)

Natürlich möchte ich auch all meinen Mitdoktoranden und Kollegen danken, die für ein gutes Arbeitsklima gesorgt haben und immer ein offenes Ohr für einen Erfahrungsaustausch hatten. Die Zusammenarbeit mit euch hat mir sehr viel Spaß gemacht.
Ein großes Dankeschön geht hier vor allem an meine Bürokollegen, insbesondere Christina und Anne, für die schöne gemeinsame Zeit und die aufbauenden Diskussionen.

Ein großes Dankeschön geht auch an meine Freunde Katrein und Stefan, die mir jederzeit zuhörten und mich in schweren Zeiten wieder aufbauten, danke für eure Geduld und euer Verständnis.

Mein wichtigster Dank geht aber an meine Eltern, die immer an mich geglaubt haben, mich ermutigt haben und mich stets auf meinem Weg unterstützt haben, auch wenn dieser mich ans andere Ende von Deutschland geführt hat. Danke für alles!

14 References

[1] E. Galia, E. Nicolaides, D. Hörter, R. Löbenberg, C. Reppas, J.B. Dressman, Evaluation of various dissolution media for predicting In vivo performance of class I and II drugs, Pharm. Res., 15 (1998) 698-705.

[2] F. Ingels, S. Deferme, E. Destexhe, M. Oth, G. Van Den Mooter, P. Augustijns, Simulated intestinal fluid as transport medium in the Caco-2 cell culture model, Int. J. Pharm., 232 (2002) 183-192.

[3] F.M. Ingels, P.F. Augustijns, Biological, pharmaceutical, and analytical considerations with respect to the transport media used in the absorption screening system, Caco-2, J. Pharm. Sci., 92 (2003) 1545-1558.

[4] F. Ingels, B. Beck, M. Oth, P. Augustijns, Effect of simulated intestinal fluid on drug permeability estimation across Caco-2 monolayers, Int. J. Pharm., 274 (2004) 221-232.

[5] N. Patel, B. Forbes, S. Eskola, J. Murray, Use of simulated intestinal fluids with Caco-2 cells and rat ileum, Drug Dev. Ind. Pharm., 32 (2006) 151-161.

[6] M. Kataoka, Y. Masaoka, S. Sakuma, S. Yamashita, Effect of food intake on the oral absorption of poorly water-soluble drugs: In vitro assessment of drug dissolution and permeation assay system, J. Pharm. Sci., 95 (2006) 2051-2061.

[7] E. Jantratid, N. Janssen, C. Reppas, J.B. Dressman, Dissolution media simulating conditions in the proximal human gastrointestinal tract: An update, Pharm. Res., 25 (2008) 1663-1676.

[8] United States Pharmacopoeia, United States Pharmacopoeial Convention Inc., Rockville, USA, 2004.

[9] N. Fotaki, Flow-through cell apparatus (USP Apparatus 4): Operation and features, Dissolution Technologies, 18 (2011) 46-49.

[10] G.L. Amidon, H. Lennernas, V.P. Shah, J.R. Crison, A theoretical basis for a biopharmaceutic drug classification: The correlation of in vitro drug product dissolution and in vivo bioavailability, Pharm. Res., 12 (1995) 413-420.

[11] FDA, Guidance for industry - waiver of in vivo bioavailability and bioequivalence studies for immediate-release solid oral dosage forms based on a biopharmaceutics classification system, (2000).

[12] C.A. Lipinski, F. Lombardo, B.W. Dominy, P.J. Feeney, Experimental and computational approaches to estimate solubility and permeability in drug discovery and development settings, Advanced Drug Delivery Reviews, 23 (1997) 3-25.

[13] P. Palumbo, U. Picchini, B. Beck, J. Van Gelder, N. Delbar, A. DeGaetano, A general approach to the apparent permeability index, Journal of Pharmacokinetics and Pharmacodynamics, 35 (2008) 235-248.

[14] P. Artursson, Epithelial transport of drugs in cell culture. I: A model for studying the passive diffusion of drugs over intestinal absorptive (Caco-2) cells, J. Pharm. Sci., 79 (1990) 476-482.

[15] I.J. Hidalgo, T.J. Raub, R.T. Borchardt, Characterization of the human colon carcinoma cell line (Caco-2) as a model system for intestinal epithelial permeability, Gastroenterology, 96 (1989) 736-749.

[16] P. Artursson, J. Karlsson, Correlation between oral drug absorption in humans and apparent drug permeability coefficients in human intestinal epithelial (CACO-2) cells, Biochem. Biophys. Res. Commun., 175 (1991) 880-885.

[17] H. Lennernäs, K. Palm, U. Fagerholm, P. Artursson, Comparison between active and passive drug transport in human intestinal epithelial (Caco-2) cells in vitro and human jejunum in vivo, Int. J. Pharm., 127 (1996) 103-107.

[18] C. Brimer, J.T. Dalton, Z. Zhu, J. Schuetz, K. Yasuda, E. Vanin, M.V. Relling, Y. Lu, E.G. Schuetz, Creation of polarized cells coexpressing CYP3A4, NADPH cytochrome P450 reductase and MDR1/P-glycoprotein, Pharm. Res., 17 (2000) 803-810.

[19] K.E. Thummel, C. Brimer, K. Yasuda, J. Thottassery, T. Senn, Y. Lin, H. Ishizuka, E. Kharasch, J. Schuetz, E. Schuetz, Transcriptional control of intestinal cytochrome P-4503A by 1α,25-dihydroxy vitamin D3, Mol. Pharmacol., 60 (2001) 1399-1406.

[20] F. Thiebaut, T. Tsuruo, H. Hamada, M.M. Gottesman, I. Pastan, M.C. Willingham, Cellular localization of the multidrug-resistance gene product P-glycoprotein in normal human tissues, Proc. Natl. Acad. Sci. U. S. A., 84 (1987) 7735-7738.

[21] J.H. Lin, M. Yamazaki, Role of P-glycoprotein in pharmacokinetics: Clinical implications, Clin. Pharmacokinet., 42 (2003) 59-98.

[22] A. Tsuji, I. Tamai, Carrier-mediated intestinal transport of drugs, Pharm. Res., 13 (1996) 963-977.

[23] I. Tamai, A. Tsuji, Drug delivery through the blood-brain barrier, Advanced Drug Delivery Reviews, 19 (1996) 401-424.

[24] V.J. Wacher, L. Salphati, L.Z. Benet, Active secretion and enterocytic drug metabolism barriers to drug absorption, Advanced Drug Delivery Reviews, 46 (2000) 89-102.

[25] J.M. Meerum Terwogt, M.M. Malingré, J.H. Beijnen, W.W. Ten Bokkel Huinink, H. Rosing, F.J. Koopman, O. Van Tellingen, M. Swart, J.H.M. Schellens, Coadministration of oral cyclosporin A enables oral therapy with paclitaxel, Clin. Cancer Res., 5 (1999) 3379-3384.

[26] T. Chang, L.Z. Benet, M.F. Hebert, The effect of water-soluble vitamin E on cyclosporine pharmacokinetics in healthy volunteers, Clin. Pharmacol. Ther., 59 (1996) 297-303.

[27] M.J. Ginski, R. Taneja, J.E. Polli, Prediction of dissolution-absorption relationships from a continuous dissolution/caco-2 system, AAPS PharmSci, 1 (1999) 1-12.

[28] M. Kobayashi, N. Sada, M. Sugawara, K. Iseki, K. Miyazaki, Development of a new system for prediction of drug absorption that takes into account drug dissolution and pH change in the gastro-intestinal tract, Int. J. Pharm., 221 (2001) 87-94.

[29] M. Kataoka, Y. Masaoka, Y. Yamazaki, T. Sakane, H. Sezaki, S. Yamashita, In Vitro System to Evaluate Oral Absorption of Poorly Water-Soluble Drugs: Simultaneous Analysis on Dissolution and Permeation of Drugs, Pharm. Res., 20 (2003) 1674-1680.

[30] M. Kataoka, T. Yokoyama, Y. Masaoka, S. Sakuma, S. Yamashita, Estimation of P-glycoprotein-mediated efflux in the oral absorption of P-gp substrate drugs from simultaneous analysis of drug dissolution and permeation, Eur. J. Pharm. Sci., 44 (2011) 544-551.

[31] M. Kataoka, K. Sugano, C. Da Costa Mathews, J.W. Wong, K.L. Jones, Y. Masaoka, S. Sakuma, S. Yamashita, Application of dissolution/permeation system for evaluation of formulation effect on oral absorption of poorly water-soluble drugs in drug development, Pharm. Res., 29 (2012) 1485-1494.

[32] S.A. Motz, U.F. Schaefer, S. Balbach, T. Eichinger, C.M. Lehr, Permeability assessment for solid oral drug formulations based on Caco-2 monolayer in combination with a flow through dissolution cell, Eur. J. Pharm. Biopharm., 66 (2007) 286-295.

[33] S.A. Motz, J. Klimundová, U.F. Schaefer, S. Balbach, T. Eichinger, P. Solich, C.M. Lehr, Automated measurement of permeation and dissolution of propranolol HCl tablets using sequential injection analysis, Anal. Chim. Acta, 581 (2007) 174-180.

[34] M. Muendoerfer, U.F. Schaefer, P. Koenig, J.S. Walk, P. Loos, S. Balbach, T. Eichinger, C.M. Lehr, Online monitoring of transepithelial electrical resistance (TEER) in an apparatus for combined dissolution and permeation testing, Int. J. Pharm., 392 (2010) 134-140.

[35] R.B. Van Breemen, Y. Li, Caco-2 cell permeability assays to measure drug absorption, Expert Opinion on Drug Metabolism and Toxicology, 1 (2005) 175-185.

[36] M. Kansy, F. Senner, K. Gubernator, Physicochemical high throughput screening: Parallel artificial membrane permeation assay in the description of passive absorption processes, J. Med. Chem., 41 (1998) 1007-1010.

[37] A. Avdeef, The rise of PAMPA, Expert opinion on drug metabolism & toxicology, 1 (2005) 325-342.

[38] G. Camenisch, G. Folkers, H. Van De Waterbeemd, Comparison of passive drug transport through Caco-2 cells and artificial membranes, Int. J. Pharm., 147 (1997) 61-70.

[39] A. Avdeef, M. Strafford, E. Block, M.P. Balogh, W. Chambliss, I. Khan, Drug absorption in vitro model: Filter-immobilized artificial membranes: 2. Studies of the permeability properties of lactones in Piper methysticum Forst, Eur. J. Pharm. Sci., 14 (2001) 271-280.

[40] J.A. Ruell, K.L. Tsinman, A. Avdeef, PAMPA - A drug absorption in vitro model: 5. Unstirred water layer in iso-pH mapping assays and pK_a^{flux} - Optimized design (pOD-PAMPA), Eur. J. Pharm. Sci., 20 (2003) 393-402.

[41] F.T.T. Huque, K. Box, J.A. Platts, J. Comer, Permeability through DOPC/dodecane membranes: Measurement and LFER modelling, Eur. J. Pharm. Sci., 23 (2004) 223-232.

[42] A. Avdeef, Absorption and Drug Development - Solubility, Permeability and Charge State, John Wiley & Sons, New York, USA, 2003.

[43] A. Avdeef, O. Tsinman, PAMPA - A drug absorption in vitro model: 13. Chemical selectivity due to membrane hydrogen bonding: In combo comparisons of HDM-, DOPC-, and DS-PAMPA models, Eur. J. Pharm. Sci., 28 (2006) 43-50.

[44] K. Sugano, H. Hamada, M. Machida, H. Ushio, High throughput prediction of oral absorption: Improvement of the composition of the lipid solution used in parallel artificial membrane permeation assay, Journal of Biomolecular Screening, 6 (2001) 189-196.

[45] K. Sugano, N. Takata, M. Machida, K. Saitoh, K. Terada, Prediction of passive intestinal absorption using bio-mimetic artificial membrane permeation assay and the paracellular pathway model, Int. J. Pharm., 241 (2002) 241-251.

[46] K. Sugano, Y. Nabuchi, M. Machida, Y. Aso, Prediction of human intestinal permeability using artificial membrane permeability, Int. J. Pharm., 257 (2003) 245-251.

[47] F. Wohnsland, B. Faller, High-throughput permeability pH profile and high-throughput alkane/water log P with artificial membranes, J. Med. Chem., 44 (2001) 923-930.

[48] C. Zhu, L. Jiang, T.M. Chen, K.K. Hwang, A comparative study of artificial membrane permeability assay for high throughput profiling of drug absorption potential, European Journal of Medicinal Chemistry, 37 (2002) 399-407.

[49] G. Corti, F. Maestrelli, M. Cirri, S. Furlanetto, P. Mura, Development and evaluation of an in vitro method for prediction of human drug absorption: I. Assessment of artificial membrane composition, Eur. J. Pharm. Sci., 27 (2006) 346-353.

[50] G. Corti, F. Maestrelli, M. Cirri, N. Zerrouk, P. Mura, Development and evaluation of an in vitro method for prediction of human drug absorption: II. Demonstration of the method suitability, Eur. J. Pharm. Sci., 27 (2006) 354-362.

[51] G.E. Flaten, A.B. Dhanikula, K. Luthman, M. Brandl, Drug permeability across a phospholipid vesicle based barrier: A novel approach for studying passive diffusion, Eur. J. Pharm. Sci., 27 (2006) 80-90.

[52] G.E. Flaten, H. Bunjes, K. Luthman, M. Brandl, Drug permeability across a phospholipid vesicle-based barrier. 2. Characterization of barrier structure, storage stability and stability towards pH changes, Eur. J. Pharm. Sci., 28 (2006) 336-343.

[53] G.E. Flaten, M. Skar, K. Luthman, M. Brandl, Drug permeability across a phospholipid vesicle based barrier: 3. Characterization of drug-membrane interactions and the effect of agitation on the barrier integrity and on the permeability, Eur. J. Pharm. Sci., 30 (2007) 324-332.

[54] H. Fischer, M. Kansy, A. Avdeef, F. Senner, Permeation of permanently positive charged molecules through artificial membranes-Influence of physico-chemical properties, Eur. J. Pharm. Sci., 31 (2007) 32-42.

[55] G.E. Flaten, K. Luthman, T. Vasskog, M. Brandl, Drug permeability across a phospholipid vesicle-based barrier. 4. The effect of tensides, co-solvents and pH changes on barrier integrity and on drug permeability, Eur. J. Pharm. Sci., 34 (2008) 173-180.

[56] S.M. Fischer, G.E. Flaten, E. Hagesæther, G. Fricker, M. Brandl, In-vitro permeability of poorly water soluble drugs in the phospholipid vesicle-based permeation assay: The influence of nonionic surfactants, J. Pharm. Pharmacol., 63 (2011) 1022-1030.

[57] S.M. Fischer, S.T. Buckley, W. Kirchmeyer, G. Fricker, M. Brandl, Application of simulated intestinal fluid on the phospholipid vesicle-based drug permeation assay, Int. J. Pharm., 422 (2012) 52-58.

[58] J. Kanzer, I. Tho, G.E. Flaten, P. Hölig, G. Fricker, M. Brandl, In-vitro permeability screening of melt extrudate formulations containing poorly water-soluble drug compounds using the phospholipid vesicle-based barrier, J. Pharm. Pharmacol., 62 (2010) 1591-1598.

[59] X. Chen, A. Murawski, K. Patel, C.L. Crespi, P.V. Balimane, A novel design of artificial membrane for improving the PAMPA model, Pharm. Res., 25 (2008) 1511-1520.

[60] L. Di, E.H. Kerns, K. Fan, O.J. McConnell, G.T. Carter, High throughput artificial membrane permeability assay for blood-brain barrier, European Journal of Medicinal Chemistry, 38 (2003) 223-232.

[61] B. Sinkó, T.M. Garrigues, G.T. Balogh, Z.K. Nagy, O. Tsinman, A. Avdeef, K. Takács-Novák, Skin-PAMPA: A new method for fast prediction of skin penetration, Eur. J. Pharm. Sci., 45 (2012) 698-707.

[62] C.Y. Wu, L.Z. Benet, Predicting drug disposition via application of BCS: Transport/absorption/ elimination interplay and development of a biopharmaceutics drug disposition classification system, Pharm. Res., 22 (2005) 11-23.

[63] L.Z. Benet, F. Broccatelli, T.I. Oprea, BDDCS applied to over 900 drugs, AAPS Journal, 13 (2011) 519-547.

[64] J. Brouwers, J. Tack, F. Lammert, P. Augustijns, Intraluminal drug and formulation behavior and integration in in vitro permeability estimation: A case study with amprenavir, J. Pharm. Sci., 95 (2006) 372-383.

[65] F. Föger, K. Kafedjiiski, H. Hoyer, B. Loretz, A. Bernkop-Schnürch, Enhanced transport of P-glycoprotein substrate saquinavir in presence of thiolated chitosan, J. Drug Target., 15 (2007) 132-139.

[66] B.D. Rege, X. Yu Lawrence, A.S. Hussain, J.E. Polli, Effect of common excipients on Caco-2 transport of low-permeability drugs, J. Pharm. Sci., 90 (2001) 1776-1786.

[67] A.M. Al-Mohizea, Influence of intestinal efflux pumps on the absorption and transport of furosemide, Saudi Pharmaceutical Journal, 18 (2010) 97-101.

[68] E.M. Collnot, C. Baldes, M.F. Wempe, J. Hyatt, L. Navarro, K.J. Edgar, U.F. Schaefer, C.M. Lehr, Influence of vitamin E TPGS poly(ethylene glycol) chain length on apical efflux transporters in Caco-2 cell monolayers, J. Controlled Release, 111 (2006) 35-40.

[69] A.H. Schinkel, E. Wagenaar, C.A.A.M. Mol, L. Van Deemter, P-glycoprotein in the blood-brain barrier of mice influences the brain penetration and pharmacological activity of many drugs, J. Clin. Invest., 97 (1996) 2517-2524.

[70] A.A. El Ela, S. Härtter, U. Schmitt, C. Hiemke, H. Spahn-Langguth, P. Langguth, Identification of P-glycoprotein substrates and inhibitors among psychoactive compounds - Implications for pharmacokinetics of selected substrates, J. Pharm. Pharmacol., 56 (2004) 967-975.

[71] K. Bogman, Y. Zysset, L. Degen, G. Hopfgartner, H. Gutmann, J. Alsenz, J. Drewe, P-glycoprotein and surfactants: Effect on intestinal talinolol absorption, Clin. Pharmacol. Ther., 77 (2005) 24-32.

[72] L. Yu, A. Bridgers, J. Polli, A. Vickers, S. Long, A. Roy, R. Winnike, M. Coffin, Vitamin E-TPGS increases absorption flux of an HIV protease inhibitor by enhancing its solubility and permeability, Pharm. Res., 16 (1999) 1812-1817.

[73] M.V.S. Varma, R. Panchagnula, Enhanced oral paclitaxel absorption with vitamin E-TPGS: Effect on solubility and permeability in vitro, in situ and in vivo, Eur. J. Pharm. Sci., 25 (2005) 445-453.

[74] F. Faassen, G. Vogel, H. Spanings, H. Vromans, Caco-2 permeability, P-glycoprotein transport ratios and brain penetration of heterocyclic drugs, Int. J. Pharm., 263 (2003) 113-122.

[75] E.M. Collnot, Modulation of the apical efflux transporter P-glycoprotein by Vitamin E TPGS: Structure-activity relationships and mechanism of inhibition, in: Department of Biopharmaceutics and Pharmaceutical Technology, Saarland University, Saarbruecken, 2007.

[76] E.M. Collnot, C. Baldes, U.F. Schaefer, K.J. Edgar, M.F. Wempe, C.M. Lehr, Vitamin e TPGS P-glycoprotein inhibition mechanism: Influence on conformational flexibility, intracellular ATP levels, and role of time and site of access, Molecular Pharmaceutics, 7 (2010) 642-651.

[77] A. Belu, C. Mahoney, K. Wormuth, Chemical imaging of drug eluting coatings: Combining surface analysis and confocal Raman microscopy, J. Controlled Release, 126 (2008) 111-121.

[78] M. Haaser, M. Windbergs, C.M. McGoverin, P. Kleinebudde, T. Rades, K.C. Gordon, C.J. Strachan, Analysis of matrix dosage forms during dissolution testing using raman microscopy, J. Pharm. Sci., 100 (2011) 4452-4459.

[79] M. Windbergs, M. Haaser, C.M. McGoverin, K.C. Gordon, P. Kleinebudde, C.J. Strachan, Investigating the relationship between drug distribution in solid lipid matrices and dissolution behaviour using Raman spectroscopy and mapping, J. Pharm. Sci., 99 (2010) 1464-1475.

[80] D.P. Cherney, J.C. Conboy, J.M. Harris, Optical-Trapping Raman Microscopy Detection of Single Unilamellar Lipid Vesicles, Anal. Chem., 75 (2003) 6621-6628.

[81] C. Matthäus, A. Kale, T. Chernenko, V. Torchilin, M. Diem, New ways of imaging uptake and intracellular fate of liposomal drug carrier systems inside individual cells, based on raman microscopy, Molecular Pharmaceutics, 5 (2008) 287-293.

[82] A.J. López, T. Rivas, J. Lamas, A. Ramil, A. Yáñez, Optimisation of laser removal of biological crusts in granites, Applied Physics A: Materials Science and Processing, 100 (2010) 733-739.

[83] J. Feys, P. Vermeir, P. Lommens, S.C. Hopkins, X. Granados, B.A. Glowacki, M. Baecker, E. Reich, S. Ricard, B. Holzapfel, P. Van Der Voort, I. Van Driessche, Ink-jet printing of YBa 2Cu 3O 7 superconducting coatings and patterns from aqueous solutions, J. Mater. Chem., 22 (2012) 3717-3726.

[84] L.M. Formosa, B. Mallia, T. Bull, J. Camilleri, The microstructure and surface morphology of radiopaque tricalcium silicate cement exposed to different curing conditions, Dent. Mater., 28 (2012) 584-595.

[85] L. Franzen, C. Mathes, S. Hansen, M. Windbergs, Advanced chemical imaging and comparison of human and porcine hair follicles for drug delivery by confocal Raman microscopy, Journal of biomedical optics, 18 (2013) 061210-061210.

[86] B. Kann, M. Windbergs, Chemical Imaging of Drug Delivery Systems with Structured Surfaces–a Combined Analytical Approach of Confocal Raman Microscopy and Optical Profilometry, AAPS J, (2013) 1-6.

[87] V. Filipe, A. Hawe, W. Jiskoot, Critical evaluation of nanoparticle tracking analysis (NTA) by NanoSight for the measurement of nanoparticles and protein aggregates, Pharm. Res., 27 (2010) 796-810.

[88] A. Steimer, E. Haltner, C.M. Lehr, Cell culture models of the respiratory tract relevant to pulmonary drug delivery, Journal of Aerosol Medicine: Deposition, Clearance, and Effects in the Lung, 18 (2005) 137-182.

[89] National Center for Biotechnology Information, http://pubchem.ncbi.nlm.nih.gov/, in: PubChem Compound Database, Jan. 05, 2013.

[90] B.A. Chavan, K.K. Mali, R.J. Dias, L.D. Kate, Solid state characterization of multicomponent inclusion complex of domperidone with β-cyclodextrin, polyvinyl pyrrolidone and citric acid, Der Pharmacia Lettre, 3 (2011) 281-290.

[91] A.K. Mandagere, T.N. Thompson, K.K. Hwang, Graphical model for estimating oral bioavailability of drugs in humans and other species from their Caco-2 permeability and in vitro liver enzyme metabolic stability rates, J. Med. Chem., 45 (2002) 304-311.

[92] P.E. Nielsen, A. Avdeef, PAMPA - A drug absorption in vitro model: 8. Apparent filter porosity and the unstirred water layer, Eur. J. Pharm. Sci., 22 (2004) 33-41.

[93] FDA, Guidance for industry - bioavailability and bioequivalence studies for orally administered drug products - general considerations, (2003).

[94] J.W. Moore, H.H. Flanner, Mathematical Comparison of Dissolution Profiles, Pharm. Technol., 20 (1996) 64-74.

[95] J.D. Gómez-Mantilla, V.G. Casabó, U.F. Schaefer, C.M. Lehr, Permutation Test (PT) and Tolerated Difference Test (TDT): Two new, robust and powerful nonparametric tests for statistical comparison of dissolution profiles, Int. J. Pharm., 441 (2013) 458-467.

[96] P. Costa, J.M. Sousa Lobo, Modeling and comparison of dissolution profiles, Eur. J. Pharm. Sci., 13 (2001) 123-133.

[97] S.A. Motz, Combined assessment of dissolution and epithelial permeability of solid oral dosage forms, in: Department of Biopharmaceutics and Pharmaceutical Technology, Saarland University, Saarbruecken, 2007.

[98] M. Muendoerfer, Combined assessment of drug dissolution and epithelial permeability: Implementationn of online TEER measurement and extension to BCS class III and IV compounds, in: Department of Biopharmaceutics and Pharmaceutical Technology, Saarland University, Saarbruecken, 2010.

[99] N.E. Basci, A. Temizer, A. Bozkurt, A. Isimer, Optimization of mobile phase in the separation of β-blockers by HPLC, J. Pharm. Biomed. Anal., 18 (1998) 745-750.

[100] K. Yamamoto, M. Hagino, H. Kotaki, T. Iga, Quantitative determination of domperidone in rat plasma by high-performance liquid chromatography with fluorescence detection, Journal of Chromatography B: Biomedical Sciences and Applications, 720 (1998) 251-255.

[101] K. Westphal, A. Weinbrenner, T. Giessmann, M. Stuhr, G. Franke, M. Zschiesche, R. Oertel, B. Terhaag, H.K. Kroemer, W. Siegmund, Oral bioavailability of digoxin is enhanced by talinolol: Evidence for involvement of intestinal P-glycoprotein, Clin. Pharmacol. Ther., 68 (2000) 6-12.

[102] L.Y. Kong, B.G. Su, Z.B. Bao, H.B. Xing, Y.W. Yang, Q.L. Ren, Direct quantification of mono- and di-d-α-tocopherol polyethylene glycol 1000 succinate by high performance liquid chromatography, J. Chromatogr. A, 1218 (2011) 8664-8671.